AFCRL-69-0205

CONTRACT AF 61 (052) - 965 Jan 1969

FINAL SCIENTIFIC REPORT

STUDIES OF SIZE DISTRIBUTIONS AND GROWTH WITH HUMIDITY OF NATURAL AEROSOL PARTICLES

1 Nov 1966 - 31 Dec 1968

NIKOLAUS ABEL, PETER WINKLER and CHRISTIAN JUNGE

MAX-PLANCK-INSTITUT FÜR CHEMIE
(OTTO-HAHN-INSTITUT)
MAINZ, Germany

THIS RESEARCH HAS BEEN SPONSORED IN PART BY THE AIR FORCE CAMBRIDGE RESEARCH LABORATORY THROUGH THE EUROPEAN OFFICE OF AEROSPACE RESEARCH (OAR), UNITED STATES AIR FORCE UNDER CONTRACT AF 61 (052) - 965

AFCRL-69-0205

CONTRACT AF 61 (052) - 965 Jan 1969

FINAL SCIENTIFIC REPORT

STUDIES OF SIZE DISTRIBUTIONS AND GROWTH WITH HUMIDITY OF NATURAL AEROSOL PARTICLES

1 Nov 1966 - 31 Dec 1968

NIKOLAUS ABEL, PETER WINKLER and CHRISTIAN JUNGE

MAX-PLANCK-INSTITUT FÜR CHEMIE
(OTTO-HAHN-INSTITUT)
MAINZ, Germany

THIS RESEARCH HAS BEEN SPONSORED IN PART BY THE AIR FORCE CAMBRIDGE RESEARCH LABORATORY THROUGH THE EUROPEAN OFFICE OF AEROSPACE RESEARCH (OAR), UNITED STATES AIR FORCE UNDER CONTRACT AF 61 (052) - 965

Abstract.

Part I.

The sensitive large-ion counter which had been previously developed (JUNGE and ABEL 1965, and ABEL and JUNGE 1966) has been improved and tested under field conditions. It can be used to determine aerosol particle size distributions between 10^{-6} cm and 10^{-5} cm particle radius at total particle number concentrations down to 500 cm^{-3} with moderate resolution. Errors of measurement and restrictions with respect to the electrical charge distribution in the aerosol are discussed. The instrument was tested and measurements were made at the following locations in more or less clean air: 1. Schauinsland, 1200 m above sea level in the Black Forest, Germany, August 1967; 2. Bay of Biscay, on research vessel "Meteor", October 1967; 3. Observatory Izaña, 2360 m above sea level on Tenerife, Canary Islands, March 1968. Some of the results obtained at these places are discussed.

Part II.

A gravimetric method is described for the determination of the growth of aerosol samples in vapors of water and organic solvents. Results of measurements for samples of natural and artificial aerosols for water vapor are discussed to demonstrate the possibilities of the method and some special characteristics of these growth curves, such as the smooth form of the curves and the hysteresis effect.

Experiments are discussed which show that the typical smooth form of the growth curves of natural continental aerosols can be explained by the presence of salt mixtures and insoluble material. It is found that both the mutual influence on solubility among the various ions as well as interaction between dissolved and insoluble material tends to smooth the shape of these curves.

The study of hysteresis indicated that this effect is due partly to the supersaturation of solutions and partly to the existence of pores in the aerosol particles or at least in the aerosol sample. There is evidence that the effect of the pores is enhanced by the interaction between soluble and insoluble material.

The study of growth of natural aerosol particles in organic vapors showed that organic material is present which results in similar growth curves as in the case of water vapor. It became clear, however, that growth in organic vapors will influence the subsequent growth in water vapor, i.e. that exposure of the aerosol samples to organic vapors is not reversible. Heating of aerosol samples up to 150° C resulted in mass losses up to 35%. This mass loss is due to both organic and inorganic components.

For further systematic study of the organic components in aerosols we developed the so-called "solution" method. In this method the mass losses are determined after exposure of the sample to a certain sequence of solvents.

Table of Contents.

List of Symbols.

Part I.

a, b = relative amplitudes of ion concentration fluctuations before and after passing a damping vessel
C = effective capacity of electrometer system
e = electrical elementary charge
E_ξ = radial electrical field strength in cylindrical aspiration condenser
$f(k)$ = ion mobility distribution function
I = ion current flowing to the receiving electrode
k = ion mobility
k_c = critical mobility of aspiration condenser
l = length of cylindrical aspiration condenser
m = factor defined by eq. (12a)
N_{av} = average ion number concentration in case of fluctuations
N_{in} = ion number concentration entering damping vessel
N_{out} = ion number concentration leaving damping vessel
N = total particle number concentration
N_o = numbe concentration of uncharged particles
N_p = number concentration of particles carrying p elementary charges of one sign
N_i = number concentration of large-ions
N_i' = fraction of ions arriving at the receiving electrode
p = number of elementary charges on a particle
$p(r)$ = charge distribution factor
Q = volume of damping vessel
r = particle radius
r_1, r_a = inner and outer radius of cylindrical aspiration condenser
r_e = radius at which ions enter the cylindrical aspiration condenser just arriving at the end of the receiving electrode
t = time
V = driving voltage at cylindrical aspiration condenser
V_a = electrometer signal voltage
$v_z(\xi)$ = air flow velocity in cylindrical aspiration condenser
z = axial coordinate in cylindrical aspiration condenser
Φ = air flow rate through the cylindrical aspiration condenser
Φ' = fraction of air flow rate within radius r_e
φ = phase shift of concentration fluctuations after passing damping vessel
ξ = radial coordinate in cylindrical aspiration condenser
τ = period of ion concentration fluctuation (assumed sinusoidal)

Part II.

m = mass of the sample at vapor pressure p

m_w = mass of water or organic solvent picked up by the sample at vapor pressure p

m_o = mass of the sample at vapor pressure p = o

m_{os} = mass of the soluble fraction of the sample

Part I.: A Sensitive Large-Ion Counter for Studying Size Distributions of Atmospheric Aerosol Particles with Radii Smaller than 0.1 Micron.

1. Introduction.

The study of particle size distributions of atmospheric aerosols in unpolluted areas is the objective of a research group at our institute. These size distributions range over many orders of magnitude in particle concentration as well as in particle size. Since the predominant physical properties of particles which can be used for size determination, such as diffusion, mobility, light scattering, inertia, vary strongly with particle size it is not possible to cover the whole size range from 10^{-7} to 10^{-2} cm radius by one single method. In view of the additional difficulty of rather low concentrations under clean air conditions it is, therefore, necessary to use several methods in parallel for the whole size range. Most of the methods available are, however, only useful for concentrations which are higher than those which we intended to study. It was, therefore, necessary to develop and refine existing methods in order to meet the requirements.

The total particle concentration in clean air ranges from about 10^2 to 10^3 particles per cm^3, most of which are found between 3.10^{-7} and 10^{-5} cm radius. The particle size range for radii larger than 10^{-5} cm can be studied by methods which use light scattering, inertia (impactor) or the optical microscope. The particle size range below about 10^{-5} cm radius is difficult to measure if it is intended to use methods applicable for routine measurements in the field. The methods, which might be considered for our objective were following:

a) Electron microscope
b) Diffusional separation of aerosols in connection with a condensation nuclei counter
c) Determination of the ion mobility spectrum and conversion of this ion spectrum into an aerosol spectrum
d) Electrical separation of ions in connection with a condensation nuclei counter.

With method a) it is difficult under clean air conditions to obtain electron microscope samples which are concentrated enough for statistical evaluation. In addition natural aerosols with radii smaller than 10^{-5} cm are at least partly volatile and spread out on the collection substrate so that size determinations by electron microscope are dubious. Method b) works best for particles smaller than about 10^{-6} cm radius and this well established method together with a reliable condensation nuclei counter for low concentration is one of the methods used in our program. Method c) is a well established method for the size range between 10^{-6} and 10^{-5} cm radius and for aerosol concentrations found in polluted or partly polluted atmosphere. The fact that this method is not applicable for particles smaller than about 10^{-6} cm radius is rather new and was not clear when we selected this method for our program.

The purpose of the present study was to refine the method c) for measurements of low concentration aerosols in a clean atmosphere. As the discussion will show it became clear during the course of this work that the usable size range does not cover the small end of the spectrum below 10^{-6} cm radius and that it is not possible with the present technical means to make the method sensitive enough for clean air conditions and for field operations. For this reason we have now switched to a combination of b) for $r < 10^{-6}$ cm and d) for 10^{-6} cm $< r < 10^{-5}$ cm after we were successful in developing a very reliable and accurate condensation nuclei counter for the concentration range of 30 to 1000 per cm^3. This work is, however, not covered in the present report.

The method c) which will be discussed in this report determines the number (total charge) and mobility of ions by deflecting them from a laminar air flow by an electrical field. Such a measurement gives the mobility spectrum of the charged aerosol particles. For conversion of this ion spectrum into an aerosol spectrum one has to know the charge distribution and fraction of charged particles. With

continuous bipolar ionization in the atmosphere due to cosmic radiation and natural radioactivity, a stationary charge distribution forms within a certain time if the aerosol itself does not change. The assumption of this ionization equilibrium can be expected to be valid at clean air conditions, remote from any local aerosol sources or aerosol sinks, i.e., for conditions which we intended to study. It was only during the course of this study that more reliable calculations about the charge distribution on aerosols under such conditions became known by several authors, and that it became clear that a reliable conversion of ion spectra into aerosol spectra is principally impossible for radii below about 10^{-6} cm.

The ion counter and its use for ion mobility analysis are known since many years (ZELENY 1900, GERDIEN 1905, ISRAEL 1931). We built our instrument on the basis of the best technical means available at present in order toachieve the required sensitivity for the analysis of large-ions in clean air. Since sensitivity was more important for our problem than extreme resolution of particle sizes, we chose the so-called integral type of aspiration condenser, accepting the ions in its whole cross section and its whole length, rather than the more complicated differential types using subdivided air flow and subdivided electrodes. A careful analysis for optimal conditions of sensitivity indicated that these latter types of ions counters, which are very useful for high particle concentrations will not meet the necessary requirements. This analysis also included the establishment of optimal dimensions of the integral aspiration condenser for the required operational conditions.

2. Apparatus.

The design and construction of the large-ion counter has been described in detail in our earlier reports JUNGE and ABEL (1965) and ABEL and JUNGE (1966). A number of improvements accomplished in the meantime will be described in the present report. In the following, we give a representation of the instrument in its final form.

Fig. 1 shows the block diagram. The cylindrical aspiration condenser is given here only in principle without details. It consists of three concentric tubes: the inner "receiving electrode" connected with the electrometer, the "driving electrode" which can attain voltages between zero and 3.500 volts, and the outer shielding tube. The laminar aerosol flow fills the space between the receiving electrode and the driving electrode. The surfaces of the electrodes facing the aerosol flow are highly polished and chromium plated. The receiving electrode is mounted between its grounded end pieces by electrically heated teflon insulators. The electrometer line extends axially from the receiving electrode into the Cary 31 CV electrometer preamplifier without further insulating supports. Thus, the insulation resistance of the electrometer system was always greater than 10^{14} ohms. The driving electrode is mounted between ring-shaped insulators consisting of specially selected polyethylene material to reduce polarization effects. These insulators are mechanically and electrically subdivided by "guard rings" to shield the receiving electrode from the insulating material and to give a uniform potential drop. For more details of the aspiration condenser, we refer to our earlier report ABEL and JUNGE (1966). Only its typical dimensions and operating data are repeated in Table 1.

The lower part of the block diagram shows the electronic and other instruments necessary to operate the ion counter. The essential features of the electrometer, high voltage source and air flow system have been discussed in ABEL and JUNGE (1966). The final circuit diagram of the "control unit" is given in Fig. 2. This unit contains power supplies and variable controls for the insulator heating, the blower, and the electrometer shorting relay as well as essential parts of the compensation device described in the subsequent section.

In the earlier report we suggested a circuit for the compensation of high voltage fluctuations. The principle of this circuit is given again in Fig. 3. It uses an additional vibrating condenser electro-

meter amplifier (FRIESEKE und HÖPFNER FH 408, slightly modified), the input of which is capacitively coupled to the high voltage source while the adjustable output with inverse polarity is capacitively coupled to the input of the main electrometer. Fig. 4 shows the guarded, air insulated input coupling condenser. The requirements for insulation and corona discharge for this coupling condenser are the same as those for the ion counter itself, since it must withstand the same voltages and is also connected to a sensitive electrometer input. All controls for the compensation circuit, such as the adjustable output with a monitoring meter, input shorting relay operation and zero adjustment, are contained in the "control unit" of Fig. 2.

This compensation device reduces the fluctuations on the main electrometer by a factor of 10 to 50, depending on the frequency of the fluctuations and on the accuracy of adjustment. The completeness of compensation is limited by the time constants of the circuit, i.e., by the lowest and highest frequencies being handled by it, and by the zero drift of the auxiliary DC amplifier. In spite of these limitations, the device was very useful during the measurements and was absolutely necessary for approaching the desired sensitivity of the ion counter.

Another problem arose from the zero drift of the ion counter, which was still too large. Extensive study of this drift lead to the conclusion that its major part is systematic and is caused by contact voltage of the receiving electrode insulators. Any insulating material, including the teflon used in our case, has a certain ionic conductivity, partly due to impurities. Since each piece of the insulating material is located between two metal supports the surfaces of which are never quite identical, it forms a "galvanic cell" producing a certain EMF, but with a very high internal resistance. In our ion counter, using the "guarding" technique of the Cary electrometer in its "31" operation mode for current measurements, the recei-

ving electrode is artificially kept on ground potential by feedback action, thus reducing the detrimental influence of insulation leak and of external capacity. Therefore, the "galvanic cells" formed by the insulators are continuously short-circuited. Their short-circuit current, determined only by their EMF and internal resistance, enters the electrometer and is indicated. It may vary, e.g., with temperature or with condition of the surfaces of the insulators and metal electrodes.

Though varying, a typical value of this current was about 3×10^{-15} amperes. Since this was even larger than the smallest ion currents to be measured, it was necessary to look for methods of elimination or at least reduction. As long as it is constant or but slowly varying, it can be compensated by a counter-voltage in series with the insulator so that the latter is allowed to assume its EMF or opencircuit voltage without generating current. For this purpose, the metal parts at the grounded ends of the two insulators were insulated from the grounded end-pieces of the receiving electrode. They were electrically connected with each other and an adjustable voltage source was connected between them and ground. This battery operated voltage source is coarse and fine adjustable by potentiometers between -0.75 and +0.75 volt against ground, which was sufficient in all cases. Since this source is of low internal resistance, the additional insulation mentioned above can be of low quality, e.g. adhesive film. Adjustment of the counter-voltage to achieve minimum drift at the electrometer usually takes many hours. This time is needed by the insulators to approach their equilibrium open-circuit voltage because of their high internal resistance and because of the considerable capacity of their metal parts. The adjustment must be controlled from time to time between the measurements.

A similar contact voltage compensation, although somewhat less critical, had to be used in the input of the auxiliary DC amplifier of the voltage fluctuation compensation circuit described earlier.

As an additional precaution against contact voltage - and its variations - all metal parts of the insulators of the ion counter in direct contact with the insulating material were gold plated making the metal surfaces as equal as possible.

All these measures kept the systematic drift current of the ion counter below 2.10^{-16} amperes without using the fluctuation compensation. With the fluctuation compensation, it may be raised again to 5.10^{-16} amperes. But, for the error of the ion current measurements, the variations of this drift current are responsible. On the basis of a large number of drift and ion measurements, it can be concluded that $\pm$ $2.5.10^{-16}$ amperes is the minimum of error of ion current measurements. This is the absolute limit of the instrument and can be reached only when the latter has been working for about one day without any serious disturbances such as violent mechanical motions, abrupt temperature changes, large line voltage changes or even line voltage failure. The possible error in the presence of such disturbances depends on the actual situation and can hardly be estimated in general.

The effect of this minimum error on the measurement of the ion or aerosol spectra will be considered later in chapter 3. Of course, also for large currents a systematic relative error must be assumed, which may amount to 2 or 3 per cent. But this error is constant and thus has no considerable effect on the spectra.

We think that this accuracy in measuring small DC currents in ion counters is the limit which can be reached with present techniques. It must be considered inherent in the method. But there are further limitations and requirements with respect to the stability of the aerosol to be sampled and the air flow through the ion counter which will be discussed in the subsequent section.

With the present method particle size distributions are determined

from current-voltage-curves of the ion counter, i.e., from series of successive readings. Such a series usually can be obtained in 20 or 30 minutes, as will be seen later. For satisfactory results, the aerosol content in the sampled air must be sufficiently constant during this time. Our observations with the ion counter and with condensation nuclei counters showed fluctuations of nuclei concentrations up to 50 per cent within a few minutes to be rather frequent in the atmosphere even in the absence of local sources or sinks. Similar observations were reported earlier by other authors (ISRAEL 1957).

In order to reduce such fluctuations the air passed a damping vessel of volume Q before entering the ion counter (Fig. 1). Effective mixing within this vessel was achieved by a suitable arrangement of the inlet and outlet tubes. We used a volume of $Q = 0.5\ m^3$ the size of which was determined on the basis of the following consideration. We assume the ion concentration entering the vessel, N_{in}, to vary around the average value N_{av} by

$$N_{in} = N_{av}\left[1 + a \sin\left(\frac{2\pi}{\tau} t\right)\right] \qquad (1)$$

with an amplitude a and a period τ. Provided that mixing is ideal and loss of particles is excluded the concentration in the air leaving the vessel, N_{out}, is given by

$$N_{out} = N_{av}\left[1 + b \sin\left(\frac{2\pi}{\tau} t + \varphi\right)\right] \qquad (2)$$

with a smaller amplitude b and phase shift φ. The "damping ratio" is given by

$$\frac{a}{b} = \sqrt{1 + \frac{4\pi^2 Q^2}{\tau^2 \phi^2}} \approx \frac{2\pi}{\tau}\frac{Q}{\phi} \qquad (3)$$

$$\text{if } \frac{2\pi}{\tau}\frac{Q}{\phi} \gg 1,$$

ϕ being the flow rate. In our case ϕ = 470 cm^3/s. If we take τ = 100 s, a value which has been really observed, we have a/b = 130 for Q = 1 m^3 or a/b = 65 for Q = 0.5 m^3. The mean residence time for the air in the vessel is 40 min. and 20 min. respectively. Q = 0.5 m^3 was considered a reasonable compromise between a sufficiently high damping and the inconvenience of a long residence time and possible loss of particles in the vessel.

In reality, of course, mixing is not ideal and some particle loss occurs in the mixing vessel. Tests showed that for particle concentrations below 10^4 cm^{-3} loss in a 1 m^3 vessel was about 10% per hour.

For the final measurements with the ion counter we used a container of 0.5 m^3 volume with a residence time of 20 minutes consisting of metal in order to avoid unnecessary ion loss due to electrostatic charges on the walls. In agreement with other authors we found that this loss can be considerable [1]. Using a condensation nuclei counter, tests with outside air passing the damping vessel at the nominal rate of the ion counter showed no systematic difference within the statistical variation between the concentrations before and after passage. Using the ion counter itself, the damping effect is demonstrated by Fig. 5 which shows the ion current at maximum voltage when sampling outside air directly or through the container. The damping effect is obvious, though somewhat less than our estimate.

To prevent eddies from the damping vessel to enter the ion counter, a "honeycomb" flow rectifier, consisting of crossed metal sheets, was mounted in the entrance of the ion counter, see fig. . Its channels have a cross section of 1 cm^2 and are 5 cm long. With the

1) We observed "half-life times" of aerosol concentration of laboratory air in storage balloons of ca. 1 m^3. In a plastic balloon, this time was 5 hours; in a balloon with metallized inner surface, this time was 12 hours.

nominal flow a diffusion loss of 3 per cent for particles of 5.10^{-7} cm radius was estimated. Since the essential size range covered by the instrument is from 10^{-6} to 10^{-5} cm radius, the diffusion loss will be negligible. Likewise, sedimentation loss is negligible for all particles of interest.

Finally, an electrical small-ion filter was mounted between the flow rectifier and the ion counter. This was necessary since the atmospheric small-ions have concentrations of the same order of magnitude as the large-ions when measuring in clean air. By way of the edge-effect of the ion counter, small-ions may affect the determination of mobility distributions of large-ions (see ISRAEL 1957) and should therefore be removed. Since the gap between the mobilities of the small-ions (1.4 resp. 1.9 cm^2/Vs) and of the smallest large-ions (some 10^{-2} cm^2/Vs) we are interested in is rather large, the arrangement of the small-ion filter is uncritical. For lack of space, we used three 0.1 cm mesh wire grids perpendicular to the air flow, mounted between insulating rings at distances of 0.8 cm. The outer grids are grounded, the inner one is connected to a 9 volts battery. For the nominal air flow ions of both signs with mobility greater than about 0.7 cm^2 /Vs are removed when the air velocity profile is uniform. In the rather wide cross section near the entrance of the ion counter, deviation from a uniform velocity profile will not be very large. The wire grids had an additional effect in smoothing the air flow. The effect of the small-ion filter on the results was rather small.

Repeated qualitative air flow tests with smoke were made in the ion counter, the high voltage electrode being replaced by a lucite tube and the shielding tube removed. No deviation from the straight laminar flow in the electrical field section of the aspiration condenser could be observed. The behaviour of trails of smoke indicated that a distinct velocity profile between the electrodes is established, although the profile could not be determined in detail by this method

3. Determination of Particle Size Distributions.

The main objective of our work was to develop a suitable method to determine the particle size distribution of aerosols in clean air, i.e., at very low concentrations. Ion counters measure only the mobility or size distribution of the aerosol fraction which is electrically charged. These ion spectra have to be converted to aerosol spectra, i.e., to spectra of all particles, charged and uncharged. This problem of converting ion spectra into aerosol spectra is not entirely solved. We made an attempt to carefully look into the present status of the art, which will be summarized in the subsequent section.

The first step in the evaluation is the conversion of electrical mobility of particles charged with one or more elementary charges into particle size. For the present purpose we can only consider spherical particles. Since atmospheric aerosol particles do not in general deviate too much from spherical shape this assumption is a good approximation. In any case we determine by this assumption the equivalent size of spherical particles. For particles in the range of interest, i.e., between 10^{-5} and 10^{-7} cm radius, the mobility can be calculated by the Stokes-Millikan-Cunningham law for the larger and from statistical mechanics for the smaller particles. We used the numerical values given by ISRAEL (1957), shown in Fig. 6. They are valid for singly charged particles; for particles with multiple charges the mobility is proportionally higher.

As a second requirement we have to know the distribution of charges among the aerosol particles. Since we are primarily interested in the background aerosol the measurements are made under conditions where local aerosol sources are absent and ionization equilibrium can be expected. The stationary charge distribution resulting from this ionization equilibrium, essentially symmetrical in both polarities, can be calculated on the basis of the diffusion-mobility theory by

BRICARD (1949, 1962) or FUCHS (1963). This theory was recently refined by BAUST (1966) and MOHNEN (1966). Fig. 7 shows calculations of Baust (BAUST and PETRAUSCH, 1968) using the parameters of positive small-ions of mass 209 AMU, corresponding to clusters of one air molecule (mean mass 29 AMU) plus ten water molecules. The values of the negative small-ions give a distribution slightly different, but this difference is unimportant in view of the accuracy of the measurements. The figure gives values for the ratios N_p/N (N_p = number concentration of particles carrying p charges of one sign, p = 0, 1, 2 ...., and N = total particle number concentration) as functions of radius r. The uncertainty of the values depends on assumptions about the mass of the small-ions, their mean free path length and mean velocity. For the present time we consider the values in Fig. 7 as the most reliable.

In order to correct for multiply charged particles, also the ratios N_p/N_1 (Fig. 8) are required. The particles N_p appear as a charge $p \cdot N_p$ at the "wrong" mobility $p \cdot k$ (or corresponding radius). They must be subtracted as $p \cdot N_p$ at $p \cdot k$ and added as N_p at the correct mobility k. In the size distributions to be expected in atmospheric aerosols, for high p values the fractions N_p become negligible compared with the total particle number. Therefore, it is usually sufficient to correct only for particles with $p = 2$ and 3.

The corrected number of ions observed for the mobility k or corresponding radius r is (one sign)

$$N_i(r) = \sum_{p=1}^{\infty} N_p(r) = N \sum_{p=1}^{\infty} \frac{N_p}{N}(r) \qquad (4)$$

The total particle number N(r) is thus obtained by multiplying $N_i(r)$ with the factor

$$P(r) = \left(\sum_{p=1}^{\infty} \frac{N_p}{N}(r) \right)^{-1} \qquad (5)$$

which is also given in Fig. 8.

For particle radii smaller than 10^{-6} cm the charge distribution given by the diffusion-mobility theory becomes uncertain. Here the particles are smaller than the mean free path length of the small-ions, so that the applicability of such a macroscopic theory becomes doubtful; a more complicated gas kinetic collision theory would have to be applied. In addition, for $r < 10^{-6}$ cm the P(r) values are very large, so that the calculated aerosol size distribution becomes increasingly unreliable. The particle radius of 10^{-6} cm must therefore be considered as a principle lower limit of the ion counter method to determine aerosol size distributions. In the results reported later we will give values of the size distributions between 10^{-6} cm and $5 \cdot 10^{-7}$ cm radius in parantheses only. This is a very serious limitation of the method which was not realized to its full extent at the beginning of this study.

On the other hand $r \approx 10^{-5}$ cm is practically the upper limit of this method at least for atmospheric aerosols. For larger radii the number concentration of aerosol particles decreases so rapidly - with simultaneous decrease of mobility - that the resulting current increments in the ion counter soon drop below the limit of resolution. The size range for which mobility measurements can be applied for size distribution studies is therefore restricted to the range

$$\approx 10^{-6} \text{ cm} < r < \approx 10^{-5} \text{ cm} .$$

It is very typical that in atmospheric aerosol studies almost all methods are restricted to rather small sections of the total size spectrum for the combined reasons of shape of the spectrum and technical limitations by the method. The ion counter is no exception.

Some further remarks are necessary on the correction for multiply charged particles according to the charge distribution. Due to mul-

tiple charges, some of the particles beyond the upper limit of 10^{-5} cm radius fall into the mobility range of the large-ion counter (depending on the size distribution, the fraction of multiply charged particles in atmospheric aerosols may amount to 10 or 20 per cent). Thus, complete correction is only possible if the extension of the size distribution curve beyond 10^{-5} cm radius is known by other methods. This is the case if the large-ion counter measurements are combined with measurements of the larger particles by impactor and optical particle counter methods, which was planned in our work and which was realized in some cases. The fraction of multiply charged particles can not be corrected for when the large-ion counter is used alone without combining it with the instrumentation for larger particles.

Knowledge of the size-mobility relation and of the aerosol charge distribution enables us to determine the aerosol size distributions in the range 10^{-6} cm $< r < 10^{-5}$ cm from ion mobility distributions. We will now discuss the method of measuring ion mobility distributions.

The theory of the integral type ion counter method is well known (see e.g. ISRAEL 1931, 1957, HOEGL 1963, CHALMERS 1967) so that only the most important facts may be repeated. We assume the air containing the ions passing our cylindrical aspiration condenser (length l, inner and outer radius r_i, r_a, radial coordinate ϱ, axial coordinate z) in axial laminar flow of rate Φ and of a certain velocity profile $v_z(\varrho)$. $v_z(\varrho)$ shall be independent of z, and there shall be complete symmetry around the axis. The voltage V between the inner and outer electrode results in a radial electrical field

$$E_\varrho = - \frac{V}{\varrho \ln (r_a / r_i)} \qquad (6)$$

for $r_i \leq \varrho \leq r_a$. Ions of mobility k have the velocity components (t = time)

$$\frac{dz}{dt} = v_z(\varrho) \tag{7}$$

$$\frac{d\varrho}{dt} = k E_\varrho = -\frac{kV}{\varrho \ln(r_a/r_i)} . \tag{8}$$

This gives their equation of motion

$$\frac{dz}{d\varrho} = \frac{-v_z(\varrho)\cdot\varrho\cdot\ln(r_a/r_i)}{kV} \tag{9}$$

Of special interest ist the case when ions entering the condenser at $z = 0$; $\varrho = r_a$ just arrive at $z = l$; $\varrho = r_i$. They must have a mobility $k = k_c$, k_c being called the critical mobility of the condenser determined by l, r_a, r_i, Φ, V.

Integration of (9) yields

$$l = \int_0^l dz = -\frac{\ln(r_a/r_i)}{k_c V} \int_{r_a}^{r_i} \varrho\, v_z(\varrho)\, d\varrho . \tag{10}$$

The total air flow is

$$\Phi = \int_{r_i}^{r_a} v_z(\varrho)\cdot 2\pi\varrho\, d\varrho . \tag{11}$$

From (10) and (11) follows

$$k_c = \frac{\phi \ln(r_a/r_i)}{2\pi l V} = M \cdot \frac{1}{V} \qquad (12)$$

with $$M = \frac{\phi \ln(r_a/r_i)}{2\pi l} \qquad (12a)$$

independent of the shape of the flow profile $v_z(\varrho)$ as long as the latter is independent of z

Let us briefly discuss the current-voltage curve I(V) of the aspiration condenser for the simple case that only ions of a single mobility k_1 enter it with a number concentration N_1. For $k_c \leqq k_1$ or $V \geqq M/k_1$, all ions are captured by the (inner) receiving electrode (Fig 9a) so that we measure a saturation current

$$I = \phi e N_1 \qquad (13)$$

(e is the electrical charge of the ions) independent of V, from which N_1 can be calculated (Fig 9b, curve 1). For $k_c > k_1$ or $V < M/k_1$ only a fraction N'_1 of the ions N_1 entering the condenser between a radius r_e and the inner radius r_i are captured

The ratio N'_1/N_1 must be the same as ϕ'/ϕ, where

$$\phi' = \int_{r_i}^{r_e} v_z(\varrho) \cdot 2\pi\varrho \, d\varrho \qquad (14)$$

is that fraction of the total air flow ϕ which flows between r_i and r_e, so that it must be

$$\frac{N_1'}{N_1} = \frac{\phi'}{\phi} = \frac{\int_{r_i}^{r_e} v_z(\varrho) \cdot 2\pi\varrho \, d\varrho}{\int_{r_i}^{r_a} v_z(\varrho) \cdot 2\pi\varrho \, d\varrho} \quad . \tag{15}$$

Integrating (9) for ions of mobility k_1 just entering at $z = 0$; $\varrho = r_e$ and arriving at $z = l$; $\varrho = r_i$ yields

$$l = \int_0^l dz = -\frac{\ln(r_a/r_i)}{k_1 V} \int_{r_e}^{r_i} \varrho \, v_z(\varrho) \, d\varrho \quad . \tag{16}$$

Dividing (16) by (10) and using (15), we have

$$\frac{N_1'}{N_1} = \frac{k_1}{k_c} \quad . \tag{17}$$

This relation is again independent of the flow profile $v_z(\varrho)$. Thus, the current measured in the ion counter for $k_c > k_1$ or $V < M/k_1$ is

$$I = \phi e N_1 \cdot \frac{k_1}{k_c} = \frac{\phi e N_1 k_1}{M} \cdot V \tag{18}$$

i.e it is proportional to V (Fig. 9b, curve 1) From $V = M/k_1$ found at the edge of the measured I(V) curve, k_1 can be calculated Thus, we have determined k_1 and N_1 by measurement

Another species of ions with k_2 and N_2 would result in a similar I.V) curve, e.g curve 2 in Fig 9b If both kinds of ions are mixed

in the air flow, their currents simply add, resulting in curve 3 of Fig. 9b, from which k_1, N_1, k_2, N_2 can easily be read as shown in the figure. This procedure can be extended to an arbitrary number of ion species as long as resolution is sufficient

Atmospheric large-ions usually have a continuous spectrum of mobilities k rather than discrete values. The I(V) curve of the ion counter fed with such a mixture of ions is obtained by dividing the ions into infinitesimal mobility steps dk, each of which can be treated in the manner just described, and by integrating over the contributions of all steps to the current I (e.g. ISRAEL 1931). The number of ions dN_i between the mobilities k and k + dk can be expressed by the distribution function f(k)

$$dN_i = f(k)\, dk \qquad (19)$$

if all ions have one elementary charge e (for multiple charges a separate correction method was given earlier) For a given V or k_c of the ion counter, the ion current I is composed of two parts: the ions with $k \geq k_c$ which are all captured, and the ions with $k < k_c$, of which the fraction k/k_c is captured according to (17). This gives

$$I = \phi e \int_0^{k_c} \frac{k}{k_c} f(k)\, dk + \phi e \int_{k_c}^{\infty} f(k)\, dk , \qquad (20)$$

which results together with (12), in I as a function of V for the mobility distribution f(k) It can be shown (ISRAEL 1931) that, for a continuous distribution f(k), the slope of this curve I(V) decreases monotonically with increasing V, (Fig 9c), and that the ion content in a mobility interval $k_c \ldots k_c + dk$ is proportional to the second derivative of I(V). Since in real measurements only a limited number of points of the I(V) curve can be determined, the analysis

will also be done in finite steps of k (or corresponding particle radius r) rather than in infinitesimal steps dk. This is accomplished in the following way. We consider the slope dI/dV:
from (20) we have [1]

$$\frac{dI}{dk_c} = - \frac{\phi e}{k_c^2} \int_0^{k_c} k\, f(k)\, dk \; ; \qquad (21)$$

from (12) we have

$$\frac{dk_c}{dV} = - \frac{M}{V^2} = - \frac{k_c^2}{M} \; ; \qquad (22)$$

consequently,

$$\frac{dI}{dV} = \frac{dI}{dk_c} \cdot \frac{dk_c}{dV} = \frac{\phi e}{M} \int_0^{k_c} k\, f(k)\, dk \qquad (23)$$

---

1) since $\frac{d}{dx} \int_0^x \xi f(\xi)\, d\xi = x f(x)$

and $\frac{d}{dx} \int_x^\infty f(\xi)\, d\xi = - f(x)$,

we have $\frac{dI}{dk_c} = \phi e \left[- \frac{1}{k_c^2} \int_0^{k_c} k f(k) dk + \underbrace{\frac{1}{k_c} k_c f(k_c) - f(k_c)}_{=0} \right]$

or

$$\int_0^{k_c} k\, f(k)\, dk = \frac{M}{\phi e} \cdot \frac{dI}{dV} \quad . \tag{23a}$$

Substituting this into the first term of (20), we obtain

$$\int_{k_c}^{\infty} f(k)\, dk = \frac{I}{\phi e} - \frac{1}{k_c} \cdot \frac{M}{\phi e} \cdot \frac{dI}{dV} = \frac{1}{\phi e}\left(I - V\frac{dI}{dV}\right) \tag{24}$$

The magnitude (I-VdI/dV) can easily be read from the I(V) curve for any of its points, as shown in Fig. 9c for two points $I_1(V_1)$ and $I_2(V_2)$; it is the section $\overline{OP}$ on the I-axis (in units of I) between the origin and the intersection point of the I-axis with the tangent to the I(V) curve at the point of question, i e. $\overline{OP}_1$ or $\overline{OP}_2$ in the two examples shown. For an ion mobility interval $k_1 \ldots k_2$, the difference

$$\frac{\overline{P_1 P_2}}{\phi e} = \frac{\overline{OP_1} - \overline{OP_2}}{\phi e} = \int_{k_1}^{\infty} f(k)\, dk - \int_{k_2}^{\infty} f(k)\, dk = \int_{k_1}^{k_2} f(k)\, dk = \Delta N_i (k_1, k_2) \tag{25}$$

gives us the number concentration of ions in this mobility interval. This procedure can be repeated for a series of intervals in the range of interest

For the upper and lower end of each mobility interval the corresponding ion radii r_m, r_n can be read from Fig 6, and the magnitude

$$\frac{\Delta N_i (r_m, r_n)}{\log (r_n / r_m)}$$

versus r is drawn on log-log paper in histogram from. After correction for multiple charges, this ion size distribution is multiplied with the P(r) factor of Fig 8 (mean value for each interval) to give the particle size distribution.

After the first experiments with the large-ion-counter, it was recognized that some difficulty existed with respect to the number of mea-

suring points for each I(V) curve. In order to draw the tangents properly, which are needed for the exact evaluation method described above, the number of measuring points should be considerably larger than the number of channels chosen for the histogram size distribution. The average time required for one sensitive current measurement by the rate-or-charge method was found to be 100 seconds, and a similar time was needed for changing the driving voltage, i.e., a total of 200 seconds for each point. Even if we disregard any fine structures of the ion distribution by choosing channels which differ in radius by a factor of two (so that $\log (r_{n+1}/r_n) = \log 2 = 0{,}301$ is constant for all intervals), the time needed for one size distribution would have been too long with respect to the observed fluctuations of the aerosols. As a compromise, we tried to use only one point per channel, connected the points by straight lines and made the evaluation in the way of Fig. 9b as if there were ion groups with discrete mobilities, attributing the ion numbers to the whole channel in each case. The histogram channels in the log-log diagram are arranged symmetrical to the ion radii r_n corresponding to the measuring points, so that in each channel half of the ions appear below and half of them above r_n. This procedure seems to be the most reasonable approach in the present case. The sacrifice in resolution is considerable but the method is still capable of giving the main features of the distribution.

The errors of the resulting size distributions caused by this simplification were tested with model distributions. Fig. 10 shows an example for a circular I(V) curve. Although depending on the shape of the individual size distribution, these errors usually are considerably smaller than those caused by errors of the ion current measurements, which are discussed later. For six channels centered at radii $r = 2.5.10^{-7}$; 5.10^{-7}; 1.10^{-6}; 2.10^{-6}; 4.10^{-6}; and 8.10^{-6} cm [1]

1) Although the $\beta(r)$ factor of the charge distribution is uncertain below $r = 10^{-6}$ cm, the ion measurements were somewhat extended to smaller radii.

(see also Table 2), six current measurements are thus required; in addition, we need at least one more point near that for 8.10^{-6} cm to get an idea of the further extension of the I(V) curve, and at least one zero determination, i.e. a total of eight measurements. With 200 seconds for one measurement plus switch-over, we thus need a little less than half an hour. As shown in chapter 2, the damping vessel to reduce aerosol fluctuations was adapted to this time.

The voltages corresponding to the channel centers listed above are under normal conditions (sea level operation) V = 4.5; 17; 66; 250; 800 and 2800 volts (see Table 2).

In chapter 2, we came to the conclusion that a statistical absolute error of the ion current measurements of $\pm 2.5.10^{-16}$ amperes can be assumed under optimal conditions. The effect of this error was also tested with model size distributions in the following way: From a given size distribution we derived by calculation the corresponding I(V) curve, averaged over the same channels as in the later measurements, then the errors were applied to the current values and the re-evaluation was made for the limits of error. Two examples are shown in Fig. 11a and 11b for two model distributions with the total particle numbers of 1000 and 500 cm^{-3} [1]. Fig. 12 shows an example of a size distribution with considerable structure. It is easy to see that the error increases as we go to smaller radii and to lower concentrations. Fig. 11 corresponds to a section of a normal size distribution with a maximum between 10^{-6} and 10^{-5} cm radius, as observed in many cases in polluted or semipolluted air. Considering the errors shown in the figures we may conclude that the determination

1) The model size distribution is assumed to drop to zero outside the range shown in Figs. 11a, b and 12.

of size distributions with our large-ion counter is reasonable down to a total particle concentration of about 500 cm^{-3}, but not below this value. The original aim to get below the particle concentration of 300 cm^{-3}, which is assumed to be the average in the background aerosol, could not be fully reached. Of course, in certain cases when the aerosol is rather stable, one can take a series of successive size distributions and thus increase the reliability of the results.

For demonstration, we give an example of a measurement and evaluation before showing results from different locations in the next chapter. Fig. 13 is a copy of the recorder strip chart, showing the electrometer charging curves (100 seconds each) for the series of driving voltages corresponding to the size distribution channels, as given in Table 2, beginning with the highest voltage. The curves are positioned on the chart by proper use of the electrometer grounding switch and zero adjustment and of the chart drive; they are concentrated on the chart in order to have a compact record. Using the effective capacity of C = 10.2 picofarads (see Table 1), the signal voltages after 100 seconds (averaged if the charging curves are irregular), $V_s(100)$, give the ion currents

$$I = C\frac{V}{t} = 10.2 \cdot 10^{-12}\ \frac{\text{amp} \cdot \text{s}}{\text{volt}} \cdot \frac{V_s(100)}{100\ \text{s}} \qquad (26)$$

The I(V) curve is drawn (Fig. 14) in linear scale, usually in three branches with different voltage scales to spread its lower part. The additional point at 1800 volts shows that in this case saturation is practically reached at the upper end of the curve. In other cases, some more points may be necessary around the upper end. At the end of the series, the value for the highest voltage (2800 volts) is reproduced to see whether the total ion concentration has changed. If the changes are not too serious, the ion currents of the series can be corrected by linear interpolation with time. For the example shown,

the change was neglected. Now the ordinate sections are read in amperes according to Fig. 9b and the ion numbers ΔN of the channels calculated according to (25). For the log-log representation of $\Delta N / \Delta (\log r)$ versus r these ion numbers must be multiplied by $1/\log 2 = 3.32$, since the successive channels differ by factors of 2. With these values the histogram ion size distribution is drawn on log-log paper (Fig. 15), and after application of the P(r) factors of Table 2 we obtain the particle size distribution. Corrections for multiple charges are not made in this example since no simultaneous measurements of particles above 10^{-5} cm radius were made; on the other hand, it may be negligible here since a considerable decrease at large particles is indicated. It must be kept in mind that the reliability of this size distribution, besides the errors of measurement and evaluation, depends on the presence of electrical charge equilibrium as well as on the assumptions used in the charge distribution theory, as it has been discussed earlier.

4. Some Results Obtained at Different Locations.

To test the applicability of our large-ion counter for the determination of aerosol size distributions in more or less clean air, three field trips were made with the instrument:

1.) August 17 to 25, 1967 on the "Schauinsland" peak, 1200 meters above sea level, in the Black Forest, Germany.
2.) October 16 to November 2, 1967 on board the research vessel "Meteor", Bay of Biscay.
3.) March 1 to March 29, 1968 at the Observatory Izaña, 2360 meters above sea level, on Tenerife/Canary Islands, together with other participants and equipment for aerosol and air chemistry measurements.

Trip 2 and 3 also served to obtain preparatory experiences for aerosol measurements during the Atlantic expedition 1969 of "Meteor". Results from these locations are shown in Figs. 16 to 28 and will be discussed below. Before doing this, some general remarks on the representations may be made.

The ion spectra (solid lines) anc aerosol spectra (broken lines) shown are obtained in the manner cescribed in the preceding chapter. The limits of error of the ion spectra given in the figures were determined individually using the electrometer recordings. Due to the influence of various factors, the errors can be larger than those for optimum operational conditions as estimated in chapter 3. For steep decreases or "holes" of the spectra, sometimes only an upper limit can be given. The determination of the aerosol spectra from the ion spectra depends on the agreement of the actual electrical charge distribution and the theoretical equilibrium charge distribution used for the evaluation. Since possible deviations between both are very difficult to estimate, no errors are given for the aerosol size distributions. The channel around the smallest radius of 5.10^{-7} cm is

uncertain (see chapter 3) and, therefore, shown in brackets.

The reliability of the results is quite different for the different locations, not only because of the different concentration levels, but also because of the presence of various disturbing factors. For instance, aerosol fluctuations were not too serious at the Schauinsland and on sea, but they were considerable at Izaña. Line power constancy, which is very essential for the instrument as pointed out in chapter 2, was excellent at Schauinsland and on the ship, but very poor at Izaña, where the power even could fail several times a day. While mechanical disturbances were excluded at the mountain stations, they were serious on board the ship. By small capacity variations of the aspiration condenser, caused by the considerable accelerations during roll and pitch, unsteady charging currents were generated so that useful measurements usually were restricted to periods with wind velocities below about 8 m/s. Finally, the gold plating at the insulators, reducing the zero drift (see chapter 2), was not finished prior to the last trip to Izaña.

Besides the measurements with the large-ion counter, some additional information was obtained by parallel determination of the concentration of the condensation nuclei. At all three locations, a Scholz nuclei counter was used. At Izaña, also an automatic nuclei counter (KANTER 1969; see also JUNGE, CHAGNON, MANSON 1960) was used. The corresponding nuclei concentrations are given in the individual figures, together with the total particle concentration obtained for that part of the size distribution covered by the ion counter (broken line). For size distributions with the main maximum within the size range of the ion counter, the two particle concentrations should roughly agree. Due to the different methods used and the difficulties of measuring ion spectra at low concentrations the agreement is only within a factor of 2 or 3 in most cases [1].

1) On the average, the Scholz nuclei counter gives lower numbers. Comparison with the automatic nuclei counter (KANTER 1969) seems to support the low Scholz figures, which are most likely due to some loss during counting.

If a considerable fraction of the particle size distribution or even the maximum lies outside the range of the ion counter, the condensation nuclei counter should, of course, give higher values. All our efforts to improve the agreement further by making the ion counter more sensitive and accurate were, however, not successful.

In the following some individual results from the three field trips are discussed.

For the first trip we chose the "Schauinsland" peak in the Black Forest, which can be reached rather simply. Here the instrument was operated at the measuring station of the "Deutsche Forschungsgemeinschaft". The station is 1200 meters above sea level, about 80 meters below the summit [1]. Because of frequent rains and occasional thunderstorms, the station was often in clouds. Therefore, against the original plan the head unit of the ion counter had to be installed inside the building, with the suction tube projecting 0.5 m through the wall in southern direction. Since winds prevailed from SW, undisturbed air could be expected in most cases.

The majority of the results were similar in character as shown by the examples in Figs. 16 to 20. The maximum of the size distributions is usually found near 4.10^{-6} cm radius, total concentrations - of the sections shown - ranging between 1500 and 6000 particles per cm^3. In most of these examples a secondary peak is indicated around 5.10^{-7} cm radius, but the results in this range are too uncertain to draw any conclusions. During most measurements on Schauinsland, the relative humidity in the outside air was between 65 and 100%. In the example of Fig. 19, taken directly after an intense rainfall, it was about 100% so that growth of particles may explain the somewhat different

1) Correction of the ion mobilities for the reduced air pressure was estimated to be unimportant in this case with respect to the errors of measurement, so that it was neglected.

shape of the spectrum. On several occasions, positive and negative large-ions were measured alternately. Of course, it can not be expected that successive spectra, separated in time by about one hour, are identical. But the material was not sufficient to recognize any systematic difference between positive and negative large-ions.

The second trip was on board the "Meteor", in October 1967, to the Bay of Biscay (cruise No. 11 of the "Meteor", especially intended for instrumental tests, starting from the North Sea and passing the English Channel). On this occasion, the function of the large-ion counter on a ship and in maritime air was to be tested. The instrument was mounted in a special room on the radar deck, the air being taken from a permanently installed air sampling system, about 17 meters above the sea surface. During heavy sea no measurements were possible due to capacity variations of the electrodes of the ion counter caused by the ship movements; this was the case all the time when passing the North Sea. At wind velocities below 8 m/s measurements were possible when the electrometer charging time for every ion current determination was increased from 100 seconds (see chapter 3) to 300 seconds. This could be done without difficulty since aerosol fluctuations were not very large.

Fig. 21 shows the first result which could be obtained, though in semipolluted air in the English Channel near Dover. Over the open sea in the Bay of Biscay, rather reliable results (Figs 22 to 24) were obtained when slowly cruising around 47^{o} N/7^{o} W, about 300 km off the nearest European coasts. Unfortunately, during this period of relatively calm sea, easterly winds prevailed so that conditions of pure maritime air were not encountered. The size distributions in Figs. 22 to 24 show a somewhat asymmetrical maximum around 2 to 4.10^{-6} cm radius with a slowly increasing slope to smaller radii, and an apparently steep slope to larger sizes. Total particle concentrations were between 2000 and 4000 per cm^{3}. The relative humidity during these measurements was between 80 and 85%.

In a third field trip we finally attempted to perform measurements in air masses which really were typical for undisturbed tropospheric "background" conditions. The Observatory Izaña on the Island of Tenerife appeared to be a suitable place which was fairly easily accessible. By courtesy of the Spanish National Meteorological Service (Air Ministery), a group of our institute could be stationed at the observatory during March 1968 to perform aerosol and air chemistry studies. The Observatory Izaña is situated at 2360 m height above sea level at 28.3^{0} N/16.5^{0} W, about 20 km NE of the central peak (3800 m height) of the island. The distance to the African coast is about 300 km. At times, the station is located above the trade wind inversion (which may form between 1500 m and 2500 m), in which case very clean air can be expected. During this time of the year NW winds and clean maritime air masses prevail.

The reduced air pressure of about 750 mb at Izaña required considerable corrections concerning the ion mobilities and the air flow measurements. The driving voltages, the air flow and the flow meter (rotameter) calibration were changed in such a way that the same channel subdivisions resulted for the ion and aerosol spectra. Frequent difficulties with line power reduced the number and accuracy of the measurements. At times the total particle concentration was below 500 cm^{-3} which is the lower limit for application of the large-ion counter as already pointed out in chapter 3. The lowest concentrations determined by the two condensation nuclei counters were 130 cm^{-3}.

The size distribution shown in Fig. 25 was obtained in a situation of a weak inversion between 2100 and 2600 meters with the station being mostly in clouds. The height of the inversion layer, the northerly winds and the relatively high particle concentrations suggest some contamination from the island before the air has reached the observatory. Comparison of this size distribution with cases of lower concentrations (e.g. Fig. 26 and 27) suggests that in this case the

contamination might be restricted to particles larger than about 4.10^{-6} cm radius.

Fig. 26 shows a case, where the observatory was above a strong inversion layer. The particle concentration is fairly characteristic of clean tropospheric air and already close to the limit of the ion counter. But the aerosol and the weather were rather stable so that four measurements could be made within four hours, resulting in a fairly reliable distribution. Fig. 27 shows a similar situation, although the total concentration was higher. Here the distribution was obtained by a single measurement, resulting in somewhat larger errors.

Finally, in Fig. 28 an aerosol size distribution is shown obtained at Izaña by combination of different methods of measurement so that the size range from 10^{-6} cm up to 10^{-2} cm radius is covered. The results above 10^{-5} cm radius were obtained by impactors and an optical particle counter (JAENICKE 1968). The part below 10^{-5} cm radius (line -.-.-.-) represents the data of the large-ion counter, an average over three single spectra measured within three hours. The weather situation was stable with the inversion layer below the station. The total particle concentration of about 800 cm^{-3} of our spectrum is lower in this case than the condensation nuclei concentration of about 2000 cm^{-3}. This, as well as the shape of the left end of the spectrum, suggests the presence of a considerable number of smaller particles between 10^{-7} cm and 10^{-6} cm radius.

These size distributions from Izaña are the first ones available for particles smaller than 10^{-5} cm radius under clean air conditions. Although the accuracy of the data and their number leave much to be desired they are of basic interest with respect to the origin of the condensation nuclei in clean, unpolluted tropospheric air masses. If the tropospheric background aerosol represents aged aerosols from continents and from polluted areas one would expect the maximum of the distribution to be close to 10^{-5} cm radius, with particles

around 10^{-6} cm and below almost missing (JUNGE and ABEL, 1965). The few data at hand indicate already that this is apparently not true. This points to the other alternative that even in clean air there is always a production of rather small particles and that the total concentrations found in clean air represent equilibrium values between production and destruction, e.g. coagulation. However, more and better data are, no doubt, required to confirm this.

It was not intended, and the material gathered until now is by no means comprehensive enough, to investigate systematic relationships between the aerosol spectra and meteorological conditions, e.g. air masses, on a larger scale. The results obtained can only be considered as random samples to demonstrate the capability and limitation of the ion counter method particularly under clean air conditions.

5. Conclusions.

The result of our development was a large-ion counter which can determine atmospheric aerosol size distributions over the particle size range of 10^{-6} cm to 10^{-5} cm radius, at particle number concentrations down to about 500 cm^{-3}. In this lower concentration range, the operation of the instrument is rather laborious and the accuracy of the results still unsatisfactory, depending to a large extent on the presence or absence of different environmental perturbations, the influence of which has been investigated. We think that the sensitivity we have reached can not be improved very much with the presently available technique. In order to obtain reliable information on the size distribution of tropospheric background aerosols the sensitivity has to be improved by at least a factor of 5 and the range has to be extended down to 10^{-7} cm radius. Ion mobility measurements are not capable to meet these requirements for basic and technological reasons. We have now started efforts to reach this goal by using precision nuclei counters in connection with electrical denuders and diffusion chambers.

6. References

ABEL, N. and JUNGE, C., 1966: Development of a Large-Ion Counter of High Sensitivity Final Technical Report, Contract DA 91-591-EUC-3910, Mainz (1966)

BAUST, E., 1966: Untersuchung des radioaktiven Aerosols der bodennahen Atmosphäre mittels des Goetzspektrometers. Dissertation (1966) Universität Heidelberg.

BAUST, E., PETRAUSCH, D., 1968: Private communication.

BRICARD, J., 1949: L'Équilibre Ionique de la Basse Atmosphère. J.Geophys.Res. 54 (1949), 39-52.

BRICARD, J., 1962: La Fixation des Petits Ions Atmosphériques sur les Aérosols Ultrafins. Geofisica Pura e Appl. 51 (1962), 237.

CHALMERS, J.A., 1967: Atmospheric Electricity 2nd.Ed Pergamon Press 1967.

FUCHS, N A., 1963: On the Stationary Charge Distribution on Aerosol Particles in a Bipolar Ionic Atmosphere. Geofisica Pura e Appl. 56 (1963), 185 - 193.

GERDIEN, H., 1905: Demonstration eines Apparates zur absoluten Messung der elektrischen Leitfähigkeit der Luft. Physikalische Zeitschrift 6 (1905), 800.

HOEGL, A., 1963: Messung von Konzentration und Beweglichkeit atmosphärischer Ionen Zeitschrift für Angewandte Physik, 16 (1963), 252 - 258.

ISRAEL, H., 1931: Zur Theorie und Methodik der Grössenbestimmung von Luftionen. Gerlands Beitr.z. Geophysik, 31 (1931), 173 - 216

ISRAEL, H., 1957: Atmosphärische Elektrizität. Akad.Verlagsgesellschaft Geest u. Portig K.G., Leipzig, 1957.

JAENICKE, R., 1968: Private communication. (Meteorolog.-Geophysikal Inst.Univ Mainz)

JUNGE, C.E., CHAGNON, C.W and MANSON, J.E., 1960: Stratospheric Aerosols. GRD, Air Force Res.Div. (ARDC) Laurence G. Hanscom Field, Bedford/Mass. Contr. AT (49-7)-1431, May 1960.

JUNGE, C.E., and ABEL, N., 1965: Modification of Aerosol Size Distribution in the Atmosphere and Development of an Ion Counter of High Sensitivity. Final Technical Report, Contract DA 91-591-EUC-3484, Mainz (1965).

KANTER, H.J., 1969: Bau und Eichung eines automatischen Kondensationskernzählers mit fotografischer Registrierung. Diplomarbeit, Univ. Mainz (Nat.Fak. 1969).

MOHNEN, V., 1966: Untersuchungen über die Anlagerung von neutralen und elektrisch geladenen Emanations-Folgeprodukten an Aerosole. Dissertation (1966) Universität München.

ZELENY, P., 1900: The Velocity of Ions Produced in Gases by Röntgen Rays. Trans.Royal Soc. A 195 (1900), 193 - 234.

7. Acknowledgments

We would like to express our sincere appreciation to the European Office of Aerospace Research (OAR), United States Air Force, and to the Air Force Cambridge Research Laboratory for making this study possible.

We want to express our thanks to the "Aerosolmeßstelle Schauinsland" ("Deutsche Forschungsgemeinschaft") and its leader, Dr.G. Rönitke, for the permission to make measurements at Schauinsland; to the "Deutsche Forschungsgemeinschaft" and "Deutsches Hydrographisches Institut", for the permission to take advantage of the facilities of the research vessel "Meteor"; and to the Spanish "National Meteorological Service (Air Ministery)" and the director of the "Meteorological Observatory Izaña", Tenerife, Sr.P Rodriguez García-Prieto and his co-workers, for the permission and excellent support for the measurements at Tenerife.

We also gratefully acknowledge instrumental support by the "Schutzkommission Reinhaltung der Luft (Bundesamt für zivilen Bevölkerungsschutz, FRG)".

8. Tables.

Table 1. SIGNIFICANT DIMENSIONS AND DATA OF OPERATION OF THE LARGE-ION COUNTER

length of cylindrical condenser (electrical field section)	l = 100 cm
inner radius	r_i = 2.65 cm
outer radius	r_a = 4.50 cm
	$\ln(r_a/r_i)$ = 0.529
air flow	ϕ = 470 cm^3/s
maximum voltage	V = 2800 volts
for minimum critical mobility k_{min}	= $1.4.10^{-4}$ cm^2/Vs
corresponding to particle radius	r = $0.8.10^{-5}$ cm
maximum electrical fiel strenght E_{max}	= 2000 volts/cm
effective capacity of electrometer system	C = 10.2 picoferads
usual period for current measurements by rate-of-charge method	t = 100 s
ratio of electrometer current, I, to concentration of singly charged ions, N_1	$\frac{I}{N_1}$ = $0.745.10^{-16}$ $\frac{amp}{1/cm^3}$

insulator heating: 5 watts (1 amp) each.

Table 2. PARTICLE RADII CHANNEL CENTERS r, DRIVING VOLTAGES V(r), AND P(r) FACTORS.

r cm	V(r) volts	P(r) -
$2.5.10^{-7}$	4.5	-
$5.\ 10^{-7}$	17	(16.5)
$1.\ 10^{-6}$	66	9.0
$2.\ 10^{-6}$	250	5.5
$4.\ 10^{-6}$	880	4.0
$8.\ 10^{-6}$	2?0	3.0

9. List of Figures.

Fig. 1. Block diagram of the large-ion-counter. 1 damping vessel, 2 flexible metal tube (90 mm dia.), 3 air inlet, 4 aspiration condenser and preamplifier unit, 5 flow rectifier, 6 small-ion filter, 7 receiving electrode, 8 driving electrode, 9 shielding-tube, 10 heated insulators for receiving electrode, 11 high voltage insulators for driving electrode, 12 electrometer line, 13 compensation electrode, 14 shorting relay, 15 Cary 31 CV electrometer preamplifier, 16 Cary 31 CV electrometer main amplifier, 17 recorder matching and polarity reversal box, 18 potentiometer recorder (any, 0...100 mV or less), 19 blower (Siemens VSA 5), 20 flow meter (Rota RHN G 1), 21 control unit (see Fig. 2), 22 DC amplifier for compensation (Frieseke u. Höpfner FH 408), 23 coupling condenser on input of 22, 24 insulator bias battery, 25 high voltage supply (Knott NSHV-3.5), 26 insulator bias voltage source, 27 line voltage regulator (magnatic type, 500 wa[illegible]

Fig. 2. Circuit diagram of the control unit. Connections (compare Fig. 1): 1 from high voltage supply, 2 to driving electrode, 3 to coupling condenser on FH 408, 4 from output of FH 408, 5 to compensation electrode, 6 to zero adjustment circuit in FH 408, 7 to heaters and shorting relay of head unit, 8 to shorting relay of FH 408, 9 to blower, 10 220 V AC power input.

Fig. 3. Principle of compensation of high voltage fluctuations in the ion counter.

Fig. 4. High voltage coupling condenser. 1 highly insulated electrode, 2 high voltage electrode, 3 shield, 4 input of auxiliary DC amplifier FH 408.

Fig. 5. Effect of the damping vessel. The two curves are taken at different times (since the apparatus had to be changed) so that mean value and individual fluctuations can not be compared directly.

Fig. 6. Electrical mobility k of singly charged particles versus particle radius r.

Fig. 7. Aerosol stationary electrical charge distribution calculated by BAUST (1966). N = total particle number concentration; N_0 = uncharged particles, N_p (p = 1,2, ...) = charged particles of one sign. Calculated for positive small-ions of mass 209 AMU (= 29 + 10 H_2O), temperature 298° K.

Fig. 8. Ratios N_0/N_1 and factor P(r) obtained from the aerosol stationary electrical charge distribution calculated by BAUST (1966).

Fig. 9. Ion paths and current-voltage characteristics of integral ion counter for different cases.

Fig. 10. Example of a model size distribution with error caused by using only one measuring point per channel of radii. The corresponding I(V) curve is part of a circle. _____ is obtained with the exact method, ... with the simple method (see text).

Fig. 11. Error of a model size distribution, caused by $\pm$ $2.5.10^{-16}$ amperes absolute error of the ion currents, for total particle numbers of (a) 1000 cm^{-3}, (b) 500 cm^{-3}.

Fig. 12. Example of error of a structured model size distribution, caused by $\pm$ $2.5.10^{-16}$ amperes absolute error of the ion currents.

Fig. 13. Example of measurement (Schauinsland 21.8.1967/15 h): record of ion currents.

Fig. 14. Current-voltage curve from Fig. 13.

Fig. 15. Size distribution from Fig. 14.

Fig. 16 to 20: Size distributions measured at "Schauinsland", Aug. 1967. _____ ions (one sign), ------- particles.

Fig. 21 to 24: Size distributions measured in the Bay of Biscay on research vessel "Meteor", Oct. 1967. _____ ions (one sign), ------- particles.

Fig. 25 to 27: Size distributions measured at Izaña/Tenerife, Mar. 1968. _____ ions (one sign), ------- particles.

Fig. 28: Combined size distribution measured at Izaña/Tenerife, 23 Mar. 1968 by simultaneous use of different instruments. Part .-.-.-.- was obtained with the large-ion counter. The other parts were obtained by R. JAENICKE (1968) with following instruments: _____ (inclined): two-stage jet impactor; .....: optical particle counter "Royco"; -------: jet impactor; _____ (stepped): free-air impactor.

10. Figures to Part I.

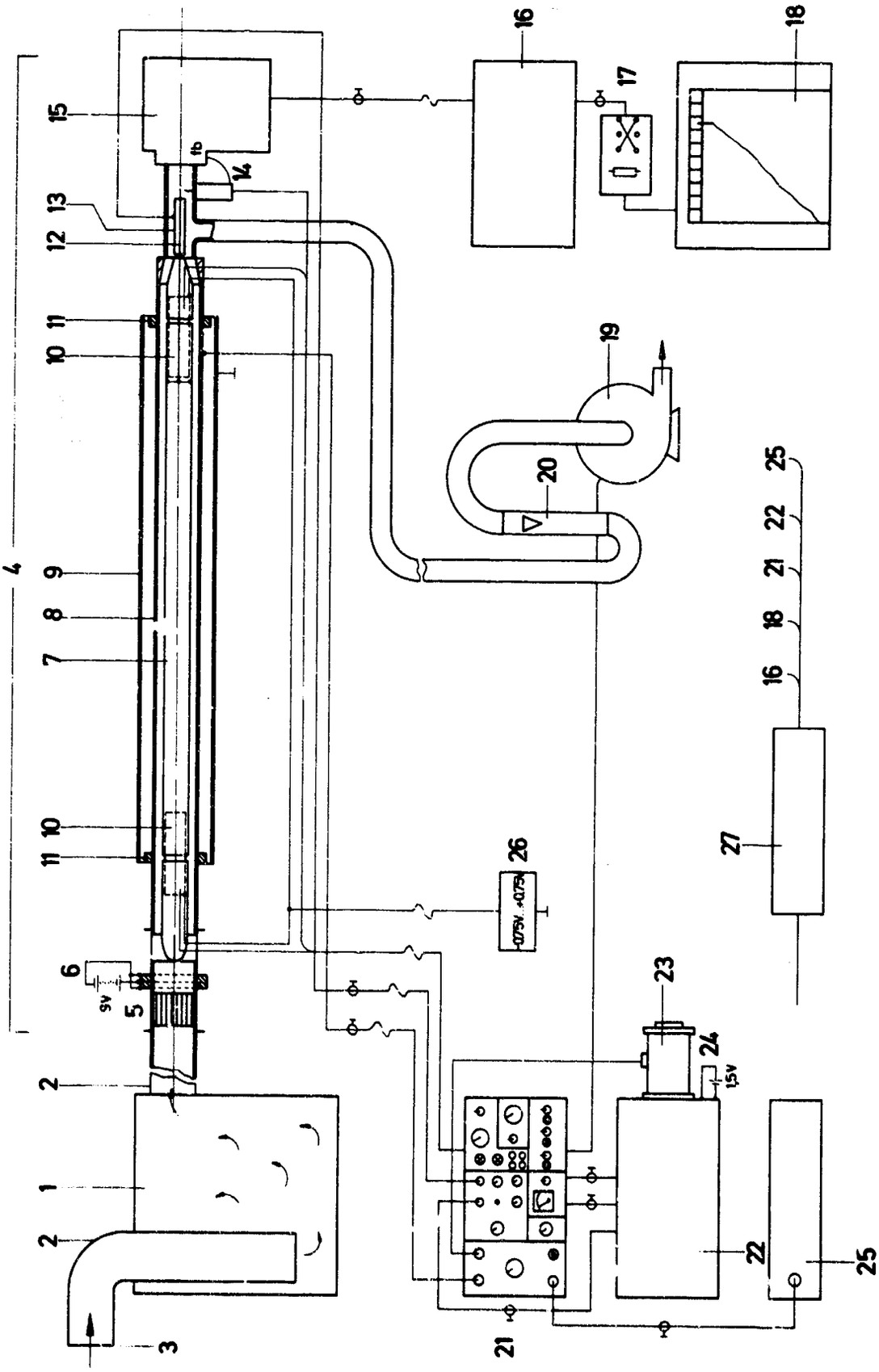
16
18
17
15
14
13
12
11
10
19
20
25
22
21
18
16
9
8
7
4
11
10
26
27
6
9V
5
23
24
15V
2
1
2
22
25
3
21

Fig.: 1

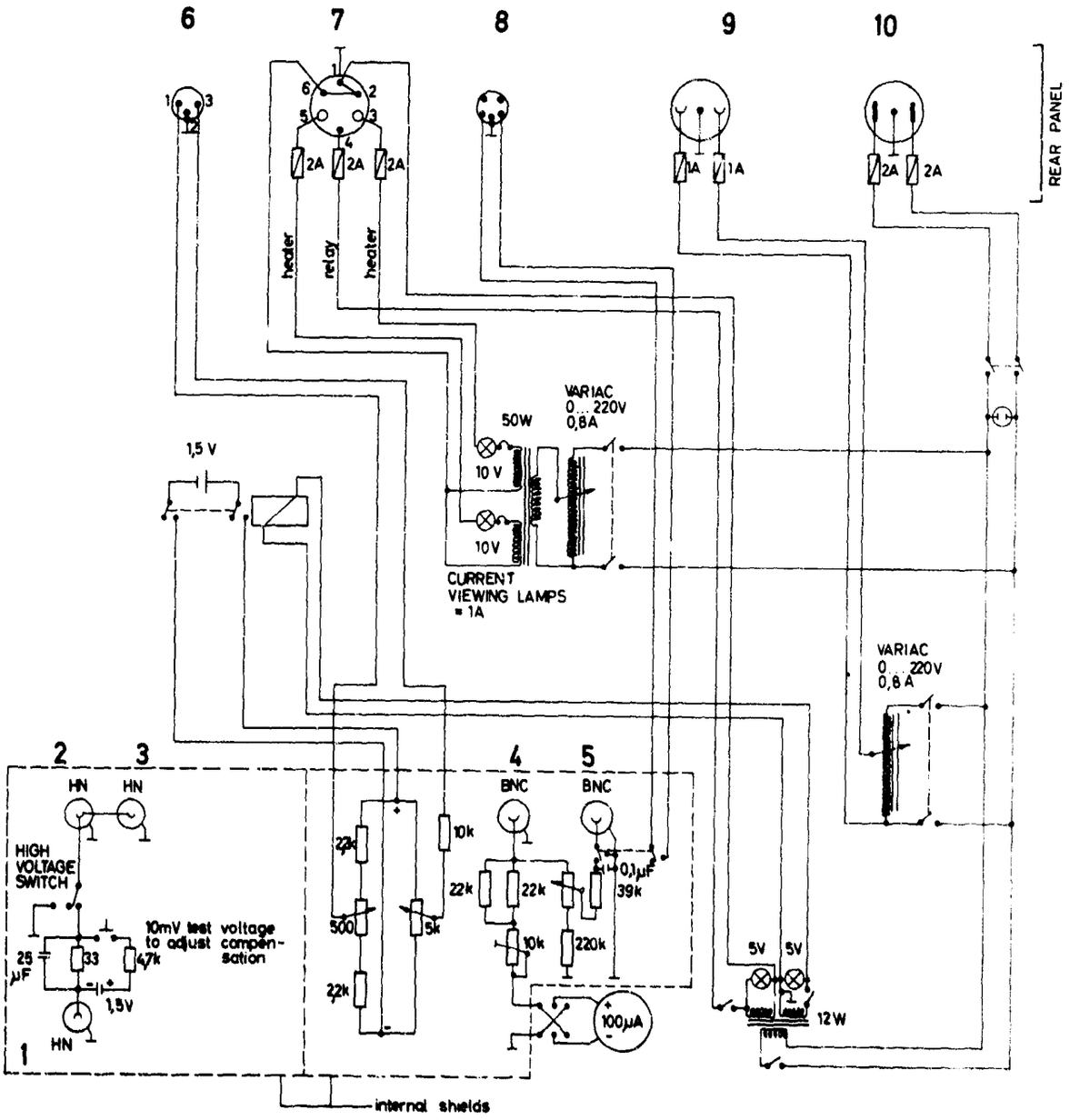
6
7
8
9
10
REAR PANEL
2A
2A
2A
1A
1A
2A
2A
heater
relay
heater
VARIAC
0 ... 220V
0,8A
50W
10 V
10V
CURRENT
VIEWING LAMPS
= 1A
1,5 V
VARIAC
0 ... 220V
0,8 A
2
3
4
5
HN
HN
BNC
BNC
HIGH
VOLTAGE
SWITCH
10mV test voltage
to adjust compen-
sation
25
µF
33
4,7k
1,5V
HN
1
22k
10k
500
5k
22k
22k
22k
0,1µF
39k
10k
220k
100µA
5V
5V
12W
internal shields

Fig.: 2

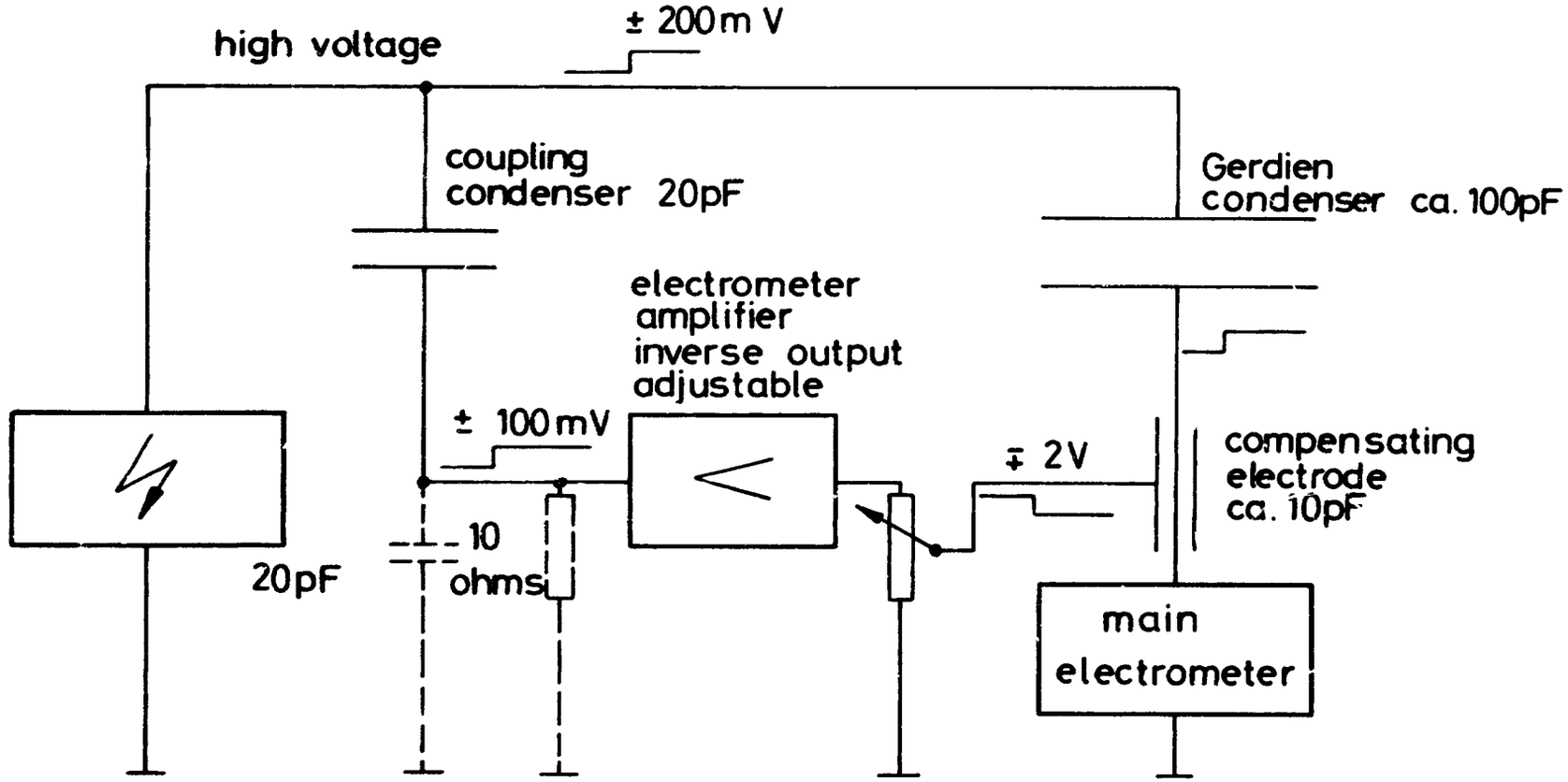
high voltage
± 200 m V
coupling
condenser 20pF
Gerdien
condenser ca. 100pF
electrometer
amplifier
inverse output
adjustable
± 100 mV
∓ 2V
compensating
electrode
ca. 10pF
20pF
10
ohms
main
electrometer

FIG. 3

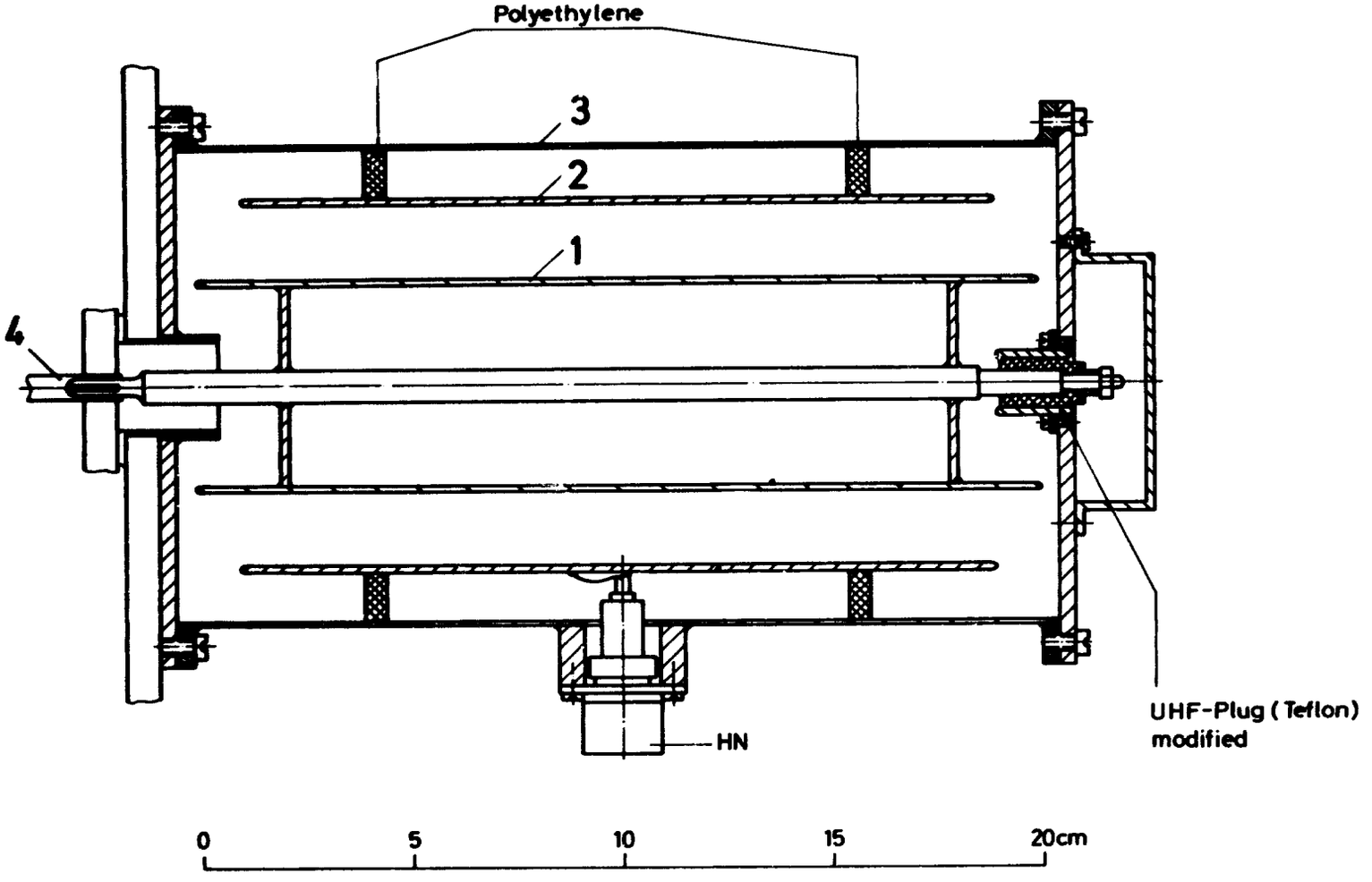

Fig. 4

Schauinsland 19.8.1967 (ca. 20.00 - 2200h)

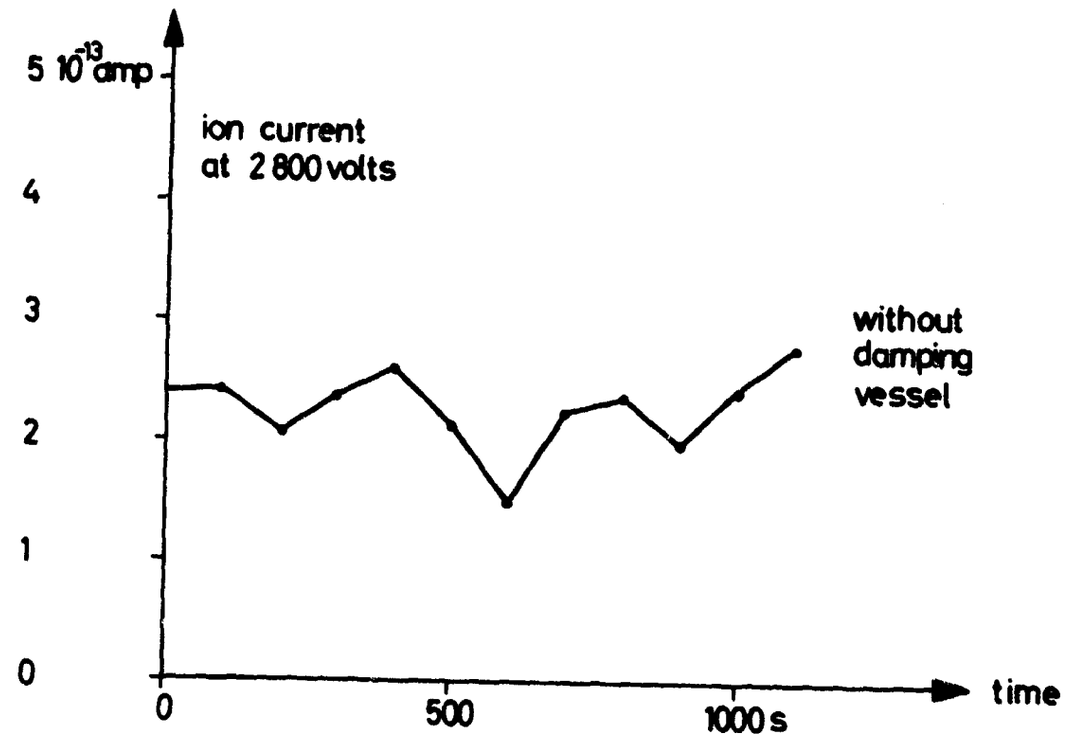

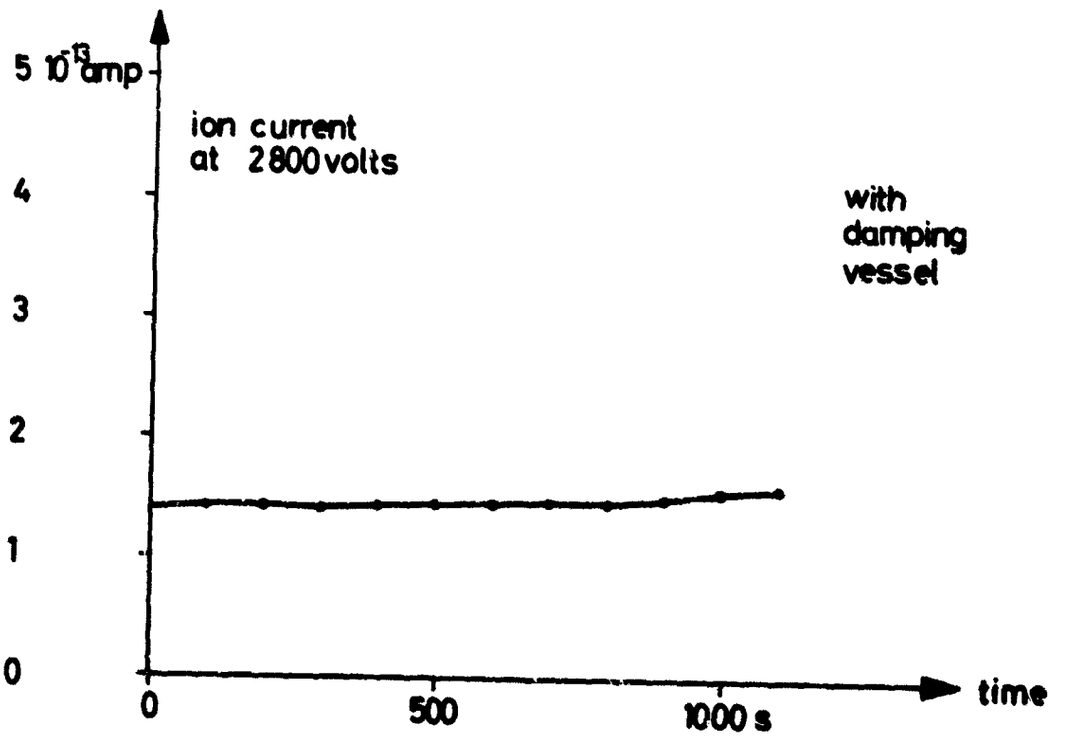

Fig: 5

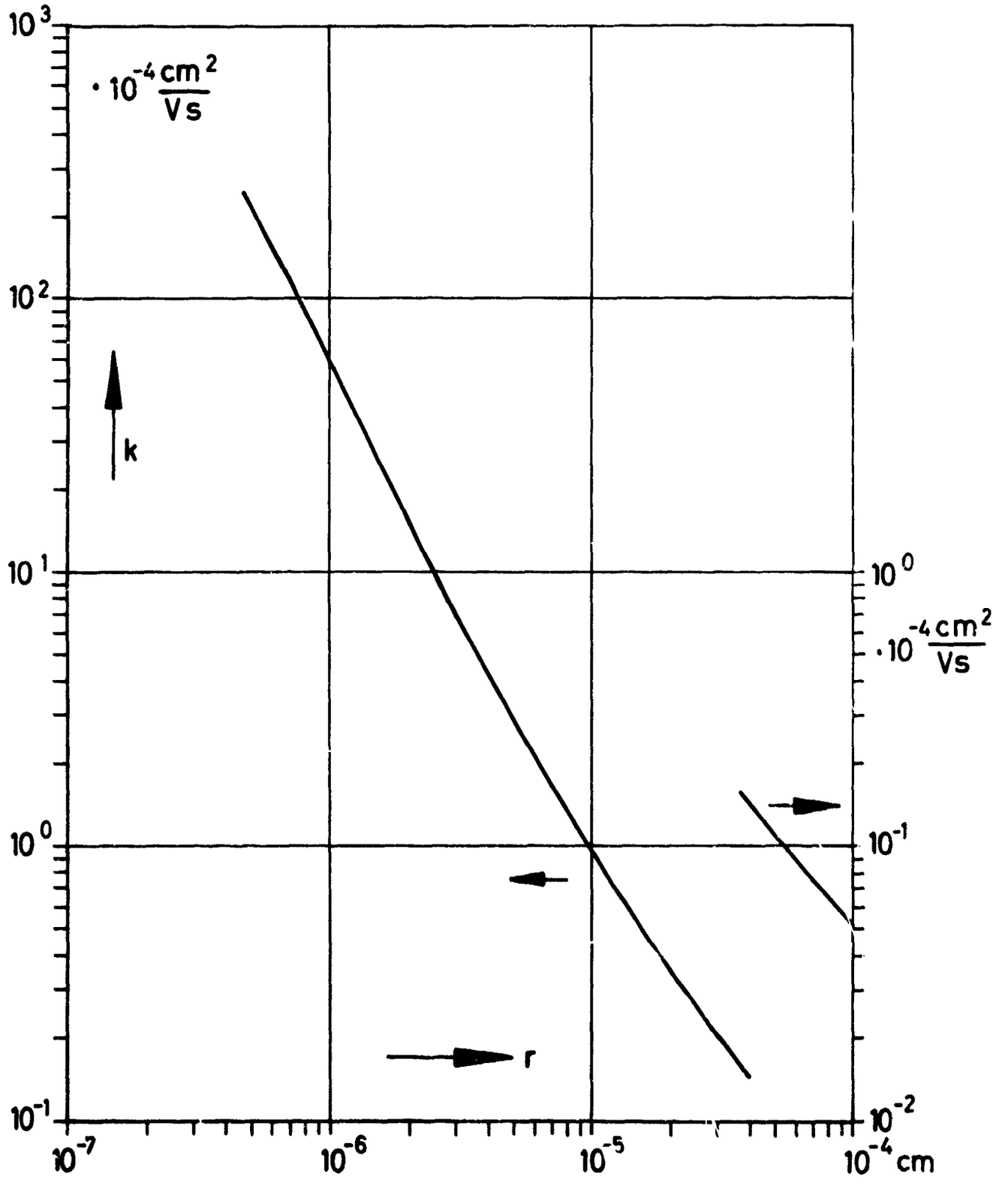
10^3
$\cdot 10^{-4} \frac{cm^2}{Vs}$
10^2
k
10^1
10^0
10^0
$\cdot 10^{-4} \frac{cm^2}{Vs}$
10^{-1}
r
10^{-1}
10^{-2}
10^{-7}
10^{-6}
10^{-5}
10^{-4} cm

Fig: 6

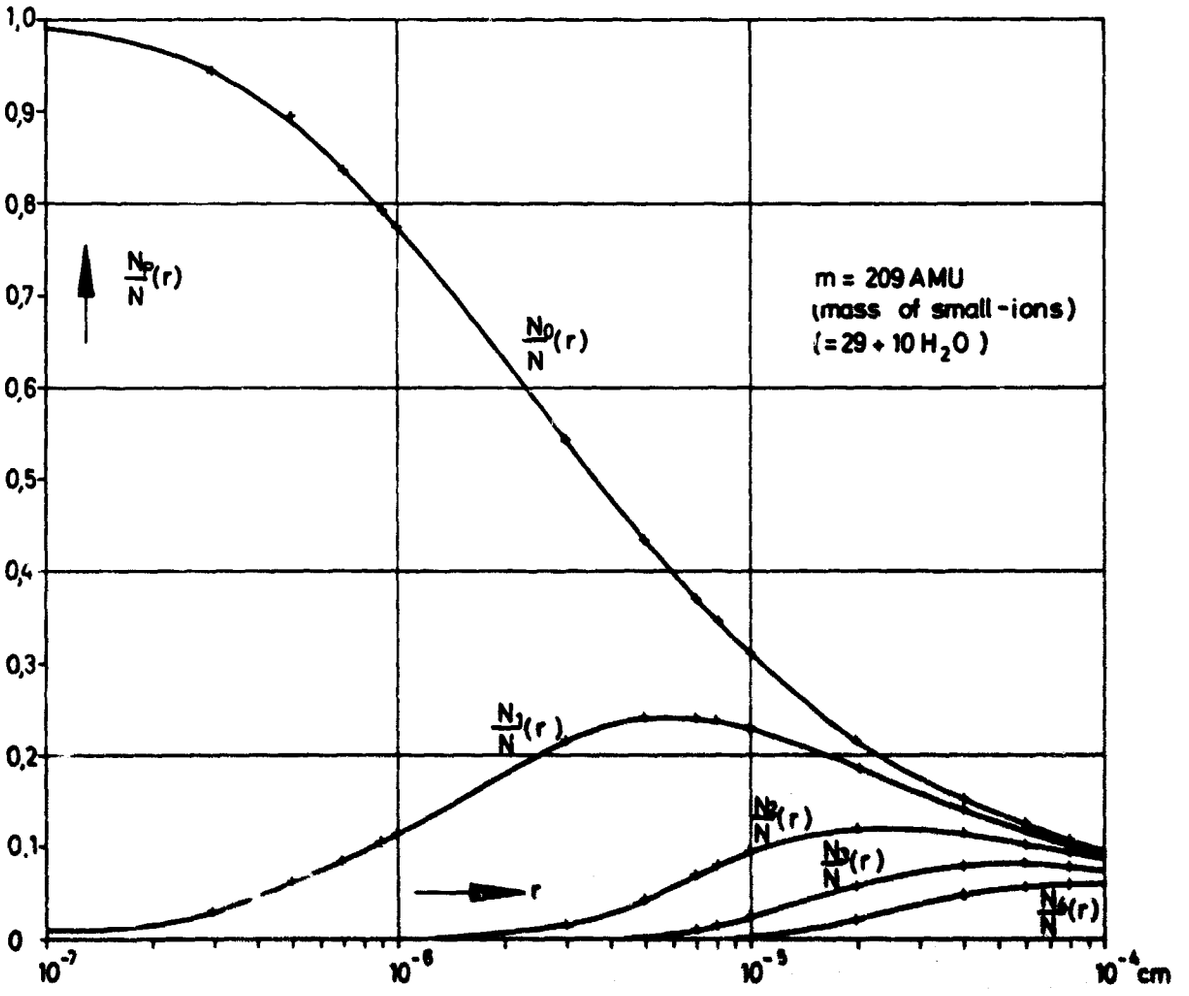
1,0
0,9
0,8
0,7
0,6
0,5
0,4
0,3
0,2
0,1
0
$\frac{N_p}{N}(r)$
$\frac{N_0}{N}(r)$
$\frac{N_1}{N}(r)$
$\frac{N_2}{N}(r)$
$\frac{N_3}{N}(r)$
$\frac{N_4}{N}(r)$
r
m = 209 AMU
(mass of small-ions)
(= 29 + 10 H_2O)
10^{-7}
10^{-6}
10^{-5}
10^{-4} cm

Fig. 7

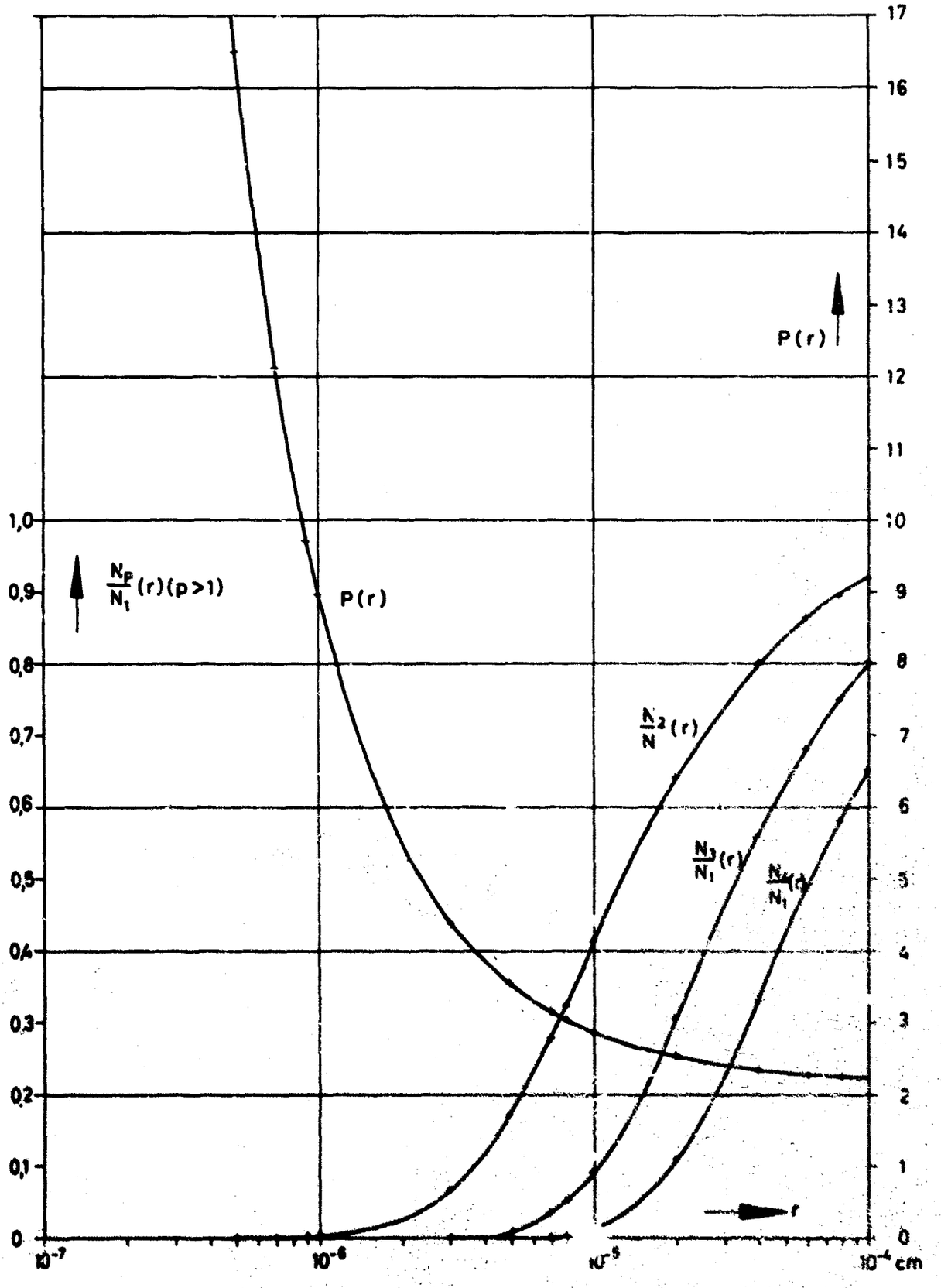
17
16
15
14
13
12
11
10
9
8
7
6
5
4
3
2
1
0
1,0
0,9
0,8
0,7
0,6
0,5
0,4
0,3
0,2
0,1
0
P(r)
$\frac{N_p}{N_1}(r)(p>1)$
P(r)
$\frac{N_2}{N_1}(r)$
$\frac{N_3}{N_1}(r)$
$\frac{N_4}{N_1}(r)$
r
10^{-7}
10^{-6}
10^{-5}
10^{-4} cm

Fig. 8

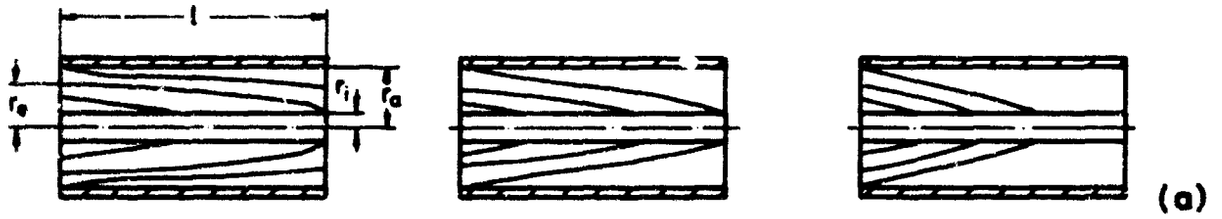

(a)

$V < \frac{M}{k_1}$ $\qquad$ $V = \frac{M}{k_1}$ $\qquad$ $V > \frac{M}{k_1}$

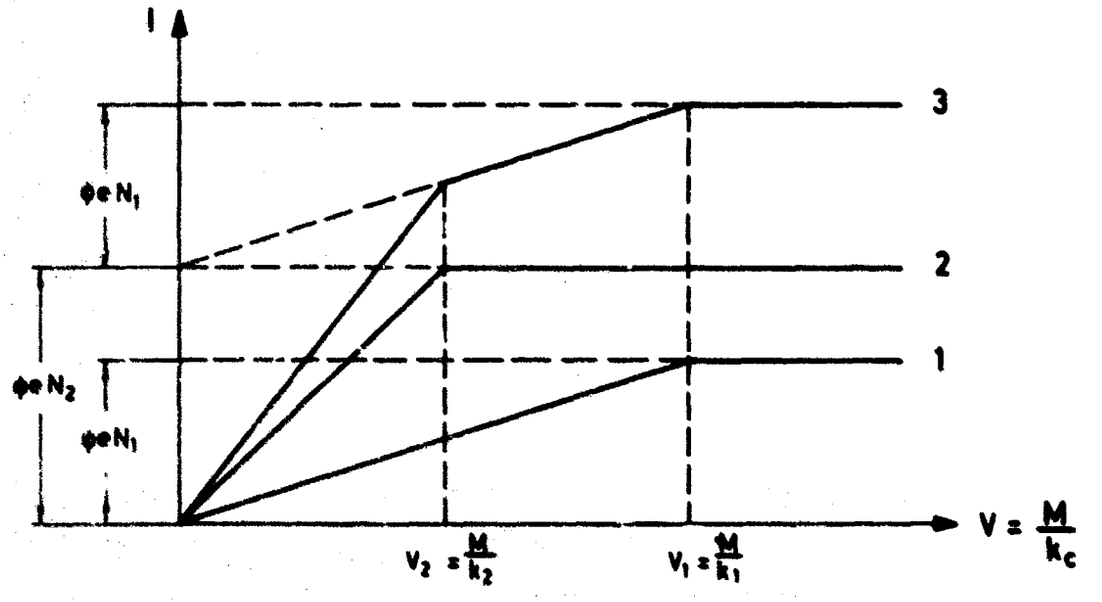

(b)

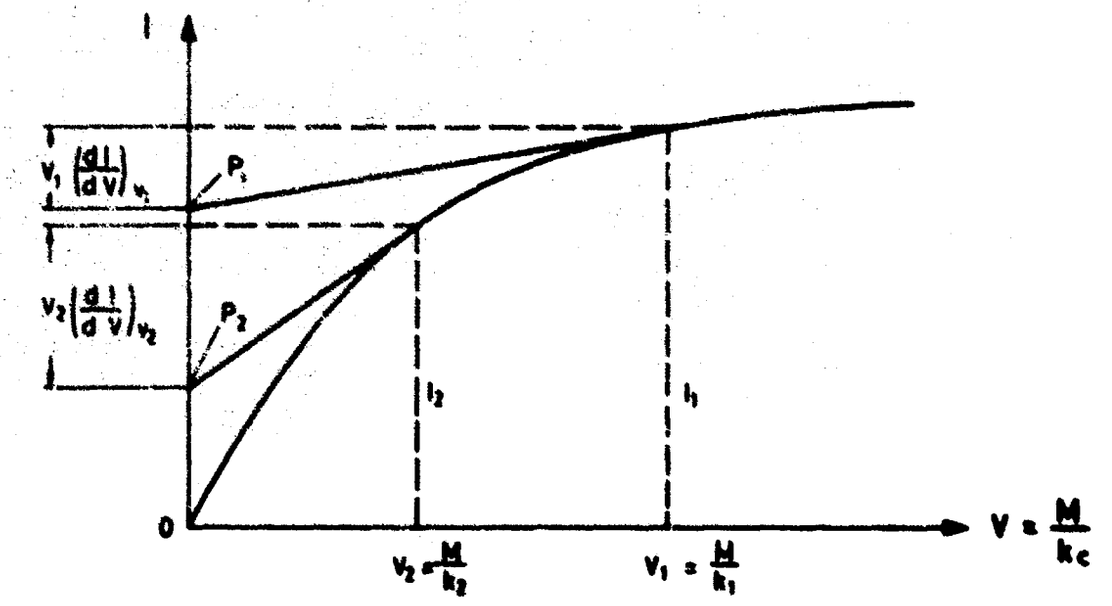

(c)

Fig : 9

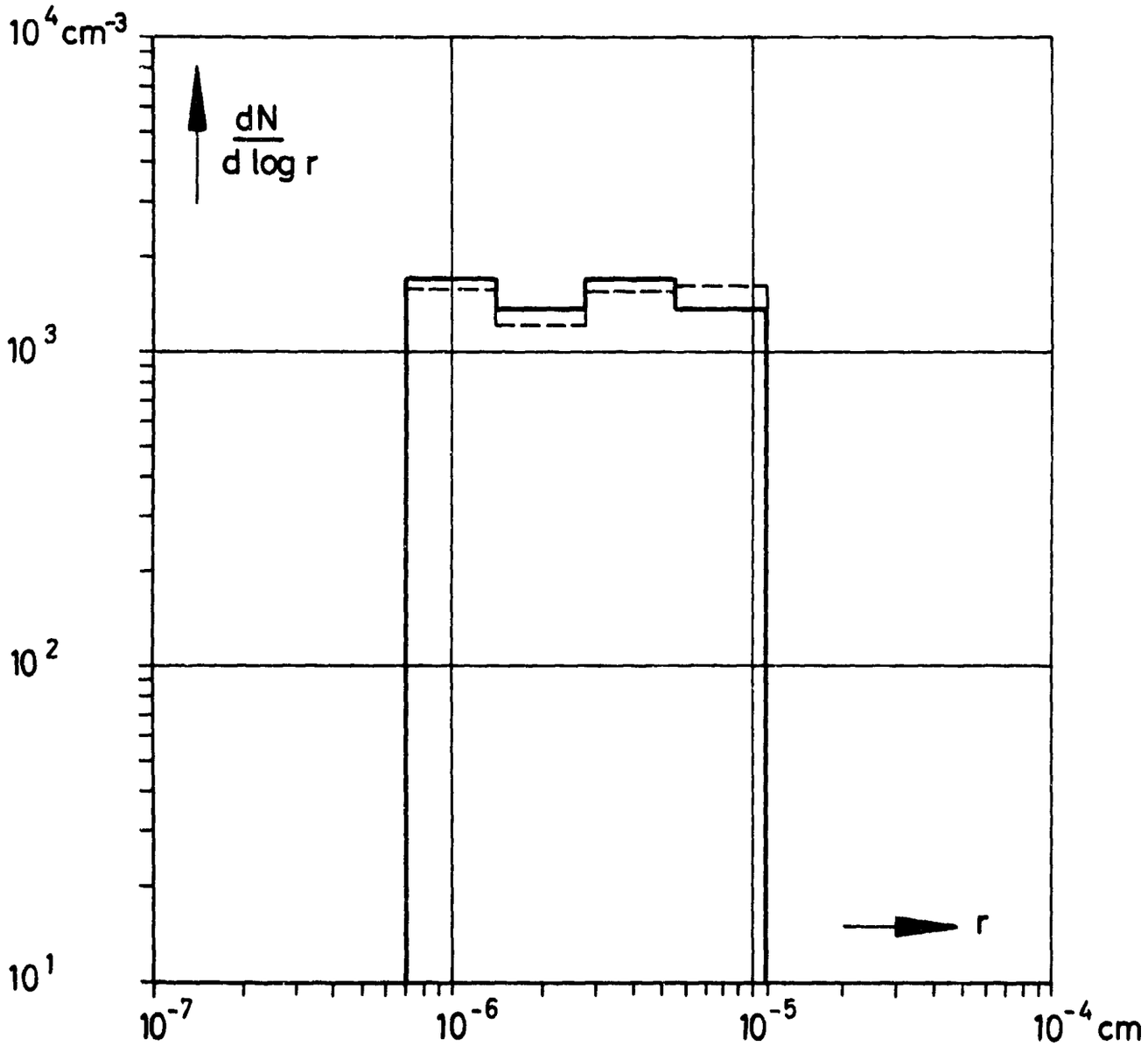

Fig.: 10

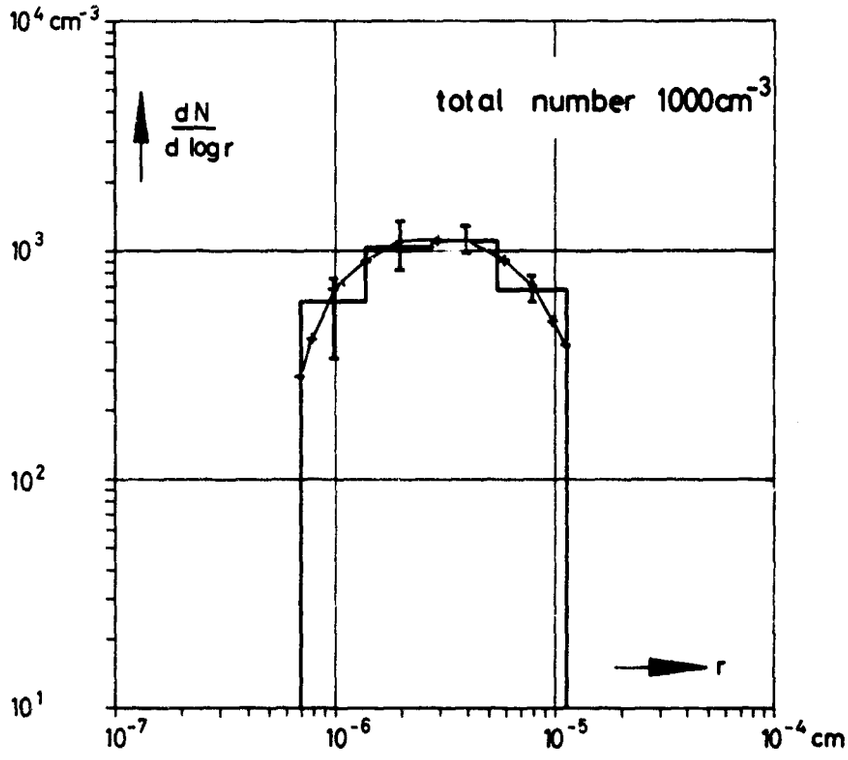
$10^4\,cm^{-3}$
$\frac{dN}{d\log r}$
total number $1000cm^{-3}$
10^3
10^2
10^1
r
10^{-7}
10^{-6}
10^{-5}
10^{-4} cm

(a)

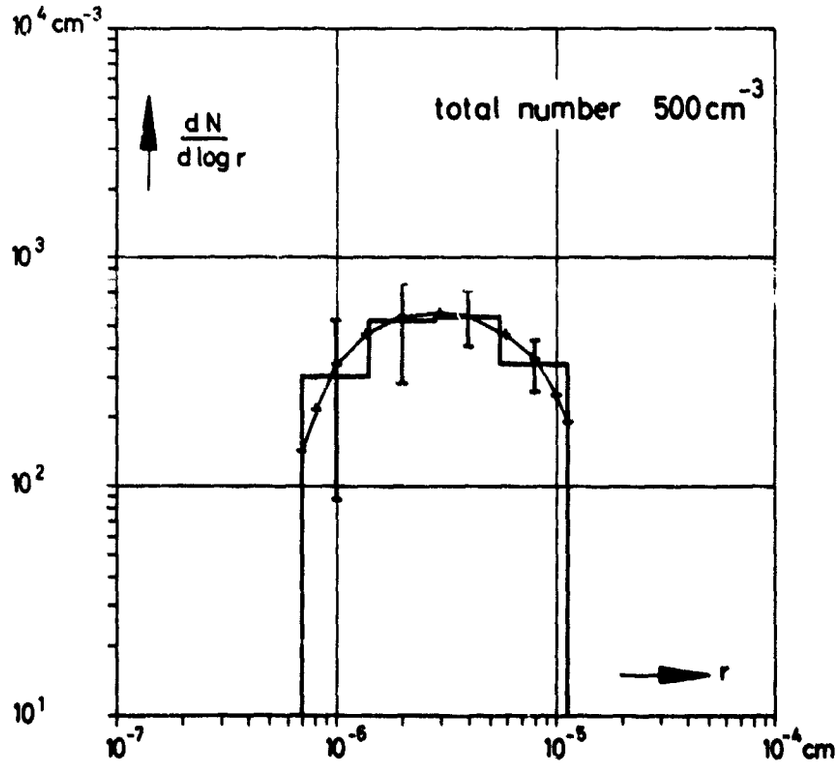
$10^4\,cm^{-3}$
$\frac{dN}{d\log r}$
total number $500cm^{-3}$
10^3
10^2
10^1
r
10^{-7}
10^{-6}
10^{-5}
10^{-4} cm

(b)

Fig.: 11

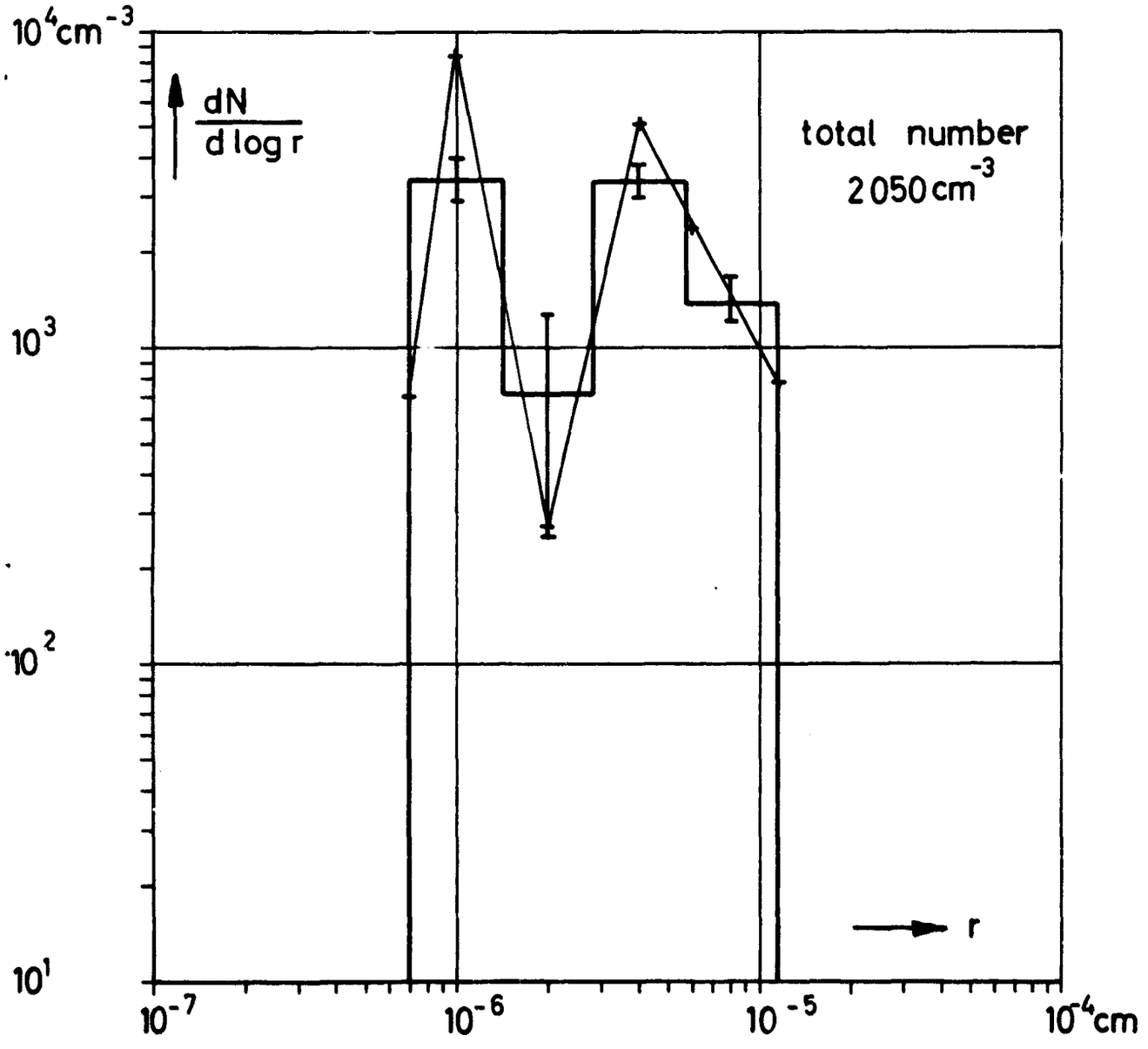
$10^4 cm^{-3}$
10^3
10^2
10^1
dN / d log r
total number
$2050 cm^{-3}$
r
10^{-7}
10^{-6}
10^{-5}
$10^{-4} cm$

Fig.: 12

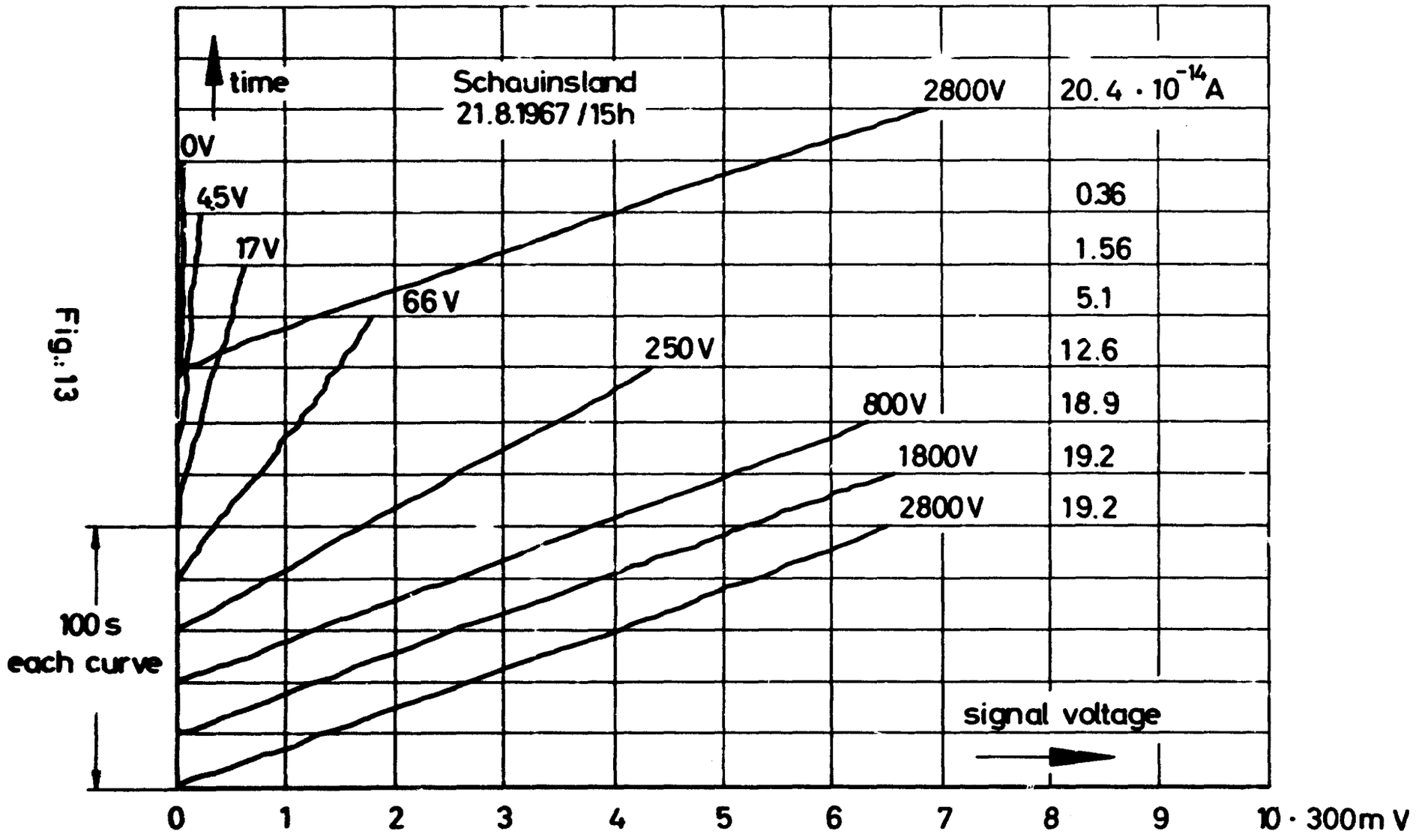
time
Schauinsland
21.8.1967 / 15h
2800V
20.4 · 10⁻¹⁴A
0V
45V
0.36
17V
1.56
66V
5.1
250V
12.6
800V
18.9
1800V
19.2
2800V
19.2
100 s
each curve
signal voltage
0
1
2
3
4
5
6
7
8
9
10 · 300m V

Fig.: 13

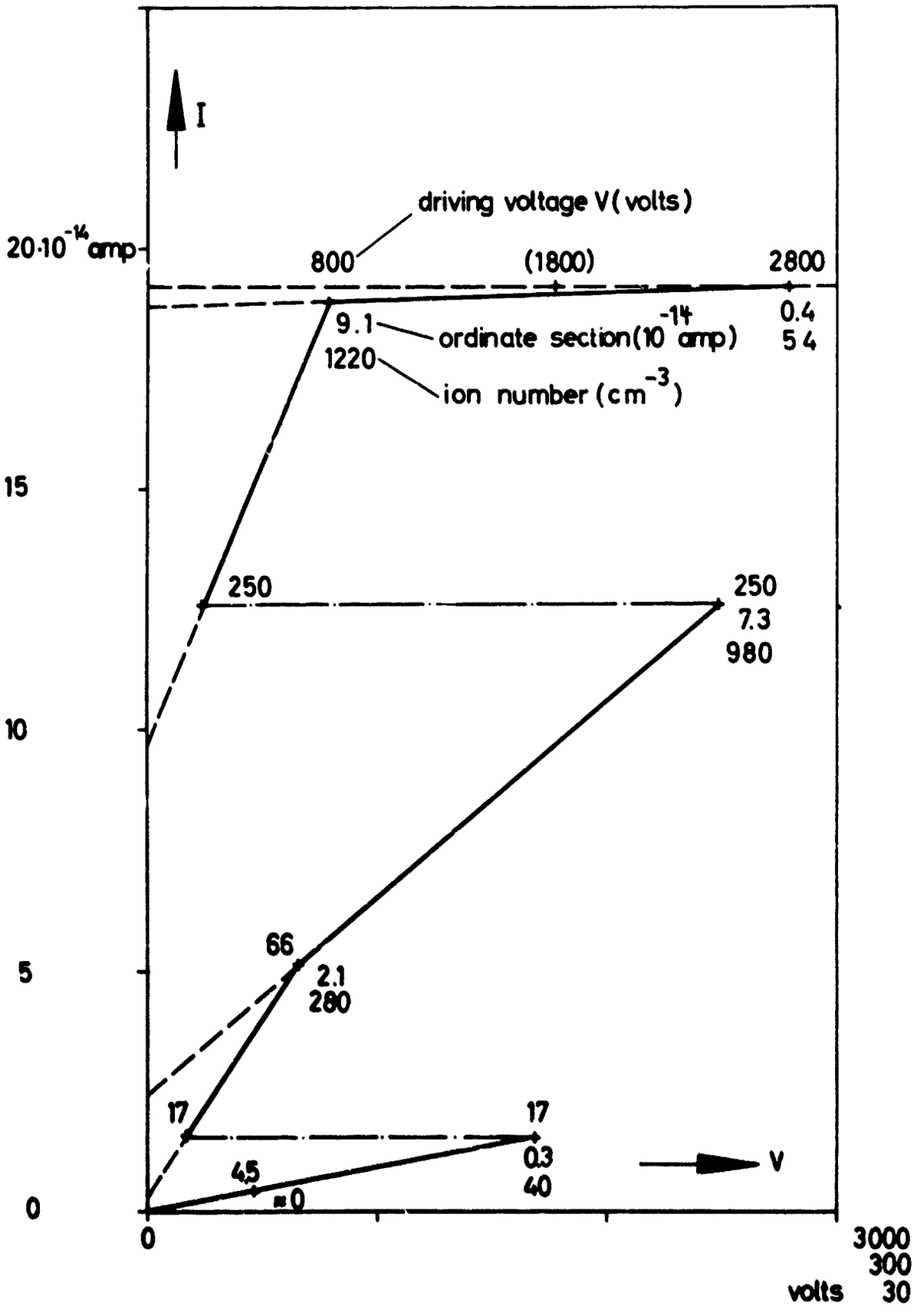
I
driving voltage V (volts)
20·10^-14 amp
800
(1800)
2800
9.1
ordinate section (10^-14 amp)
0.4
5 4
1220
ion number (cm^-3)
15
250
250
7.3
980
10
66
2.1
280
5
17
17
0.3
40
V
45
≈0
0
0
3000
300
volts
30

Fig. : 14

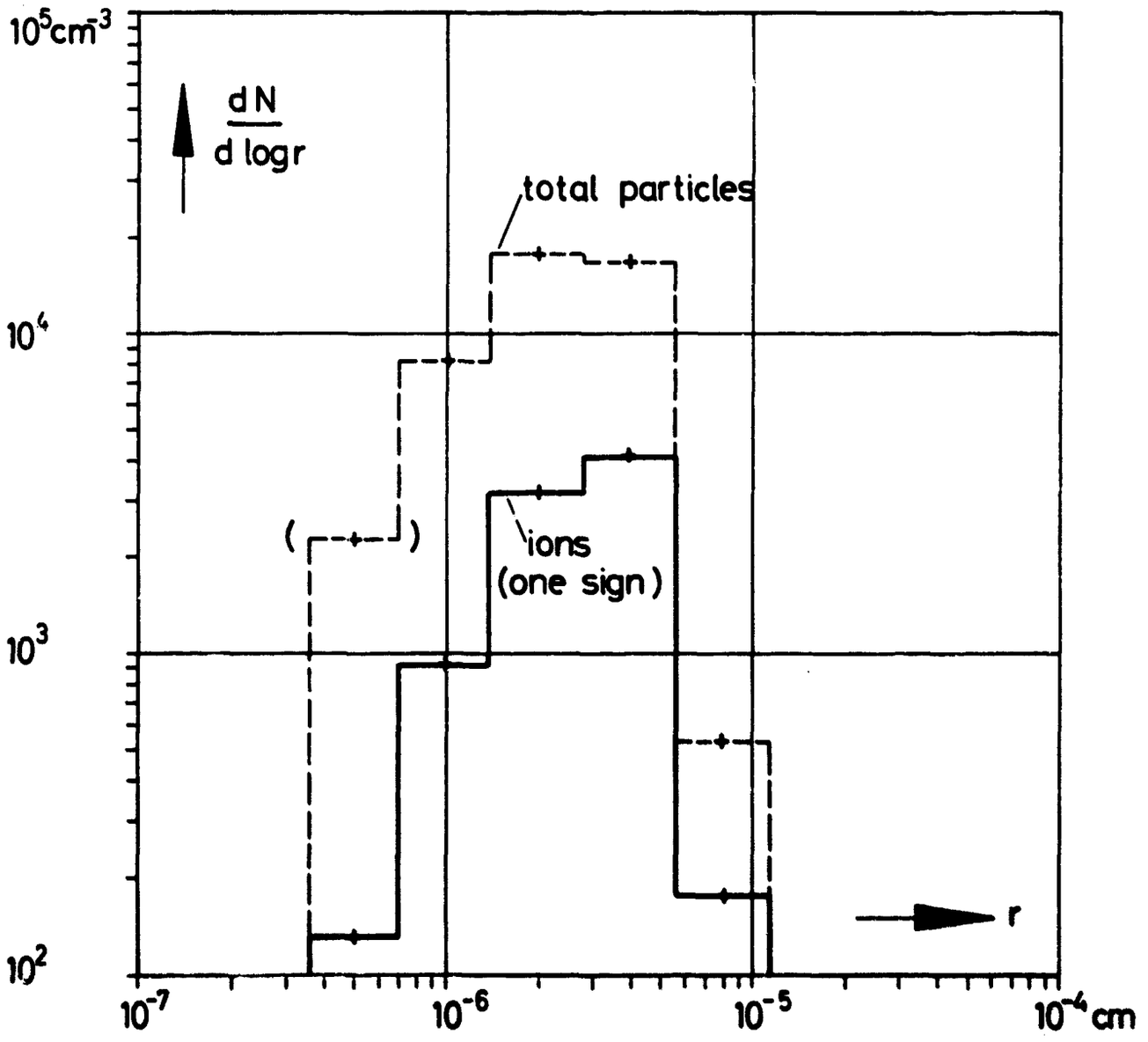
$10^5 cm^{-3}$
dN
d logr
total particles
10^4
(
)
ions
(one sign)
10^3
r
10^2
10^{-7}
10^{-6}
10^{-5}
10^{-4} cm

Fig.: 15

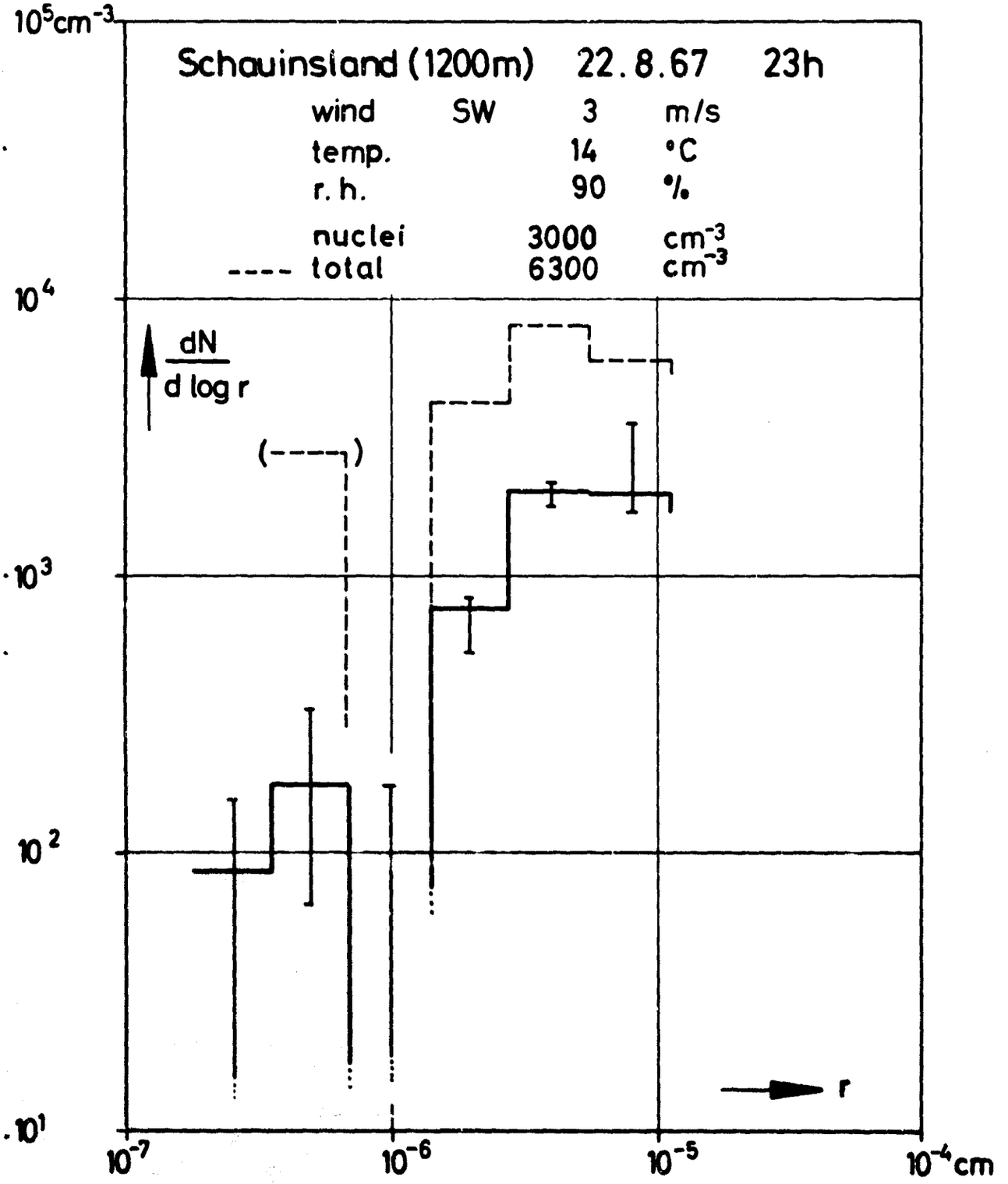
Schauinsland (1200m) 22.8.67 23h
wind SW 3 m/s
temp. 14 °C
r.h. 90 %
nuclei 3000 cm⁻³
---- total 6300 cm⁻³
10⁵cm⁻³
10⁴
10³
10²
10¹
dN / d log r
r
10⁻⁷
10⁻⁶
10⁻⁵
10⁻⁴cm

Fig.: 16

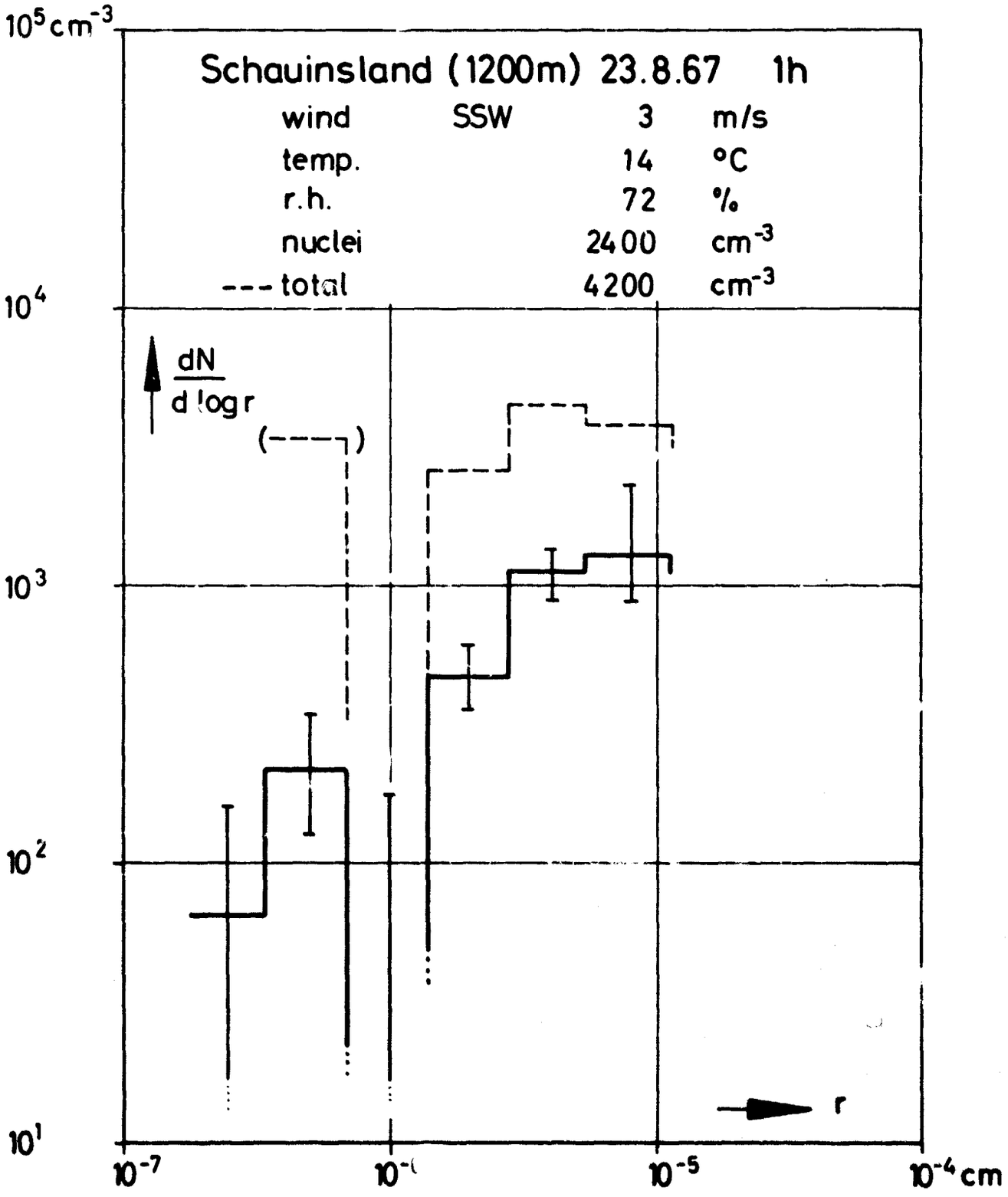
Schauinsland (1200m) 23.8.67 1h
wind SSW 3 m/s
temp. 14 °C
r.h. 72 %
nuclei 2400 cm-3
--- total 4200 cm-3
dN / d log r
(----)
r
10^5 cm^-3
10^4
10^3
10^2
10^1
10^-7
10^-5
10^-4 cm

Fig : 17

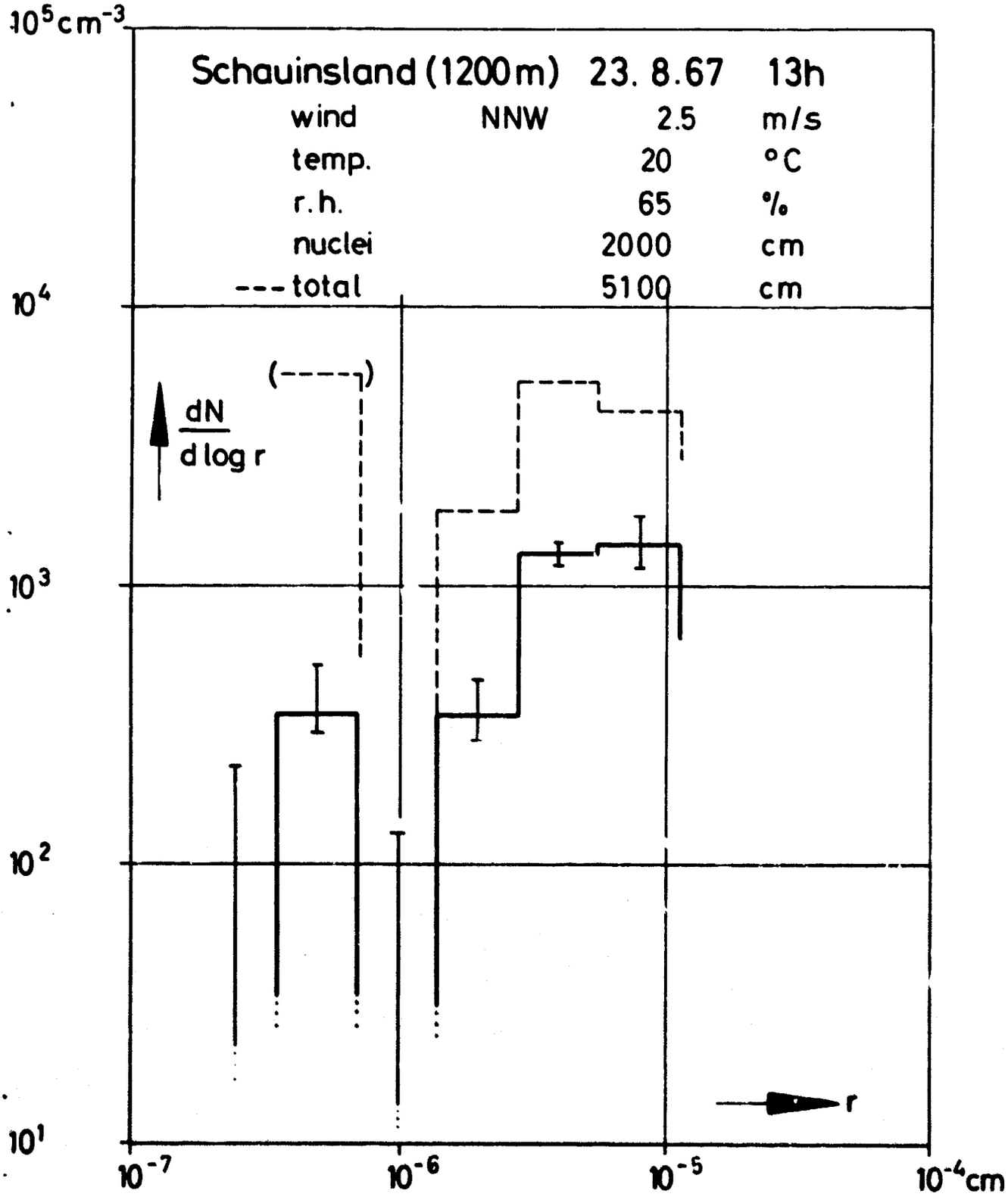
$10^5 cm^{-3}$
Schauinsland (1200m) 23. 8.67 13h
wind NNW 2.5 m/s
temp. 20 °C
r.h. 65 %
nuclei 2000 cm
--- total 5100 cm
10^4
10^3
10^2
10^1
dN / d log r
r
10^{-7}
10^{-6}
10^{-5}
10^{-4}cm

Fig.: 18

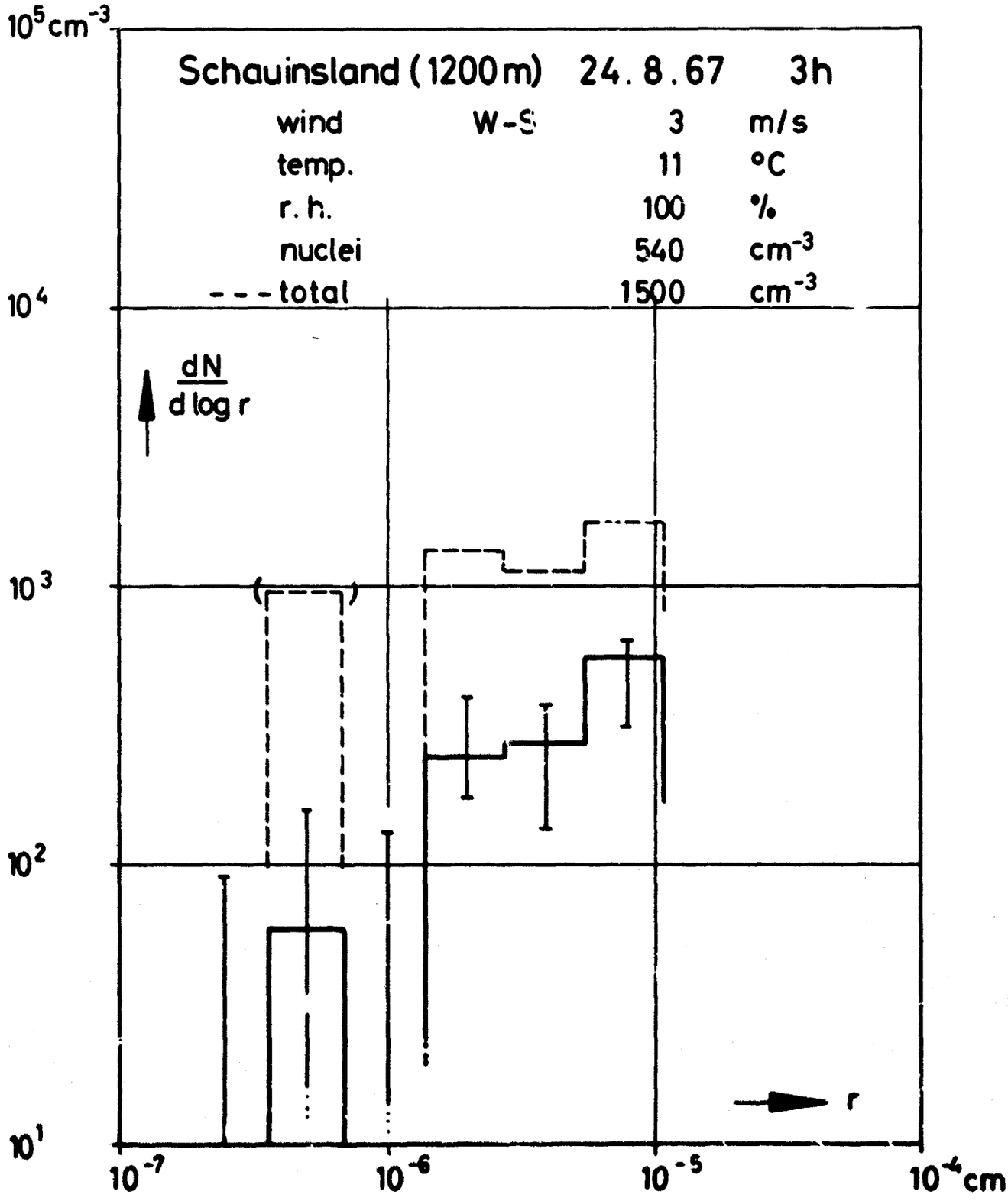
Schauinsland (1200 m) 24.8.67 3h
wind W-S 3 m/s
temp. 11 °C
r.h. 100 %
nuclei 540 cm⁻³
--- total 1500 cm⁻³
dN / d log r
r
10⁵ cm⁻³
10⁴
10³
10²
10¹
10⁻⁷
10⁻⁶
10⁻⁵
10⁻⁴ cm

Fig.: 19

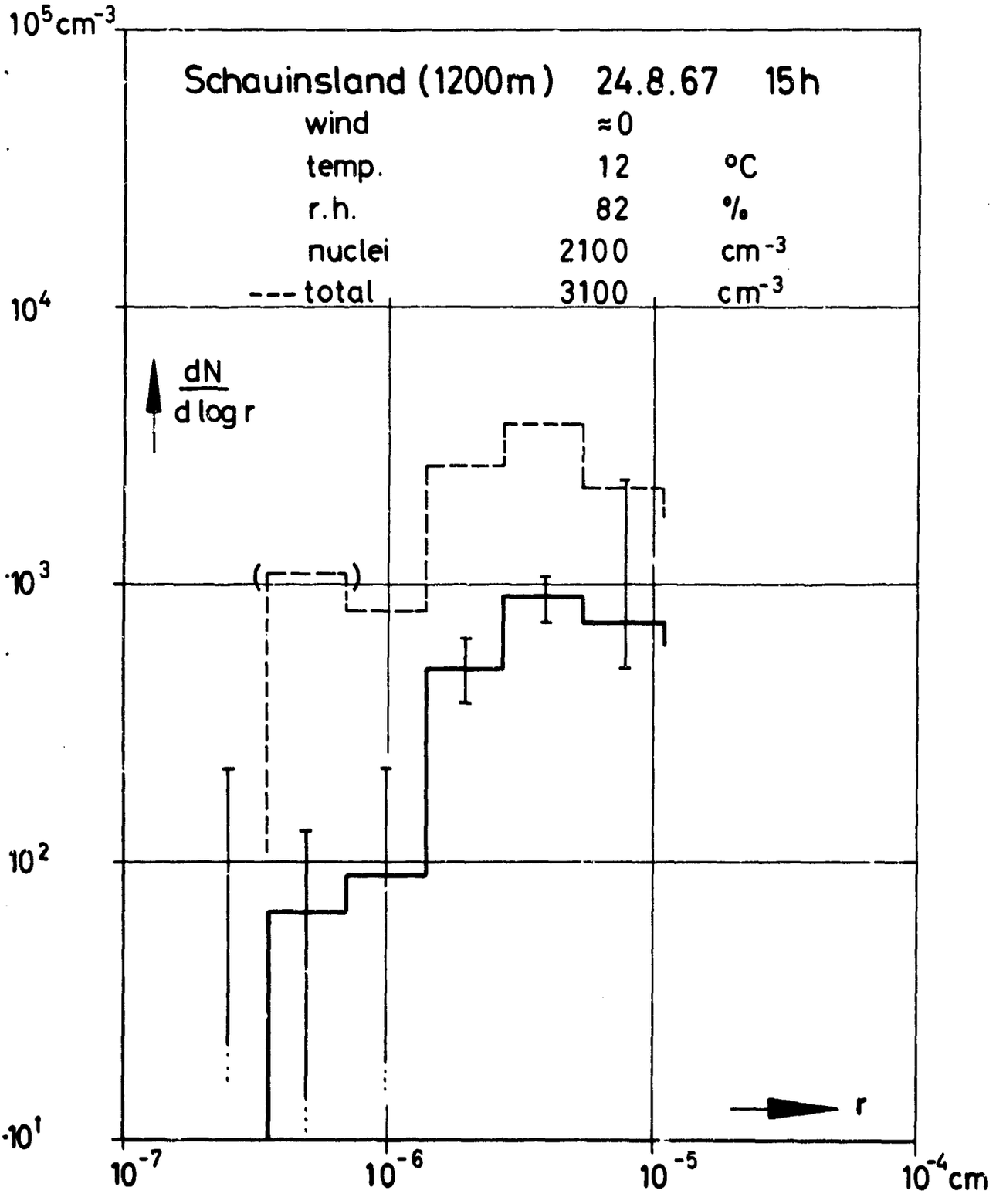
$10^5 cm^{-3}$
Schauinsland (1200m) 24.8.67 15h
wind ≈0
temp. 12 °C
r.h. 82 %
nuclei 2100 cm^{-3}
--- total 3100 cm^{-3}
10^4
$\frac{dN}{d \log r}$
10^3
10^2
10^1
r
10^{-7}
10^{-6}
10^{-5}
10^{-4} cm

Fig.: 20

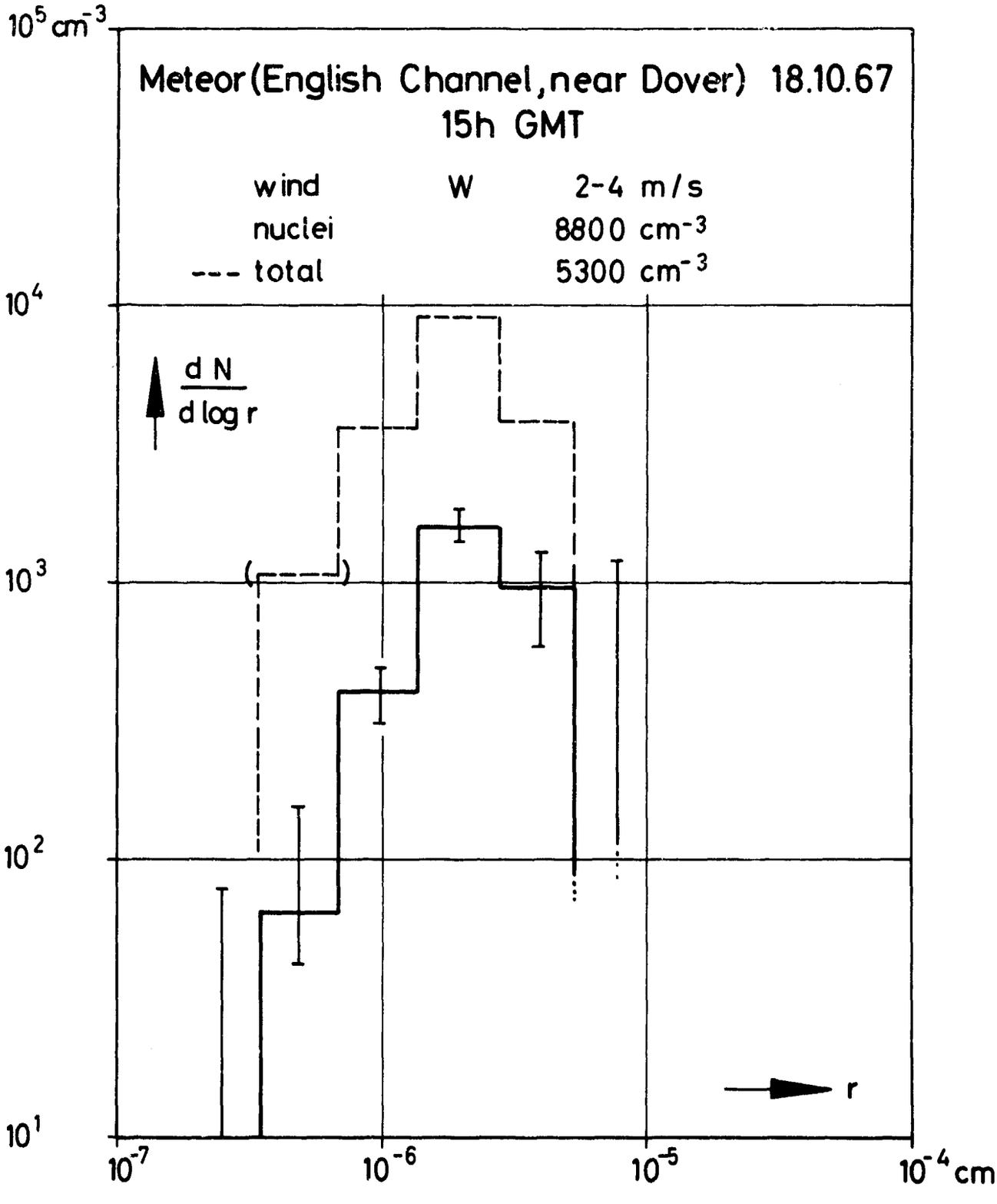
10^5 cm^{-3}
Meteor (English Channel, near Dover) 18.10.67
15h GMT
wind W 2-4 m/s
nuclei 8800 cm^{-3}
--- total 5300 cm^{-3}
10^4
$\frac{dN}{d\log r}$
10^3
10^2
10^1
r
10^{-7}
10^{-6}
10^{-5}
10^{-4} cm

Fig.: 21

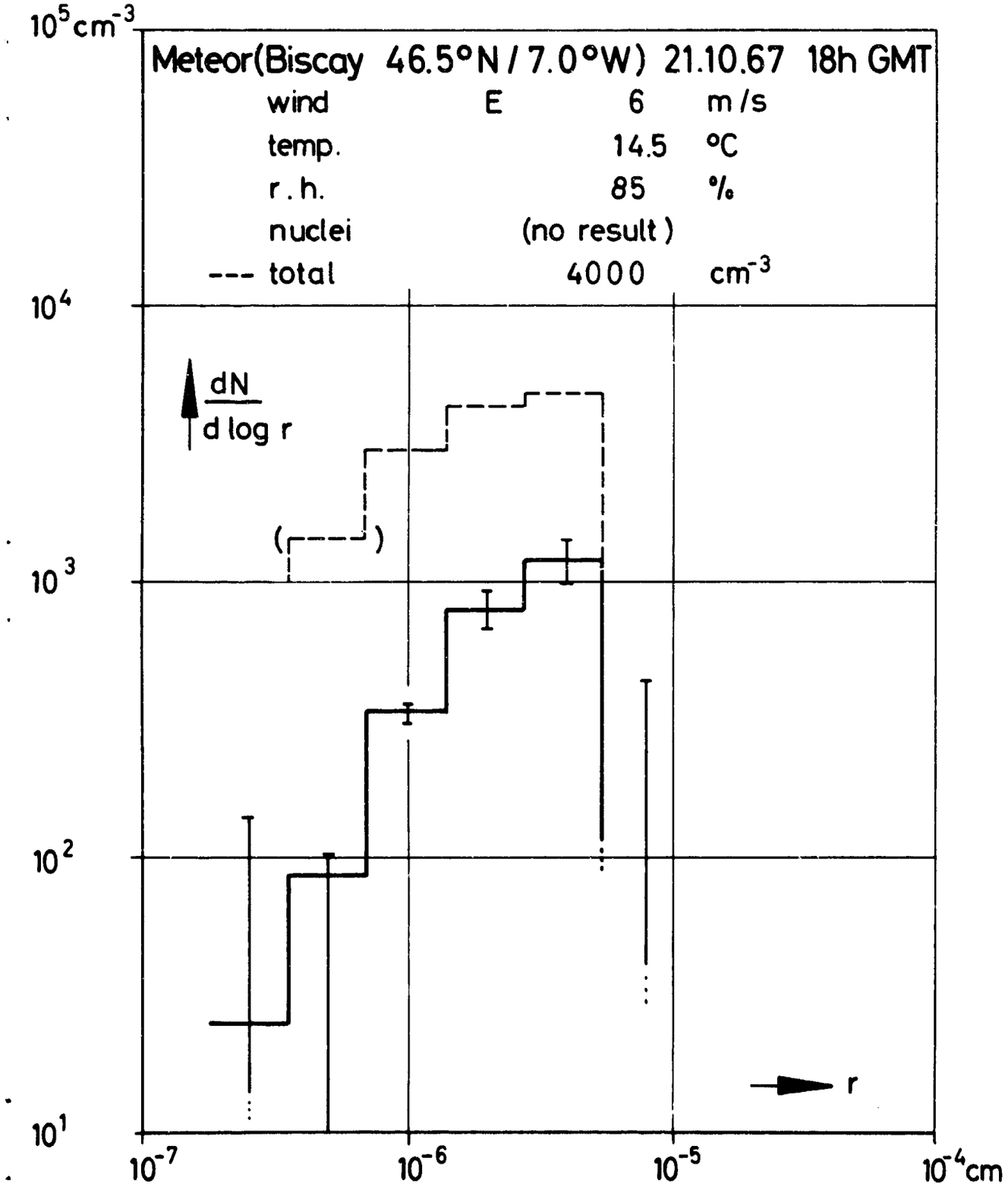
Meteor(Biscay 46.5°N / 7.0°W) 21.10.67 18h GMT
wind E 6 m/s
temp. 14.5 °C
r.h. 85 %
nuclei (no result)
--- total 4000 cm⁻³
dN / d log r
r
10⁵ cm⁻³
10⁴
10³
10²
10¹
10⁻⁷
10⁻⁶
10⁻⁵
10⁻⁴ cm

Fig. : 22

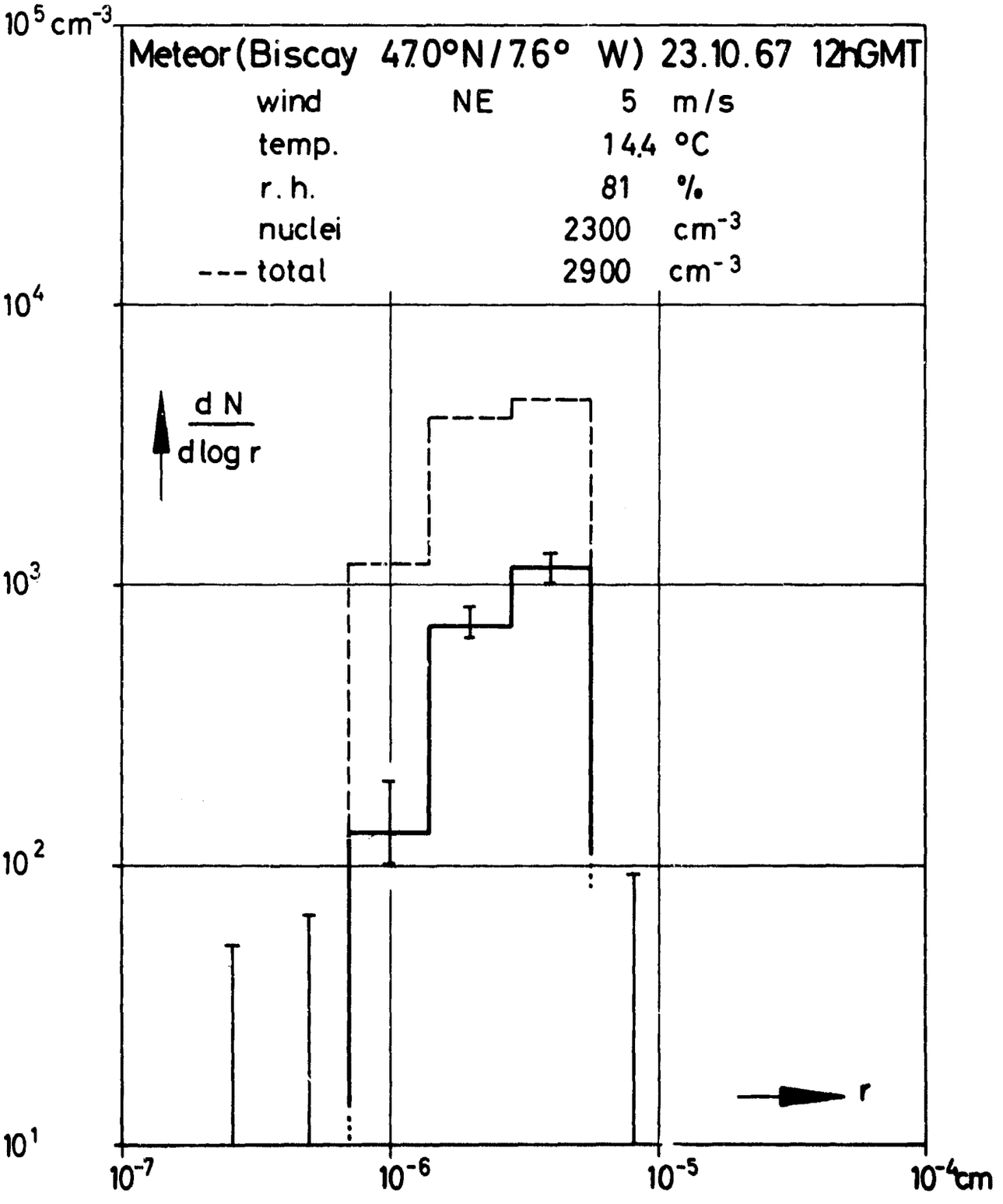
Meteor (Biscay 47.0°N / 7.6° W) 23.10.67 12h GMT
wind NE 5 m/s
temp. 14.4 °C
r.h. 81 %
nuclei 2300 cm⁻³
--- total 2900 cm⁻³
10⁵ cm⁻³
10⁴
10³
10²
10¹
d N / d log r
r
10⁻⁷
10⁻⁶
10⁻⁵
10⁻⁴ cm

Fig.: 23

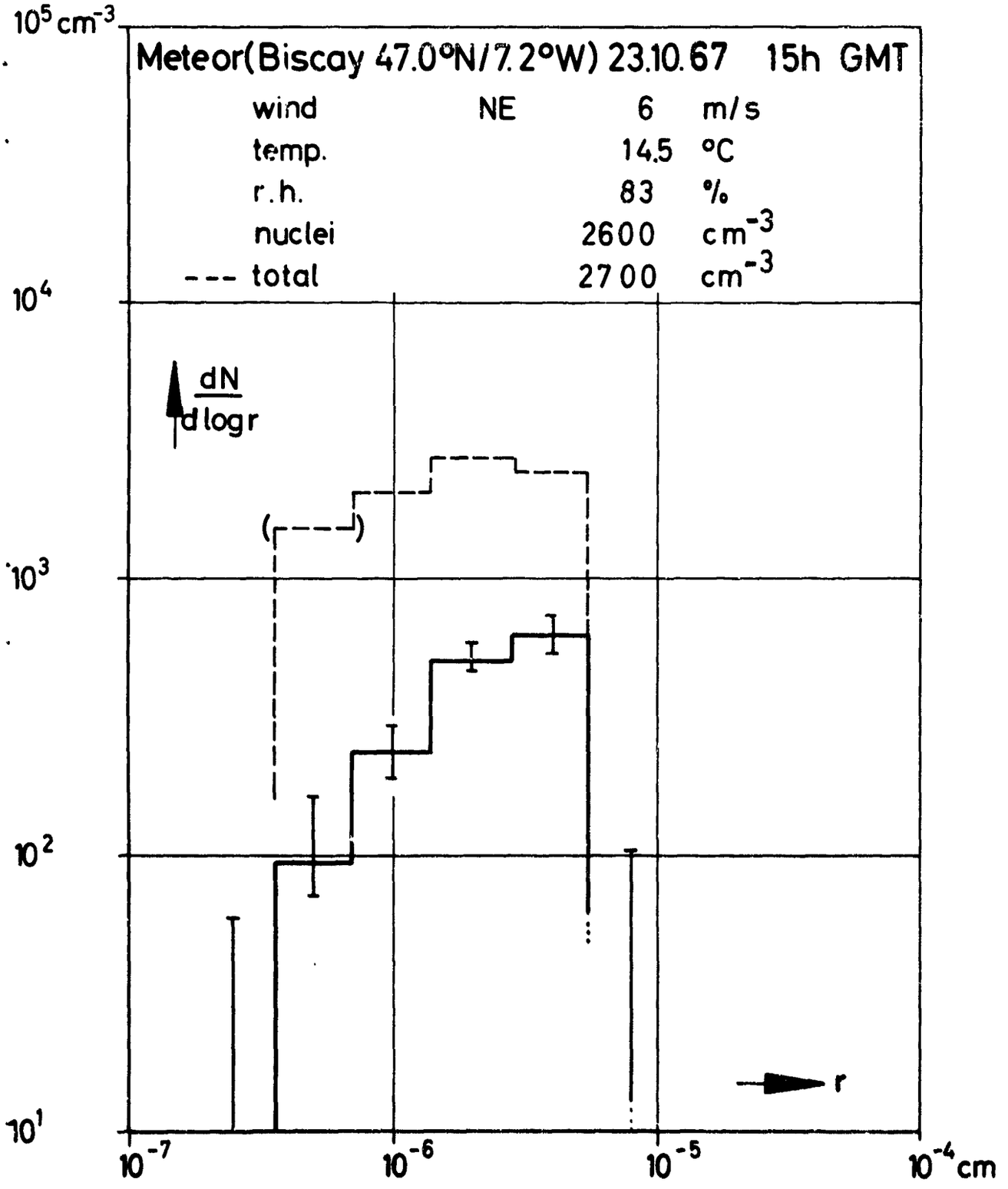
Meteor(Biscay 47.0°N/7.2°W) 23.10.67 15h GMT
wind NE 6 m/s
temp. 14.5 °C
r.h. 83 %
nuclei 2600 cm⁻³
--- total 2700 cm⁻³
10⁵ cm⁻³
10⁴
10³
10²
10¹
dN/d log r
r
10⁻⁷
10⁻⁶
10⁻⁵
10⁻⁴ cm

Fig.: 24

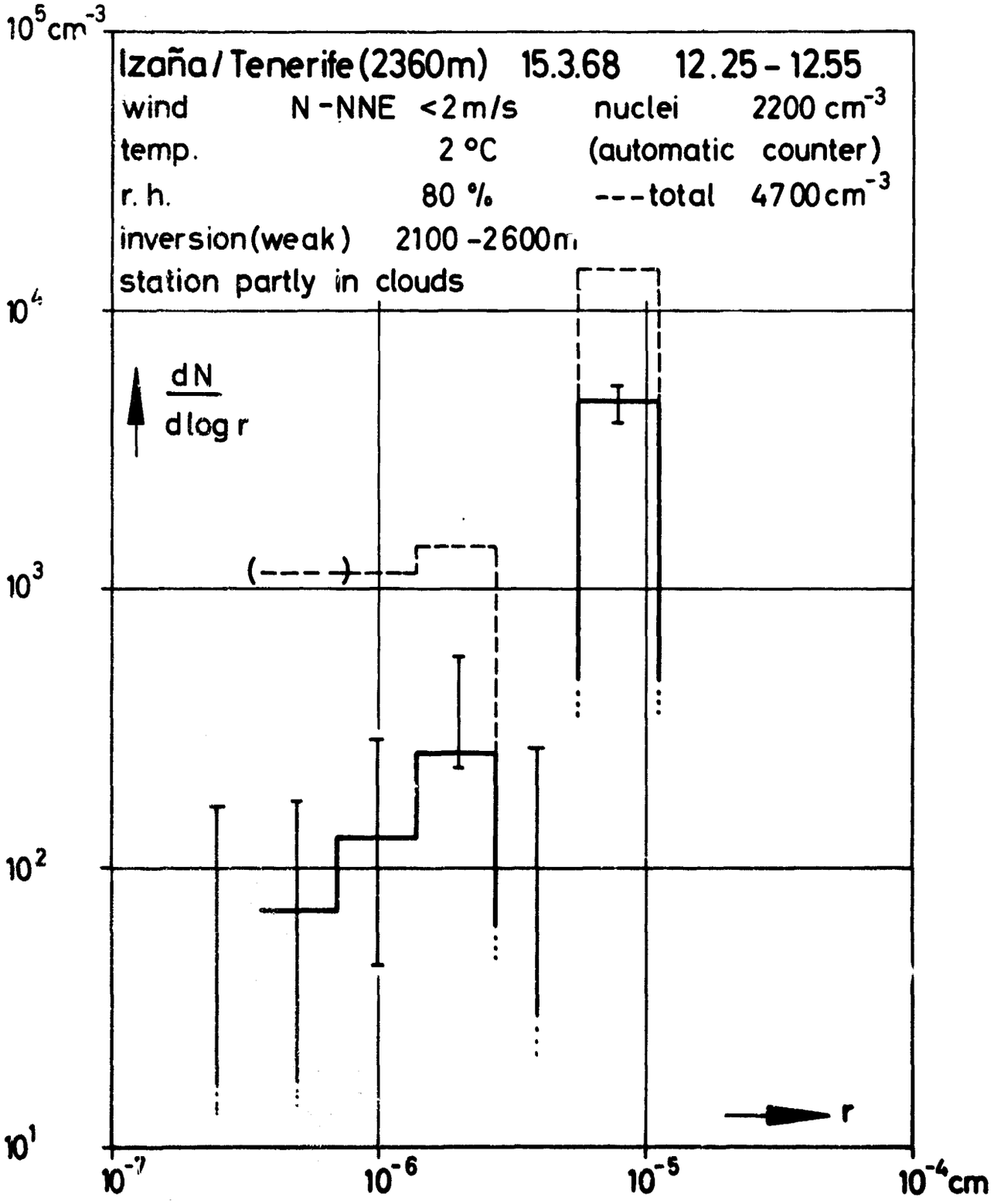
$10^5 cm^{-3}$
Izaña / Tenerife (2360m) 15.3.68 12.25 - 12.55
wind N - NNE < 2 m/s
temp. 2 °C
r. h. 80 %
inversion (weak) 2100 - 2600 m
station partly in clouds
nuclei 2200 cm^{-3}
(automatic counter)
---total 4700 cm^{-3}
10^4
10^3
10^2
10^1
$\frac{dN}{d\log r}$
r
10^{-7}
10^{-6}
10^{-5}
10^{-4} cm

Fig.: 25

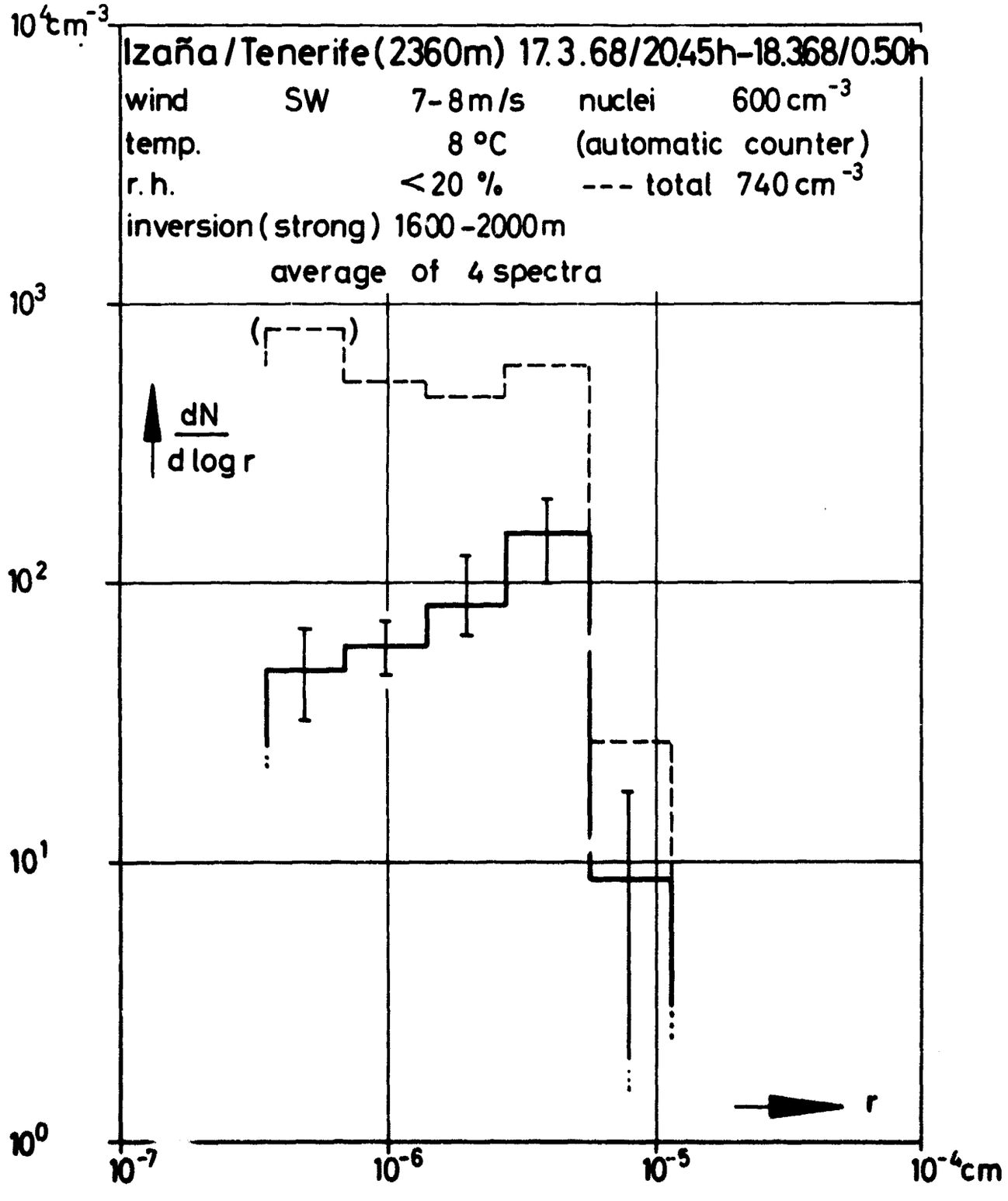
$10^4 cm^{-3}$
Izaña / Tenerife (2360m) 17.3.68/20.45h–18.3.68/0.50h
wind SW 7–8 m/s
temp. 8 °C
r. h. < 20 %
inversion (strong) 1600–2000 m
average of 4 spectra
nuclei 600 cm^{-3}
(automatic counter)
--- total 740 cm^{-3}
10^3
10^2
10^1
10^0
$\frac{dN}{d \log r}$
r
10^{-7}
10^{-6}
10^{-5}
10^{-4} cm

Fig.: 26

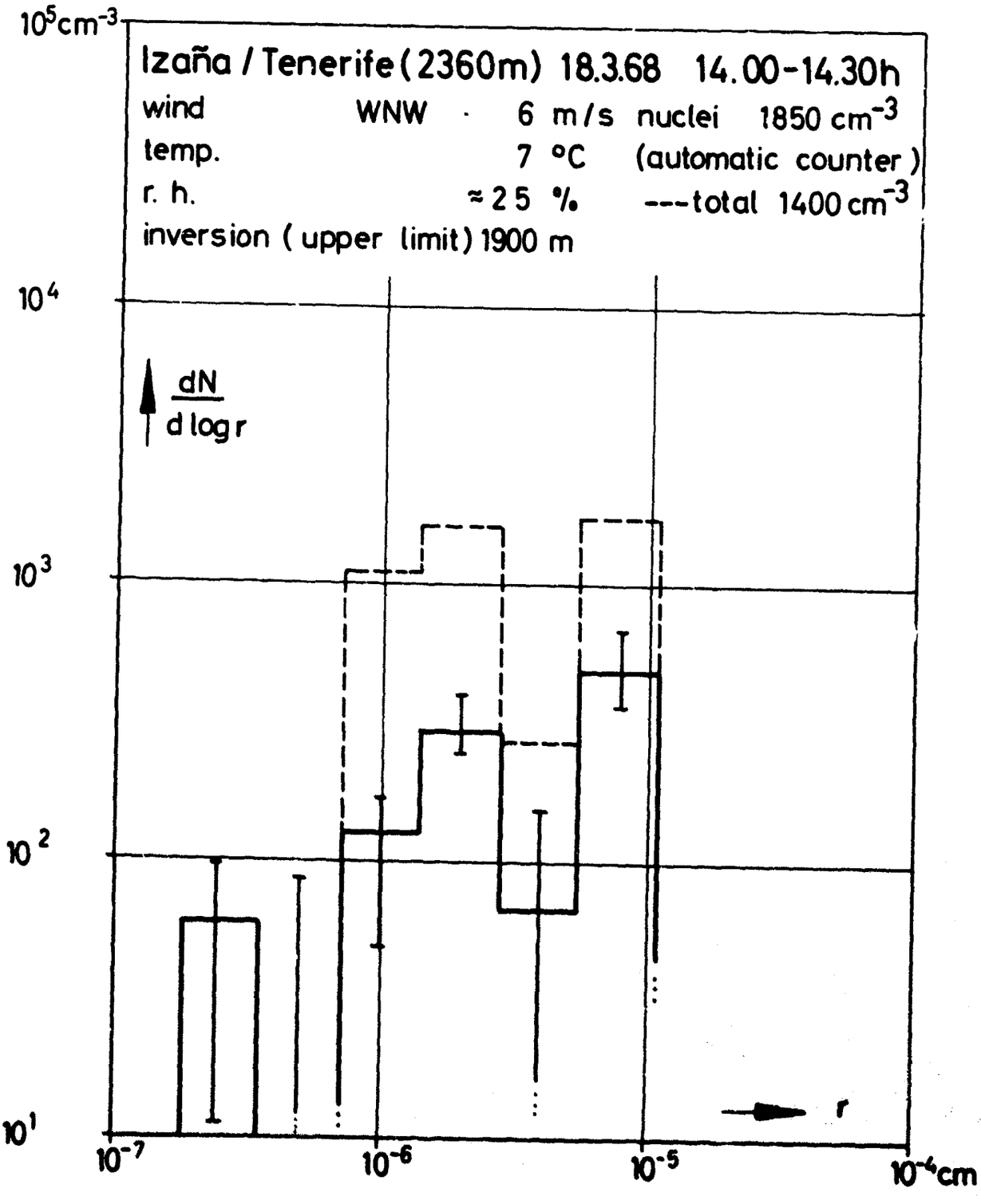
$10^5 cm^{-3}$
Izaña / Tenerife (2360m) 18.3.68 14.00-14.30h
wind WNW · 6 m/s nuclei 1850 cm^{-3}
temp. 7 °C (automatic counter)
r. h. ≈ 25 % ---total 1400 cm^{-3}
inversion (upper limit) 1900 m
10^4
10^3
10^2
10^1
$\frac{dN}{d \log r}$
r
10^{-7}
10^{-6}
10^{-5}
10^{-4}cm

Fig.: 27

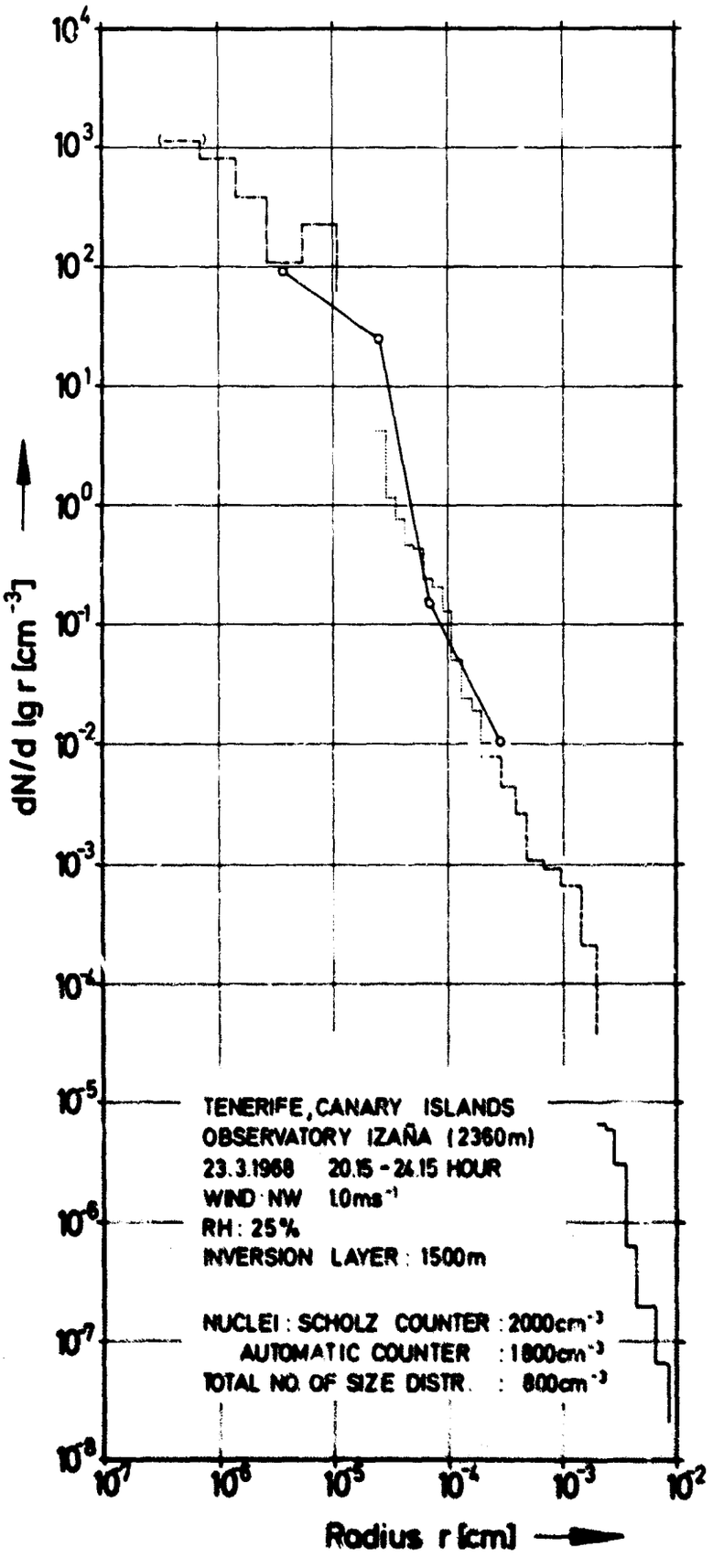
dN/d lg r [cm⁻³]
Radius r [cm]
TENERIFE, CANARY ISLANDS
OBSERVATORY IZAÑA (2360m)
23.3.1968 20.15 - 24.15 HOUR
WIND NW 10ms⁻¹
RH: 25%
INVERSION LAYER: 1500m
NUCLEI: SCHOLZ COUNTER: 2000cm⁻³
AUTOMATIC COUNTER: 1800cm⁻³
TOTAL NO. OF SIZE DISTR.: 800cm⁻³

FIG.: 28

Part II: Investigation of the Composition of Atmospheric Aerosol Particles by Measurement of particle Growth due to Absorption of Water Vapor and Organic Vapors.

1 Introduction

In earlier studies (WINKLER, 1969) we developed a method to measure the humidity growth of aerosol particles by determining gravimetrically the weight increase of an aerosol sample which is exposed to different relative humidities. With this method we determined aerosol growth curves in continental and maritime air masses. Except for clear evidence of the presence of considerable amounts of sea salt in oceanic air the growth curves were rather uniform and smooth. They also showed hysteresis for increasing and decreasing humidities. In addition the question arose if and to what extent does aerosol growth occur if exposed to organic vapors instead of water vapor. The study of this effect was expected to give interesting information on the content of the aerosols of organic matter and on the physical structure of natural aerosols. It was the purpose of the work under this contract to obtain information on these problems in accordance with the statement of work:

a) Development and refinement of a gravimetric method to study the growth of artificial and natural aerosols by absorption of water vapor and several organic vapors in order to obtain information on their chemical composition.

b) Performance of measurements of natural aerosols under various meteorological and geographical conditions in order to obtain information on the average composition of natural aerosols.

Work was started on point a) and the development and refinement of the methods was completed to a large extent. It turned out that measurement of growth curves of aerosols in organic vapors apparently modified the samples so that this method is not quite undestructive as originally expected. It further turned out that by dissolving the same sample in a sequence of water and organic solvents more and faster information could be obtained and consequently this method was

given the preference. Since it was originally expected that the contract might be extended another year systematic field measurements listed under point b) could not be performed so that this part of the work is left uncompleted under this contract. The work is, however, continued by support from other sources.

2. Method of measurement.

2.1 Micro balance.

For the present purpose a special micro balance was developed on the basis of a thin horizontal elastic fiber fixed at one end and used at the other end to put the sample on. The deflection of the fiber as a measure of the weight is practically linear and can be determined very accurately with a suitable microscope.

In order to measure growth curves of aerosol samples the elastic fiber with the sample attached to the end is enclosed in a thermostated metal case, through which air of known relative humitidy or organic vapor content is ventilated. Absorption of water or organic solvent by the aerosol sample results in a weight increase which approaches equilibrium after a certain time. By increasing or decreasing the relative vapor saturation by small increments the absorption growth curves of the aerosol samples can be determined in both directions.

The micro balance developed for our purpose had a sensitivity of 1 /ug per devision of the microscopic scale, of which fractions could be estimated. The range visible in the microscope was about 100 /ug; by adjusting the fiber in different positions the useful range could be extended to about 1000 /ug, with uniform sensitivity.

The aerosol sample is deposited on a small and very thin piece of metal foil in order to keep the weight of the sample carrier as low as possible (~ 0.6 mg). The weight of the aerosol sample is deter-

mined by the increase in weight of the foil after deposition. Another weight similar to that of the foil is used to check possible changes of the zero position of the balance.

Fig. 1 shows a diagram of the balance. Two similar balances were available, one of which was constructed of material not affected by organic vapors after we found out that this was not the case for the first balance used for water vapor.

2.2 Variation of relative vapor saturation.

The air circulated through the balance is drawn through a battery of a total of six metal bottles covered inside with blotting paper and containing small amounts of the solvent such as water, ether, acetone etc. (Fig. 2). These bottles are kept at a carefully controlled temperature by a cryostat. The vapor becames saturated within the bottles and its pressure can be determined from chemical tables. After leaving the bottles the air is passed through a preheater into the balance kept by a thermostat and by suitable insolation at a constant, but higher temperature. The temperature difference cryostat-balance gives the relative vapor saturation.

The cycle through the cryostat bottles, the balance and the pump is a closed one. For studies with organic vapors the air within the cycle is dried to exclude the influence of water vapor. The"dry weight" of the samples can be determined by flushing the balance with dried air.

With this arrangement the relative vapor saturation can be varied between 20% and 97%. For water vapor the error is less than 1%, for organic vapors it depends on the accuracy of the tables and is smaller than 2%.

2.3 Aerosol sampling.

The samples are taken by means of a slit impactor which collects particles > 0.1 μ radius. The aerosol is deposited on a small and thin aluminium foil. The great advantage of impactors consists in concentrating large amounts of aerosols on small surfaces. This makes it possible to keep the foil small and the weight ratio of sample to foil high.

2.4 Calibration of the microbalance and accuracy of the measurement.

In accordance with CUNNINGHAM and WERNER (1949) the microbalance was calibrated by putting small amounts of a carefully prepared KNO_3 solution by a micro burette on the metal foil. The salt residues after drying were used for calibration.

The calibrations turned out to be completely linear in the range used. The standart deviation for both balances was about 0.2 μg, the maximum errors were smaller than 0.5 μg.

In order to avoid changes in the zero position due to incomplete elasticity of the fiber the load of the balance was always kept approximately constant also if not in use. The aluminium foils used differed by not more than 10 μg from their average weight. Remaining small variations of the zero position can be eliminated, because they appear to be reproducible. The zero position is determined before and after each measurement, by using a standart weight.

Another error in determining the weight increase m/m_o (m = mass of the sample at vapor pressure, p, m_o = mass of the sample for $p = 0$) can occur in the determination of m_o, if the sample at $p = 0$ is not completely dried. m_o is determined twice before and after the measurements. If differences are observed the lowest value for m_o is

used.

2,5 Test of the method by use of known salts.

A very efficient way of testing the method is by measuring the growth curves of known salts. If tables are available for relative vapor saturation as function of the concentration of a salt solution the ratio m/m_o can be calculated and compared with measurements. Fig. 3 shows that the agreement is good. With increasing humidity the transition from crystal into a droplet occurs very sharptly at the humidity of the saturated solution. With decreasing humidity the solution becomes supersaturated and crystallisation occurs at a somewhat lower humidity. This branch of the curve is time dependent and not reproducible and will be discussed later (Section 4).

3. Studies of the shape of the growth curves with humidity of samples of natural aerosols.

3,1 The problem.

Fig. 3 shows that the growth curve of a pure salt is characterized by the critical relative humidity for the transition from crystal into droplet. Previous studies (WINKLER) of natural aerosol samples, of which Fig. 4 gives typical examples, showed rather smooth curves, except in maritime air masses, where the dominant NaCl content from sea salt results in a more or less pronounced growth rate near 75% relative humidity. The character of the growth curves is therefore quite different for natural aerosols and pure salts and the question arises why this is so. Besides this difference the total growth of natural aerosols is also smaller than of pure salts. This latter phenomenon was thought to be caused by the presence of insoluble matter according to the concept of mixed aerosols (JUNGE, 1952). The decrease of total particle growth of atmospheric particles consisting of a mixture of soluble and insoluble matter can be calculated, but nothing is known about the mutual influence of the vari-

ous soluble and insoluble components and why such mixtures result in smoothed curves as observed for natural aerosols.

From physico-chemical concepts it can be expected that there should be considerable influence among the various ionic constituents in a mixed solution on their solubility. Salts with the same ions will influence each other according to the law of mass action. Different ions will effect each other through changes of the activity coefficients. Because of lack of data it is practically impossible to predict the behavior of a given ionic mixture. We decided, therefore, to run a number of tests for mixtures of known composition in order to see, at least qualitatively, what effects might be expected. In these studies we found two effects which tend to smooth steps in growth curves. The more important one is due to the mutual influence in solutility of different ions, the second one is connected with the presence of insoluble matter and is most likely caused by absorbtion phenomena at its surface.

3.2 Growth curves of polyionic mixtures.

Chemical analysis of the natural aerosol (JUNGE, 1963, JUNGE and SCHEICH, 1967) have shown the presence of several ions, e.g. Na^+, K^+, NH_4^+, $SO_4^=$, CL^-, NO_3^-. Mixtures of these ions were prepared and tested. We succeeded in obtaining growth curves which were similar to those of the natural aerosols. The measurements indicate that both the composition of the components and their number is important. A few examples will demonstrate this.

Fig. 5 shows a test in which the number of components was stepwise increased. The composition of the salts was primarily chosen in such a way that new ions were added, so that the influence of solubility products is strongly reduced. We see that curve d with five components results in a curve very close to a typical example of a continental aerosol.

In these runs the total amount of soluble matter was measured at relative humidities of less than 1% before and after each run, to make sure that no loss of material occured due to possible escape of ion combinations which resulted in volatile compounds such as HCl or NH_3. It was, however, not tested, if some material escaped, while drying the sample for the first time.

The example in Fig. 5 shows that mixtures of ions can result in both smooth growth curves and also considerable reduction of total growth as compared with single salts, e.g. NaCl. The growth curves of natural aerosols could, therefore, in principle be explained without the presence of insoluble matter. Since analysis shows that considerable fractions of insoluble matter are present in natural aerosols, it is most likely that both effects are involved to various degrees.

It is quite evident that the growth curves of individual salts are modified qualitatively and quantitatively by addition of other ions and that the composite growth curves can not be obtained by any simple additive procedure, except for high humidity according to Raoults Law.

Another example, of mutual influence between various ions is shown in Fig. 6. Curve a shows a mixture with the same number of components as curve d in Fig. 5 but with a pronounced step at 69% relative humidity. Addition of HCl even increases this step (curve c), but addition of H_2SO_4 (curve b) modifies the growth curve considerably. It should be mentioned that the mixture of curve a, Fig. 6 contains salt combinations which, if being present alone, would be soluble below 60%.

3.3 Mutual influence between soluble and insoluble matter.

In view of the fact that natural aerosols are always composed of a mixture of soluble and insoluble matter (concept of mixed particles) we tested the mutual influence between these components in artificial muxtures. Fig. 7 gives an example. Here we prepared mixtures of NaCl with three different forms of SiO_2 which differ primarily in grain size, i.e. in the ratio of absorbing surface to mass. In the sample b the insoluble particles had radii between 0.1 and 1 /um (grinded sand), in sample c between 0.01 and 0.05 /um (Aerosil) and in sample d the inner surface of the porous material (silicagel) was about 400 m^2/g. The mixtures were prepared in such a manner that the insoluble fraction was always about 65% of the total weight of the sample. The data plotted in Fig. 7 give the amount of water absorbed with reference to the weight of NaCl so that the curves reflect the influence of the insoluble matter on the solubility of NaCl. The curves do not show, therefore, the reduction of the growth curves with reference to total weight which is the basis for previous calculations for mixed particles in the literature (see e.g. JUNGE, 1963).

The calculations of these reductions would be correct if the curves in Fig. 7 would be those of pure NaCl (curve a). But we see two kinds deviation from these curves:

1. The curves of NaCl are smoothed by the presence of SiO_2, curve b, c and d.
2. The total water absorption of NaCl increases somewhat in the presence of SiO_2 and this effect is larger for larger absorption surfaces. Curve e shows the growth curve for silicagel without NaCl indicating an absorption of about 65% of water at 95% relative humidity. Comparison of the curves a,d, and e shows that growth of the system silicagel plus NaCl is larger than the sum of the individual effects

From Fig. 7 we can conclude that the presence of finely divided insoluble matter in aerosol particles will not only reduce total growth according to the concept of mixed particles but will modify the shape of the growth curves, of the soluble components, in particular it will tend to smooth the growth curves of pure salts. Similar results were obtained for other salts, e.g. for $MgCl_2$. The same effect can be demonstrated for natural aerosols if the soluble and insoluble fractions are seperated. This seperation can be achieved by the following process: A droplet of very pure water is run over the sample and transfered after a while on a seperate plate and dried. This is repeated several times to make sure that no soluble matter is left with the aerosol sample. Fig. 8 shows growth curves of the original sample and of the soluble and insoluble fraction after seperation for three different aerosols. The mixture absorbs more water than both components individually particularly in the range between 30 and 70% relative humidity.

We can conclude from these experiments that the simple concept, by which the growth curves of mixed nuclei are calculated on a volume basis, is only a rough approximation. We can in general distinguish three effects by which this concept is modified

1. Smoothing of grwoth curves due to the presence of several different ions and the presence of insoluble matter with absorbing surfaces.
2. Reduction of total growth due to the presence of several different ions.
3. Enhancement of total growth due to interaction between soluble and insoluble components.

We feel that at least qualitatively these effects can explain the shape and the amplitude of the growth curves of natural aerosols in a satisfactory way.

4. Studies of the hysteresis effect.

4.1 The problem.

In our previous studies of natural aerosols we found that the same sample contained less water for stepwise increased humidity than for decreasing humidity. This effect wascalled hysteresis. It can in principle be caused by several processes:

a) Condensation in pores of dry insoluble material, in case of our aerosol samples these pores can be present in the aerosol particles prior to collection or they can be produced between the aerosol particles by collection in many layers in our impactor samples.

b) Supersaturation of salt solutions are easily formed with decreasing humidity in pure salt solutions, resulting in hysteresis below the critical humidity of the salt (humidity of the bulk saturated solution).

c) Spread of organic, water insoluble material in our aerosol samples due to the presence of such material in natural aerosols. Such films would tend to decrease the rate of water exchange during changes of humidity.

The effect a) is known for porous material (e.g. ADAMSON, 1967, COHAN, 1944). In case of process b) and c) one would expect that the effect decreases with time of observation. This time dependance was found in experiments with pure salt solutions for process b). Our measurements indicated no time effect for natural aerosol samples. We concluded therefore that in this case hysteresis was caused primarily by the presence of pores in the samples leaving the question open if the pores were present within the aerosol particles or were produced by the collection process. We tested also the possibility c) by adding to the samples organic material which spreads over the

surface of aqueous solutions (e.g. stearic acid) but we could not produce reliable effects.

We resumed these studies of the hysteresis effect in the contex of the present work.

4.2 Hysteresis for seperated soluble and insoluble fractions of natural aerosols.

Fig. 8 shows that hysteresis of natural aerosols is larger for the composite sample than for either the soluble or the insoluble fraction. The insoluble fraction should have preserved all the pores present in the original sample. It is evident from the small hysteresis effect of the insoluble fraction that process a) is of minor importance at least for our natural aerosol samples. The hysteresis of the soluble fraction is larger than that of the insoluble fraction, it is in general smaller, though sometimes comparable to the effect of the original sample. These observations seem to indicate that hysteresis might be enhanced by mutual influence between soluble and insoluble matter. In order to test this suggestion we made a number of experiments with known substances and mixtures.

4.3 Hysteresis of known materials and mixtures.

Fig. 9 shows hysteresis curves of three insoluble materials with different ratios of surface to mass. Whereas carbon black shows an effect comparable to that of the insoluble fraction of natural aerosols, both aerosil and particularly silicagel show considerable effects. This is in agreement with findings by COHAN (1944).

Fig. 10 shows measurements of salt mixtures with insoluble matter. NaCl shows a higher hysteresis with silicagel (curve b) than with grinded sand (curve a). The salt mixture alone (curve c) shows no hysteresis, but addition of aerosil produces a definite effect

(curve d).

It is evident from all these measurements that the phenomenon is quite complex. Insoluble matter of sufficient inner surface shows hysteresis apparently produced by capillary condensation. It looks as if this effect is not very important for natural aerosols, i.e. that the insoluble matter in natural aerosols has not a very large absorbing surface. Pure salt solutions may show hysteresis or not depending on the possibility of supersaturation which in turn is critically dependend on nucleation processes. There is evidence that the hysteresis in our natural aerosol samples is primarily produced by interaction between soluble and insoluble matter of sufficient absorbtion capabilities. This suggests that the hysteresis which we observe with our samples is due to the aerosols themselves and not to the special way in which the samples are collected. We could not obtain reproducible information on the influence of oil films, but we believe that this is of no great importance for our present problem.

5. Studies of the organic fraction in aerosols.

5.1 Growth curves in organic vapors.

We started measurements of growth curves of aerosols in organic vapors because it was suggested that this might be a useful non destructive method to study the composition of organic fractions in aerosols. Fig. 11 shows a few examples of such growth curves for natural aerosols. The total weight increase seems to be smaller than with water vapor which can be due to the following effects:

a) The density of organic liquid is smaller than one,
b) The soluble fraction of the aerosol in the particular solvent is smaller than that in water,
c) The solubility of the material in the particular solvent is high, so that only small amounts of vapor are absorbed.

The shape of the growth curves is similar to that for water vapor, as expected, but the hysteresis effect is smaller. This small hysteresis effect seems to support the conclusion from the water vapor results that capillary condensation in the insoluble, porous fraction is of minor importance. Otherwise it should be of similar magnitude when using organic vapors.

The possibility to use this method for non destructive analysis depends on the complete reversibility of the absorbtion process in various vapors. If this would be the case, one could expose the same sample to water and to a variety of organic vapors in order to obtain data on the mass fractions of different groups of organic components in the aerosol sample. In order to test the reversibility of the absorbtion process the same sample was exposed to water vapor, aceton vapor and again water vapor. Fig. 12 shows that the second exposure to water vapor indicates less absorbtion than the first exposure, suggesting some modification of the sample with respect to water soluble matter, during the aceton exposure. Because of this effect and the difficulty in quantitative interpretation with respect to b) and c) above we abandoned this method. Instead we developed the "solution technique" which seems to be more straight forward and which appears to work better and faster. Before discussing this method we will describe some measurements of mass decrease of aerosol samples due to heating.

5.2 Volatile material in aerosols.

Most inorganic substances, which were shown to be present in natural aerosols or which can be expected to be present have negligible vapor pressures below about 100° C. There are many organic substances, on the other hand, which are volative at much lower temperatures. GOETZ and PREINING,(1962), collected aerosol samples in clean and polluted air on chromium foils and heated them to 50 - 70° C. By measuring the light scattered by these samples he found

in most cases a considerable decrease after heating. Although it is likely that this is due to evaporation the possibility cannot be excluded that other processes are involved such as microdestillation, spread of particles on the surface etc. which can also result in a decrease of light scattering capabilities. The presence of large fractions of some organic material in atmospheric aerosols was demonstrated by their solubility in chloroform (GOETZ, 1964).

It was easy to test these interesting observations with our gravimetric method. We heated aerosol samples in steps up to 150° C and determined the loss of weight. Fig. 13 shows two typical examples. With increasing temperature increasing fractions of the sample evaporate, but in each temperature step a certain equilibrium value is reached indicating that always new components are involved when the temperature is raised. The weight losses are quite substantial but it is not certain if only organic materials are involved, since at 150° C also a few inorganic compounds such as NH_4Cl or $(NH_4)_2SO_4$ might decompose. The partial volatility of water soluble material of natural aerosols could be demonstrated by measuring growth curves in water vapor before and after heating. Fig. 14 shows examples of this effect. The sample of 17.9.68 is the same in Fig. 13 and 14. A decrease of aceton soluble matter by heating is demonstrated in Fig. 11, b.

These tests must be considered priliminary and were performed primarily to obtain a survey for the various effects and the possibilities of the method. It is apparent that these methods may be quite suitable to obtain interesting information on atmospheric aerosols.

5.3 The solution method.

Organic substances in aerosols are of increasing interest in polluted (SAWICKI, 1964, 1965; RUBIN, 1952) as well as in unpolluted at-

mospheres (WENDT, 1965, 1960; GOETZ, 1965). But our information on these materials is up to now very scanty. We were therefore interested in developping a suitable method to obtain such information on a quantitative basis. Since absorbtion measurements in various vapors were not reproducible enough and too tedeous we tried another method which proved to be more successful. In this "solution method" the aerosol samples are exposed to various solvents in a certain sequence and the losses in weight are measured. In each step the exposure to the solvent is repeated in order to ensure that no soluble material is left. In most cases we started with water followed by organic solvents with increasing capability to disolve organics (fluotropic equence). This gives information on the presence of certain groups of organics present in the aerosols and on their mass fraction.

An extension of this method consists in the collection of a number of equal samples which are treated with the same solvents but in different sequences. This program is closely connected with another one using thin layer chromatography of these aerosol samples. In this way we hope to obtain a survey about the main groups of organic substances in polluted and unpolluted aerosols.

An important requirement for a successful application of the solution method is that the individual solution steps do not remove any insoluble material from the sample by the solution process. To test this requirement always two identical samples were treated in the same way. The results are given in Table 1; they show that the requirement is satisfied. The deviations are smaller than 4% of the total mass, but can be reduced to about 2% by very careful work. With fractions of the organic matter of about 15 - 30% in the aerosols it will be possible to obtain quantitative information by this method. These tests were made with tetrahydrofuran which is a strong solvent. We have not yet made measurements with other solvents, but we expect a similar behavior.

Table 1. Tests for solution method.

Total Mass = 100%. The first and the second figure refer to the first and the second impactor respectively. The numbers in parantheses give the sequence of extraction.

	Water soluble fraction		Tetrahydro-furan-soluble fraction		volatile fraction		insoluble fraction	
1.	29.7	31.3 (3)	15.1	15.5 (1)	16.6	18.8 (2)	38.6	34.5
2.	31.2	31.5 (2)	15.3	16.2 (1)	--	--	54.5	52.4
3.	22.7	22.2 (3)	0.3	0.2 (2)	24.0	24.9 (1)	53.0	53.0
4.	28.0	28.0 (3)	0.1	6.0 (2)	18.5	18.5 (1)	47.4	47.5
5.	57.4	56.3 (1)	8.1	7.7 (2)	1.4	0.0 (3)	33.2	36.0
6.	44.1	45.0 (1)	14.0	16.4 (2)	0.0	0.0 (3)	42.0	38.6
7.	38.4	38.9 (2)	23.1	22.5 (1)	1.5	1.7 (3)	37.0	37.0
8.	59.3	56.0 (1)	5.6	6.4 (2)	0.0	1.0 (3)	35.2	36.6
9.	35.1	37.3 (2)	27.2	27.4 (1)	0	0 (3)	33.7	35.3
10.	35.0	36.1 (2)	28.9	24.6 (1)	0	0 (3)	36.9	40.1
11.	52.3	50.3 (1)	8.4	7.3 (2)	3.0	3.9 (3)	36.3	36.8
12.	38.4	37.5 (2)	24.0	25.9 (1)	2.9	0.8 (3)	34.5	35.8
13.	68.0	67.4 (1)	5.8	6.3 (2)	--	--	26.2	26.4
14.	53.4	54.4 (1)	15.0	16.1 (2)	--	--	31.7	29.5
15.	37.4	38.4 (1)	25.6	24.9 (2)	--	--	37.0	37.7

6. Appendix.

The solution method was first applied to check the operation of nozzle impactors used in the study to collect the aerosol samples. The collection efficiency of such impactors is generally increased if the collection surface is coated with a sticky film of silicon oil etc. The study of growth curves, however, does not allow the use of such materials. On the other hand the impactor is the only collection method capable of concentrating a sufficient amount of material on a small area so that the weight ratio of sample to collection plate becomes large enough.

The experiments discussed in the following are very preliminary and shall only serve to demonstrate the kind of studies which can be performed and the kind of results which can be expected. Final measurements are in preparation.

The experiments are concerned with the collection efficiency of impactors for natural aerosols as a function of the relative humidity. In one set of experiments we used two identical impactors in parallel in front of which the air is passed through two tubes of equal size, one of which was wet inside. The sample collected at higher humidity ($> 75\%$) had approximately twice the mass of the low humidity sample. ($< 65\%$). This difference can not be explained solely by the growth of the aerosol particles due to the increase in humidity. It must be assumed that in addition the collection efficiency is increased due to the higher water content of the particles. In earlier studies we found that in general the collection efficiency of natural aerosols is rather high on a plain surface in an impactor if the relative humidity is above 70%.

The relative humidity of the two samples was also different. The dry impactor showed a higher fraction of soluble matter, although the absolute amount was still smaller than with the wet impactor. The

organic fractions were about the same in both samples.

In another set of experiments both impactors were operated in series. Comparison of the composition of the samples gives information on the collection efficiencies of insoluble and water soluble material and on material soluble in various organic solvents. Use of the dry and wet tube in this case gives additional information on the dependance of the quantities on the relative humidity of the air sampled. Preliminary experiments indicate considerable differences for the different kind of material and pronounced variations with humidity.

To far as we see now there are three processes involved to produce these effects of the humidity:

a) growth of particles by humidity
b) preferred attachment of water containing "moist" particles
c) better collection efficiency of the collecting surface after formation of the first layer of "moist" particles.

7. References.

1. ADAMSON, A. (1967): The Physical Chemistry of Surfaces. 2.ed. Intersciences Publishers, New York 1967.
2. COHAN, L.H. (1944): Hysteresis and the Capillary Theory of Adsorption of Vapors. J.Am.Chem.Soc. 66, 1944, 98.
3. CUNNINGHAM, B.B., WERNER, L.B. (1949): The first isolation of plutonium. J.Am.Chem.Soc. 19, 1949, 1521.
4. GOETZ, A., PREINING, O. (1961): Beiträge zur Kenntnis des atmosphärischen Aerosols. Acta Physicy Austriaca XIV, 1961, 305.
5. GOETZ, A. (1964): Final Report Fourth Yellowstone Field Research Expedition 1964, 58.
6. GOETZ, A. (1965): Constitution of Aerocolloidal Particulates above the Ocean Surface. Proceedings of the International Conference on Cloud Physics Tokyo 1965, 42.
7. JUNGE, C. (1952): Die Konstitution des atmosphärischen Aerosols. Ann.Met. 5, 1952, 1 - 55.
8. JUNGE, C. (1963): Air Chemistry and Radioactivity. Academic Press, New York, London 1963.
9. JUNGE, C., SCHEICH, G. (1967): Studien zur chemischen Zusammensetzung atmosphärischer Aerosole unter besonderer Berücksichtigung des Gehaltes an freien Wasserstoffionen. Met.Rundschau 20, 1967, 165.
10. RUBIN, S. (1952): Liquid Particles in Atmospheric Haze. J.Atm. and Terrestrial Phys. 2, 1952, 130.
11. SAWICKI, E. (1964): Application of thin Layer chromatography to the Analysis of Atmospheric Pollutants and Determination of Benz (a) pyrene. Analyt.Chemic. 36, 1964, 497.
12. SAWICKI, E., MECKER, J.E., MORGAN, M.J. (1965) The Composition of Air Pollution Effluents in Terms of Aza Heterocyclic Compounds and Polynuclear Aromatic Hydrocarbones. Int.J. of Air and Water Pollution 9, 1965, 219.

    SAWICKI, E., McPherson, S.P., STANLEY, T.W., MECKER, J.E., ELBERT, W.C. (1965): Quantitative Composition of the Urban Atmosphere in Terms of Polynuclear Aza Heterocyclic Compounds and Aliphatic and Polynuclear Aromatic Hydrocarbons. Int.J. of Air and Water Pollution 9, 1965, 515.
13. WENT, F.W. (1960): Organic Matter in the Atmosphere, and its possible Relation to Petroleum Formation. Proc.Nat. Acad.Sci.USA 46, 1960, 212.
14. WENT, F.W., RASMUSSEN, R. (1965): Volatile Organic Material of Plant Origin in the Atmosphere. Proc.Nat.Acad.Sci. USA 53, 1965, 215.
15. WINKLER, P. (1969): Wachstum von Aerosolteilchen mit der relativen Feuchte nach einer gravimetrischen Methode. Ann.Met. Neue Folge Nr. 4, 1969. (to be published).

8. List of Figures.

Fig. 1 Schematic diagram of the microbalance

Fig. 2 Aparatus for vapor pressure variation and air circulation through microbalance.

Fig. 3 Growth curves of the pure salts NaCl, KCl, $MgCl_2$. Comparison between calculated and measured curves.

Fig. 4 Typical growth curves of continental natural aerosols in water vapor. The curves are rather smooth and show a pronounced hysteresis for decreasing relative humidity.

Fig. 5 Growth curves of artificial poly-ionic mixtures. The following table gives the composition of the several mixtures (in weight percent)

	Na^+	Mg^{++}	NH_4^+	Ca^{++}	K^+	Cl^-	SO_4^{--}	NO_3^-
curve a	24.4	9.7				65.9		
curve b	7.3	2.9	19.1			19.6	50.9	
curve c	5.1	2.0	13.3	7.4		13.1	35.6	23.0
curve d	4.4	1.8	11.4	6.4	4.2	11.8	40.7	19.4
curve e	average growth curve of natural aerosols							

Fig. 6 Growth curves of artificial poly-ionic mixtures. The following table gives the composition of the several mixtures (in weight percent).

	Na^+	NH_4^+	K^+	Cl^-	$SO_4^=$	SO_3^-	CO_3^-	CH_3COO^-
curve a	8.3	10.3	19.4	20.5	13.5	10.4	6.3	11.2
curve b	7.0	8.7	16.5	17.3	27.0	8.8	5.3	9.5
curve c	4.9	6.1	11.6	52.?	8.1	6.2	3.8	6.7

Fig. 7 Growth curves of artificial mixtures of soluble and insoluble materials. The insoluble fraction is about 65%. To show the influence of the insoluble matter, the water absorbed by the samples is related to m_{os}, the dry mass of the saltfraction.

curve a Growth curve of pure NaXl

curve b Growth curve of a mixture of 35% NaCl and 65% grinded sand ($0.1 < r < 1\ \mu$)

curve c Growth curve of a mixture of 35% NaCl and 64% Aerosil (Aerosil = SiO_2 $0.01 < r < 0.05\ \mu$)

curve d Growth curve of a mixture of 35% NaCl and 65% porous silicagel

curve e Growth curve of the silicagel fraction of sample d allone

Fig. 8 Growth curves and hysteresis of natural aerosols and the growth of the water soluble and insoluble fractions of the same sample.

curve a natural mixture

curve b water soluble fraction

curve c water insoluble fraction

9. Figures to Part II.

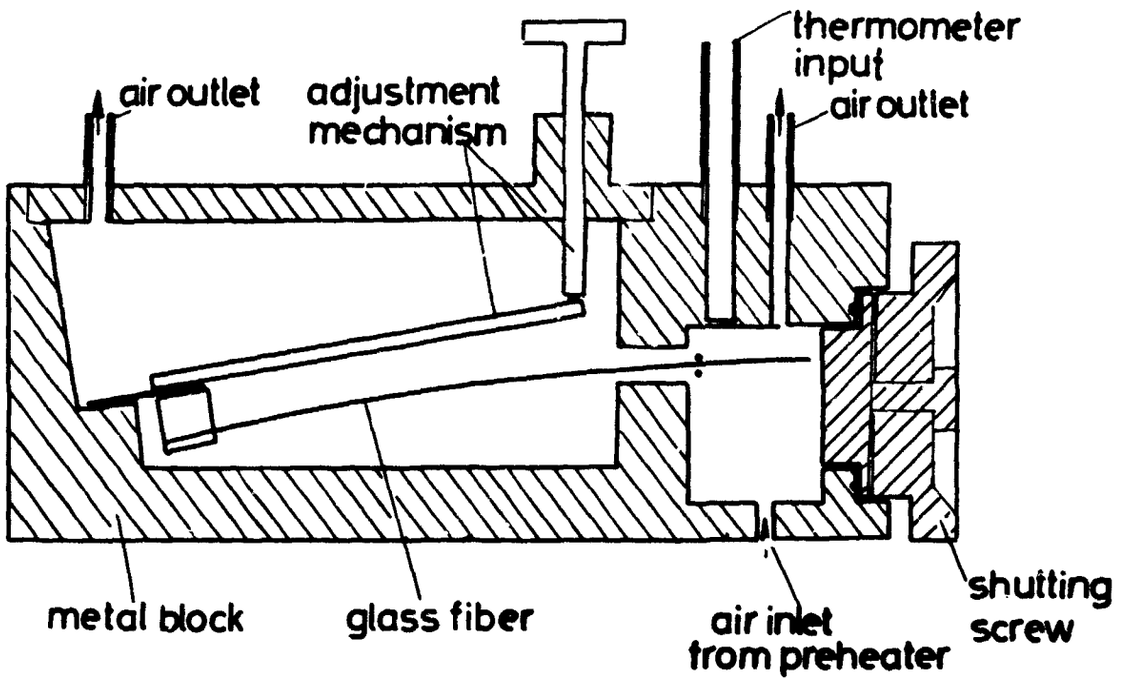

schematic diagram of the microbalance

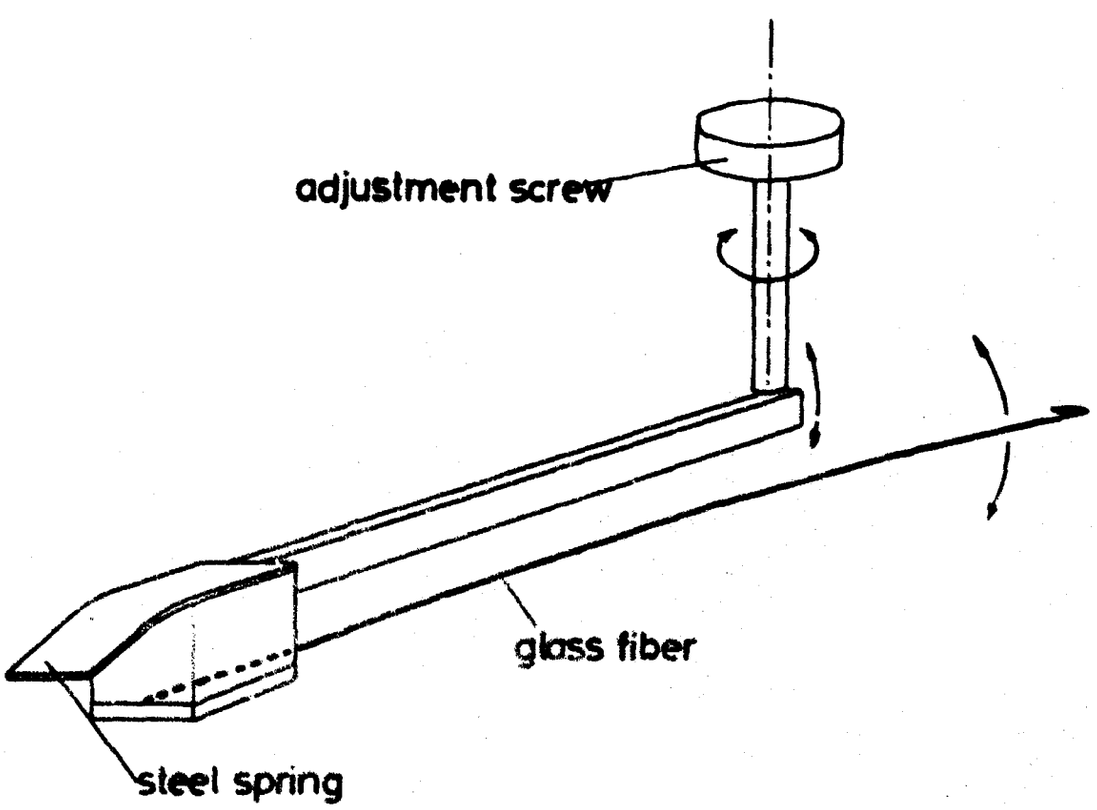

shifter for adjusting the glassfiber

Fig.1

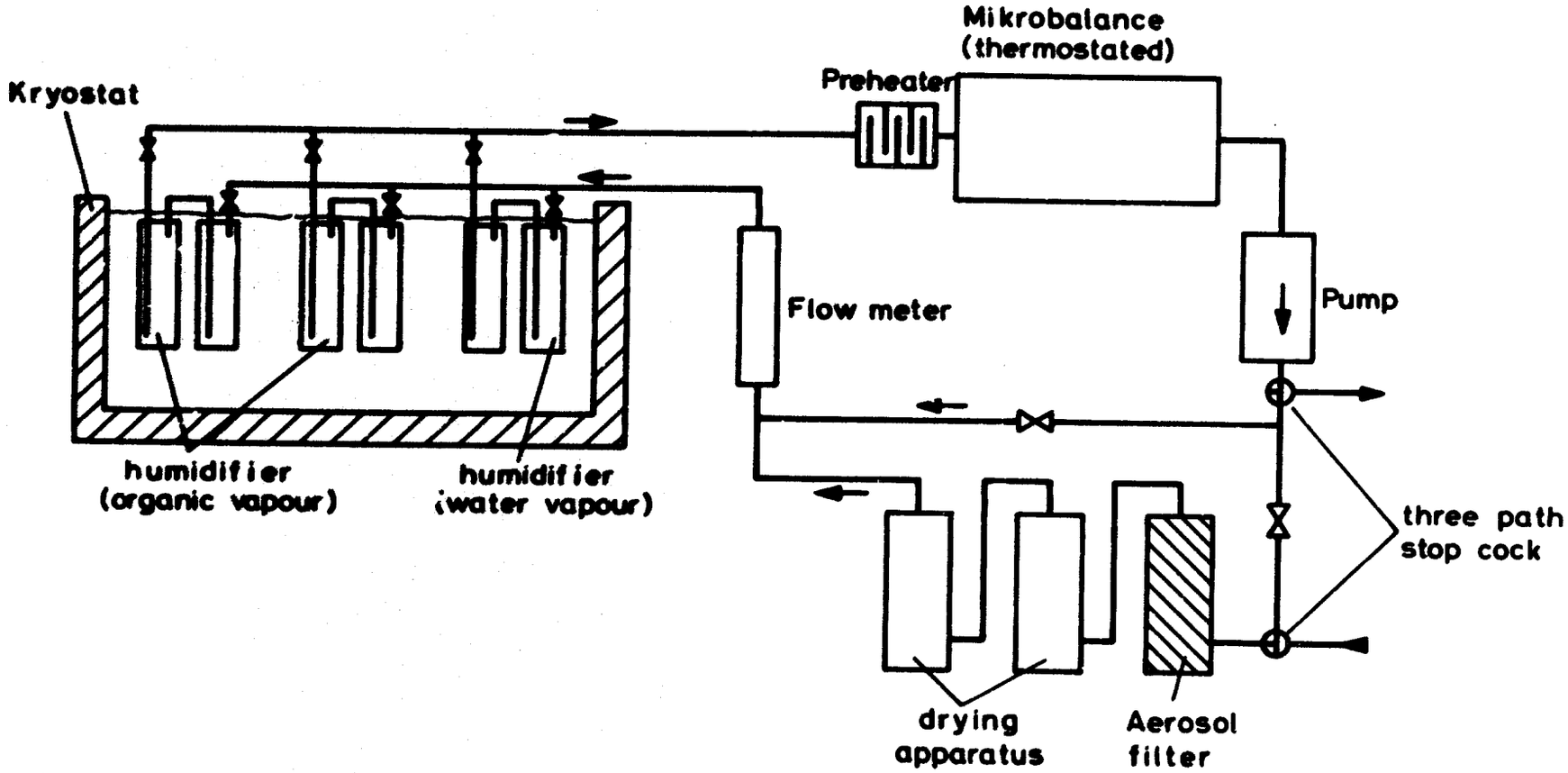

Schematic block diagram of apparatus.

Fig. 2

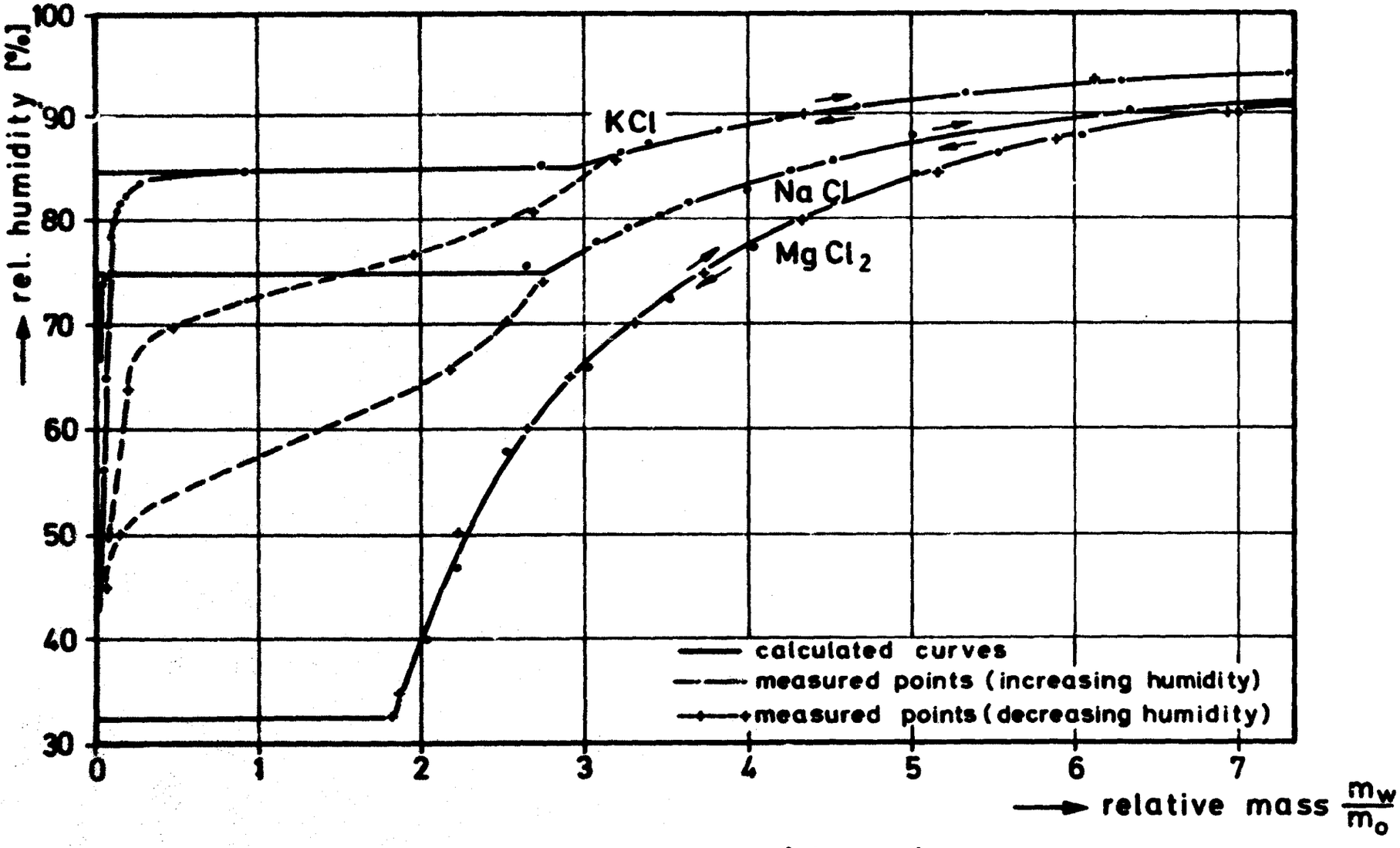

Growth curves of pure salts (25°C)

Fig. 3

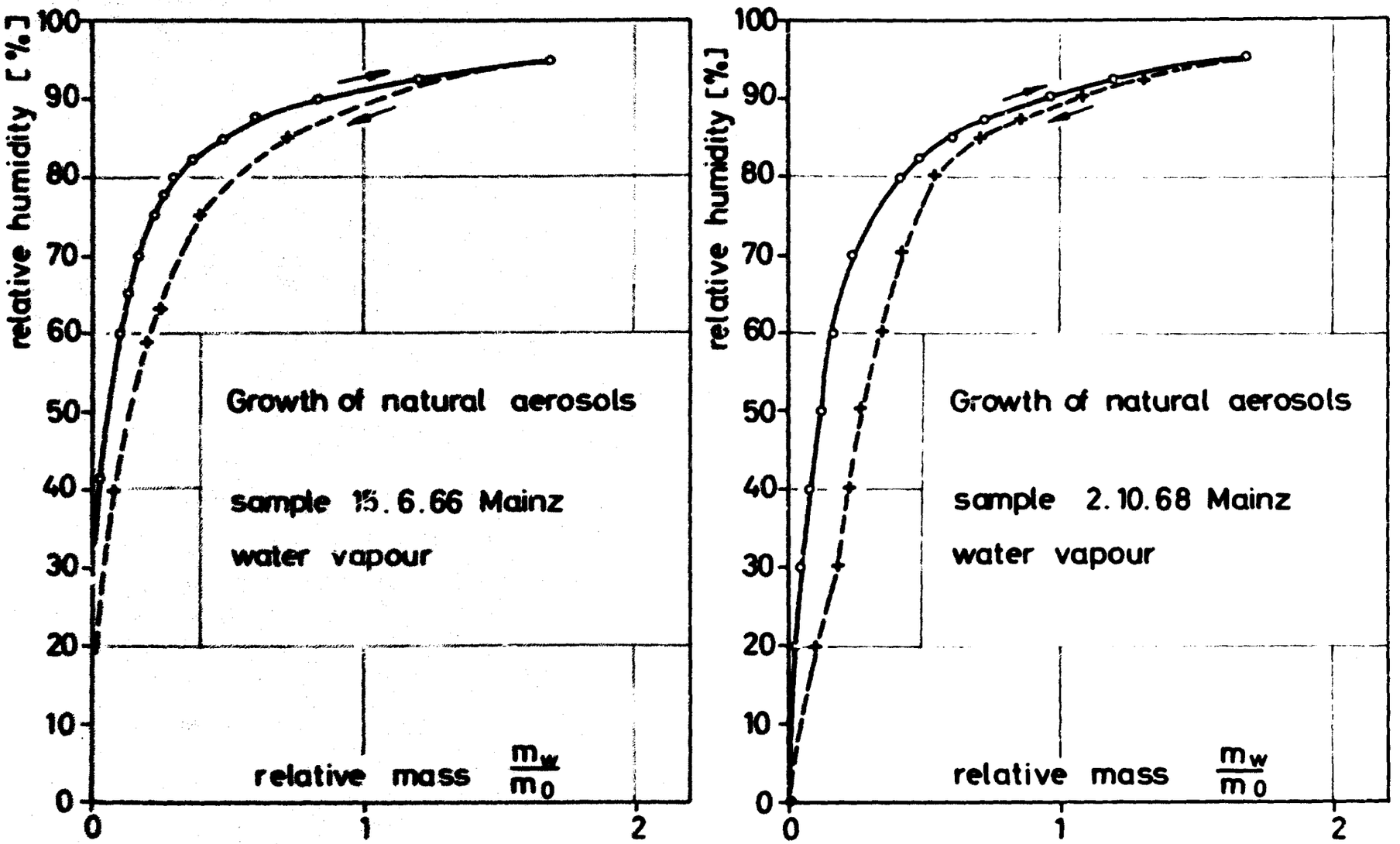
relative humidity [%]
100
90
80
70
60
50
40
30
20
10
0
0
1
2
Growth of natural aerosols
sample 15.6.66 Mainz
water vapour
relative mass $\frac{m_w}{m_0}$
relative humidity [%]
Growth of natural aerosols
sample 2.10.68 Mainz
water vapour
relative mass $\frac{m_w}{m_0}$

Fig.: 4

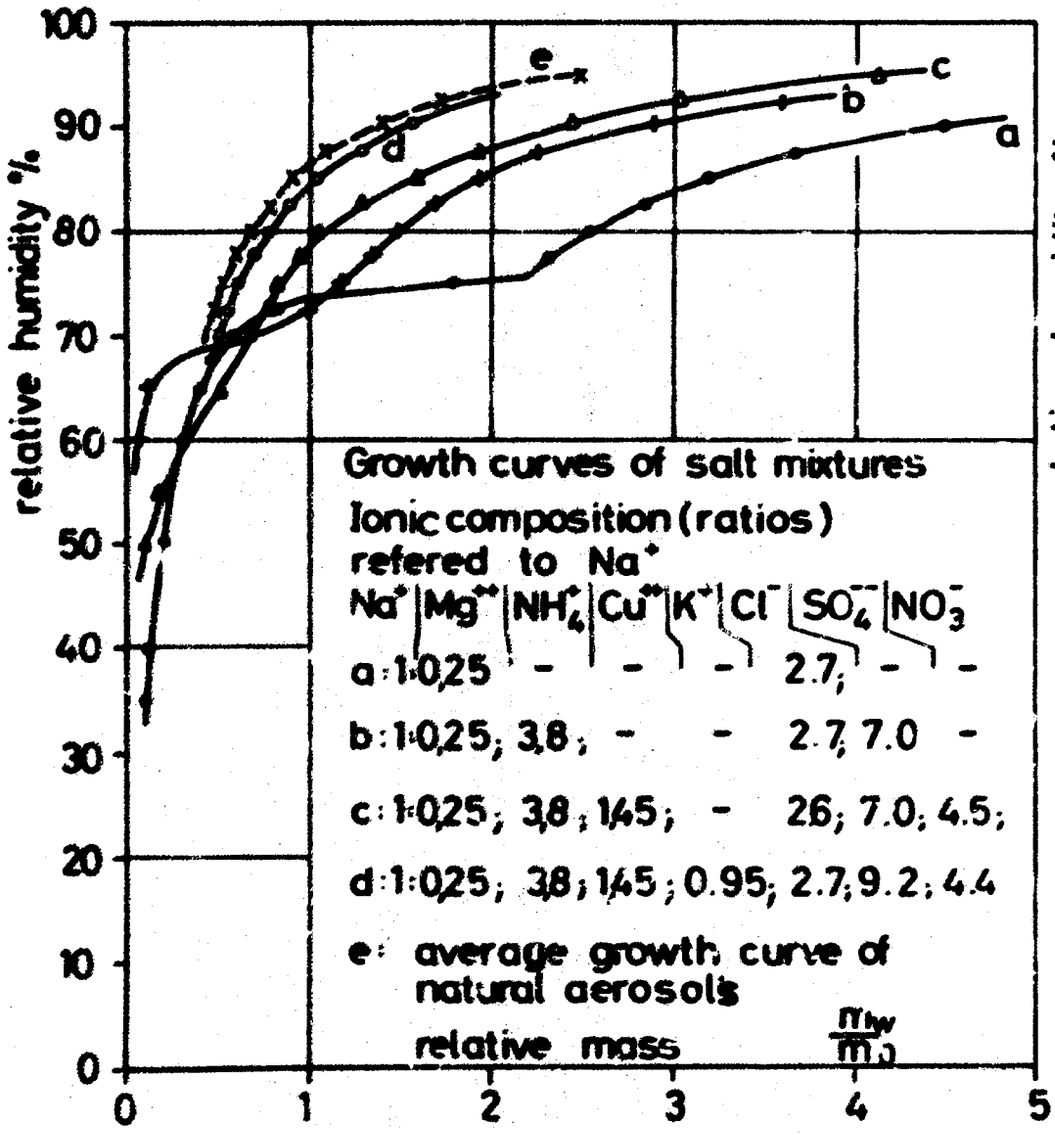
relative humidity %
100
90
80
70
60
50
40
30
20
10
0
0
1
2
3
4
5
a
b
c
d
e
Growth curves of salt mixtures
Ionic composition (ratios)
refered to Na+
Na+ | Mg++ | NH4+ | Cu++ | K+ | Cl- | SO4-- | NO3-
a: 1: 0,25 - - - 2.7; - -
b: 1: 0,25; 3,8; - - 2.7; 7.0 -
c: 1: 0,25; 3,8; 1,45; - 26; 7.0; 4.5;
d: 1: 0,25; 3,8; 1,45; 0.95; 2.7; 9.2; 4.4
e: average growth curve of natural aerosols
relative mass
mw/m0

Fig. : 5

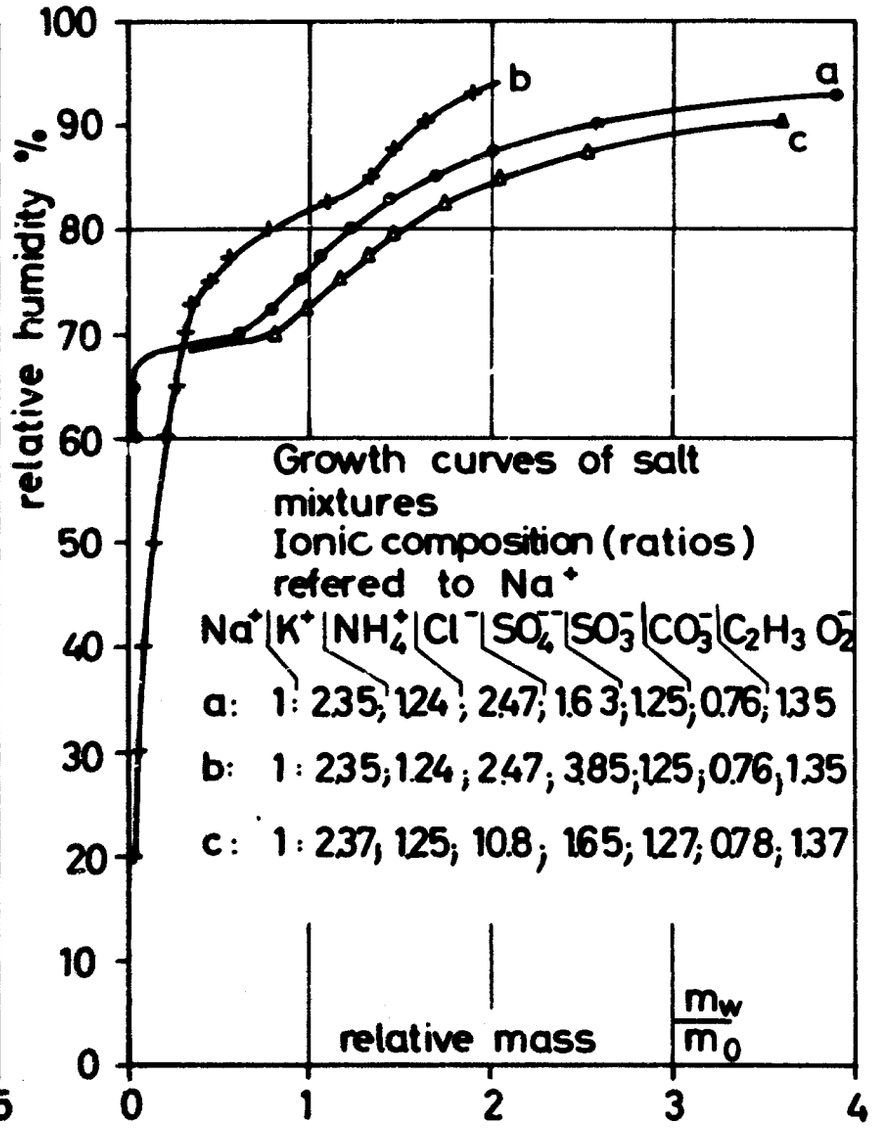
relative humidity %
100
90
80
70
60
50
40
30
20
10
0
0
1
2
3
4
a
b
c
Growth curves of salt mixtures
Ionic composition (ratios)
refered to Na+
Na+ | K+ | NH4+ | Cl- | SO4-- | SO3- | CO3- | C2H3O2-
a: 1: 2.35; 1.24; 2.47; 1.63; 1.25; 0.76; 1.35
b: 1: 2.35; 1.24; 2.47; 3.85; 1.25; 0.76; 1.35
c: 1: 2.37; 1.25; 10.8; 1.65; 1.27; 0.78; 1.37
relative mass
mw/m0

Fig. : 6

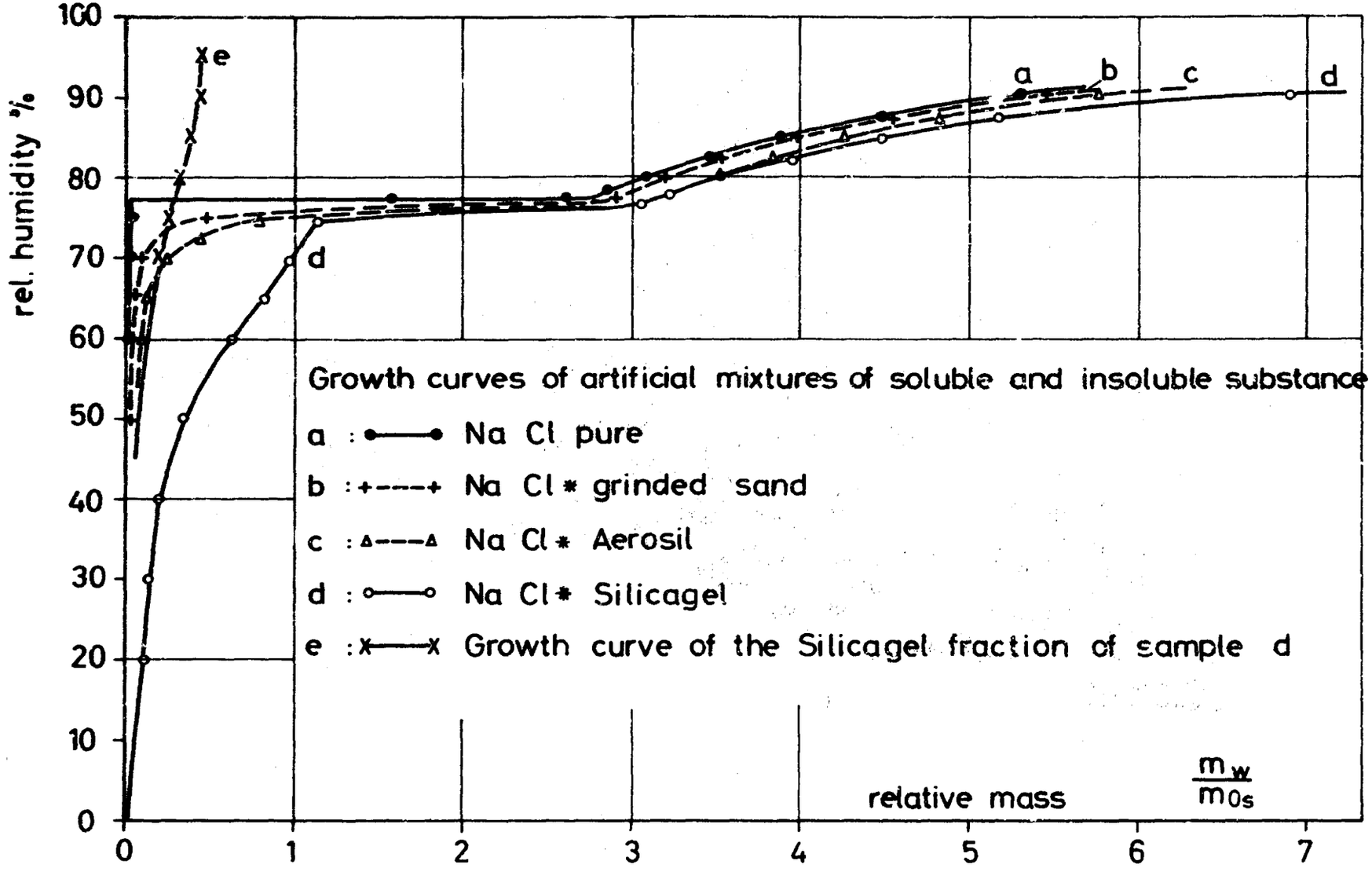
rel. humidity %
100
90
80
70
60
50
40
30
20
10
0
0
1
2
3
4
5
6
7
relative mass
$\frac{m_w}{m_{0s}}$
a
b
c
d
e
Growth curves of artificial mixtures of soluble and insoluble substance
a : Na Cl pure
b : Na Cl * grinded sand
c : Na Cl * Aerosil
d : Na Cl * Silicagel
e : Growth curve of the Silicagel fraction of sample d

Fig.: 7

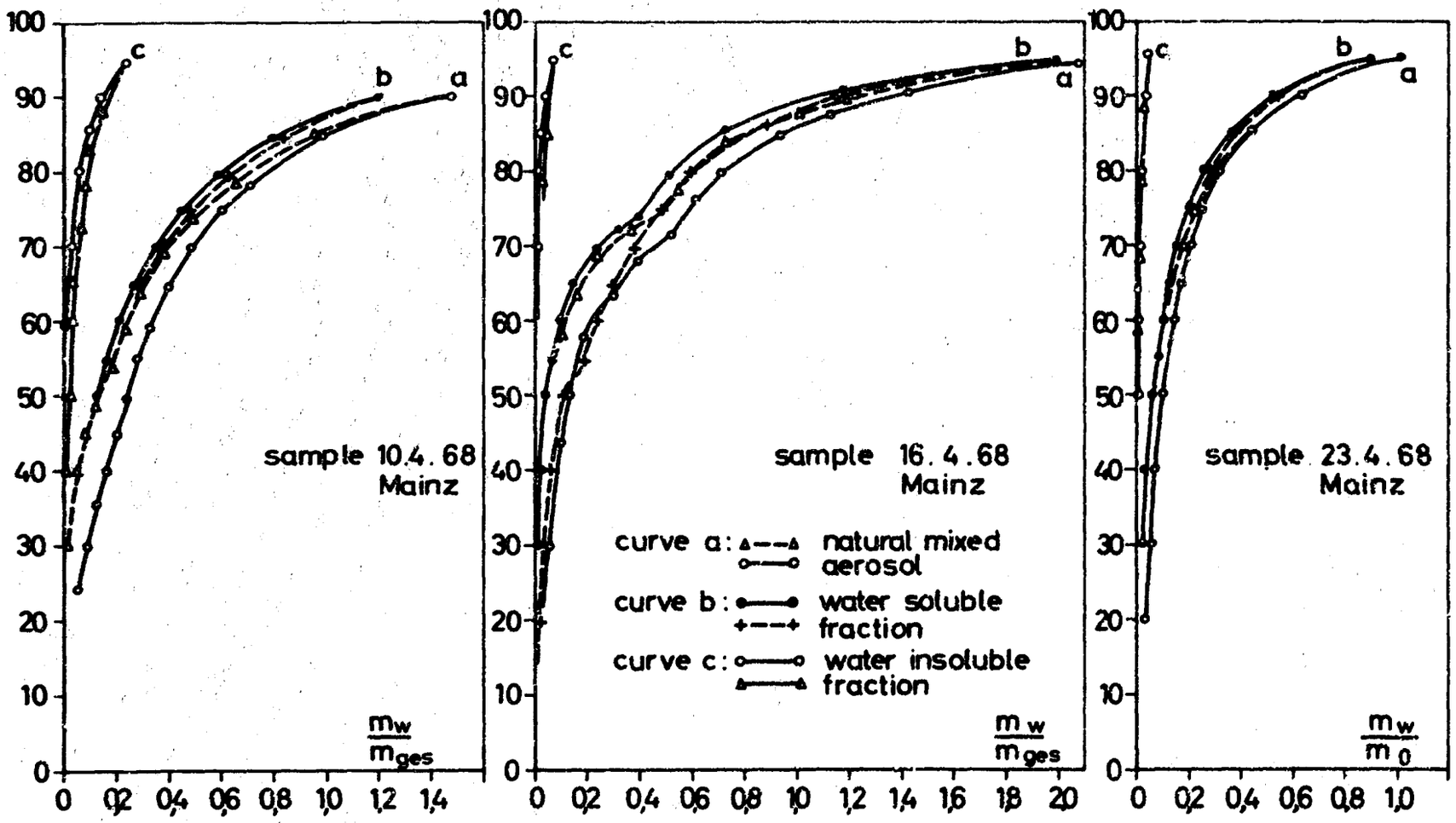
sample 10.4.68
Mainz
sample 16.4.68
Mainz
sample 23.4.68
Mainz
curve a: natural mixed aerosol
curve b: water soluble fraction
curve c: water insoluble fraction
$\frac{m_w}{m_{ges}}$
$\frac{m_w}{m_0}$

Fig.: 8

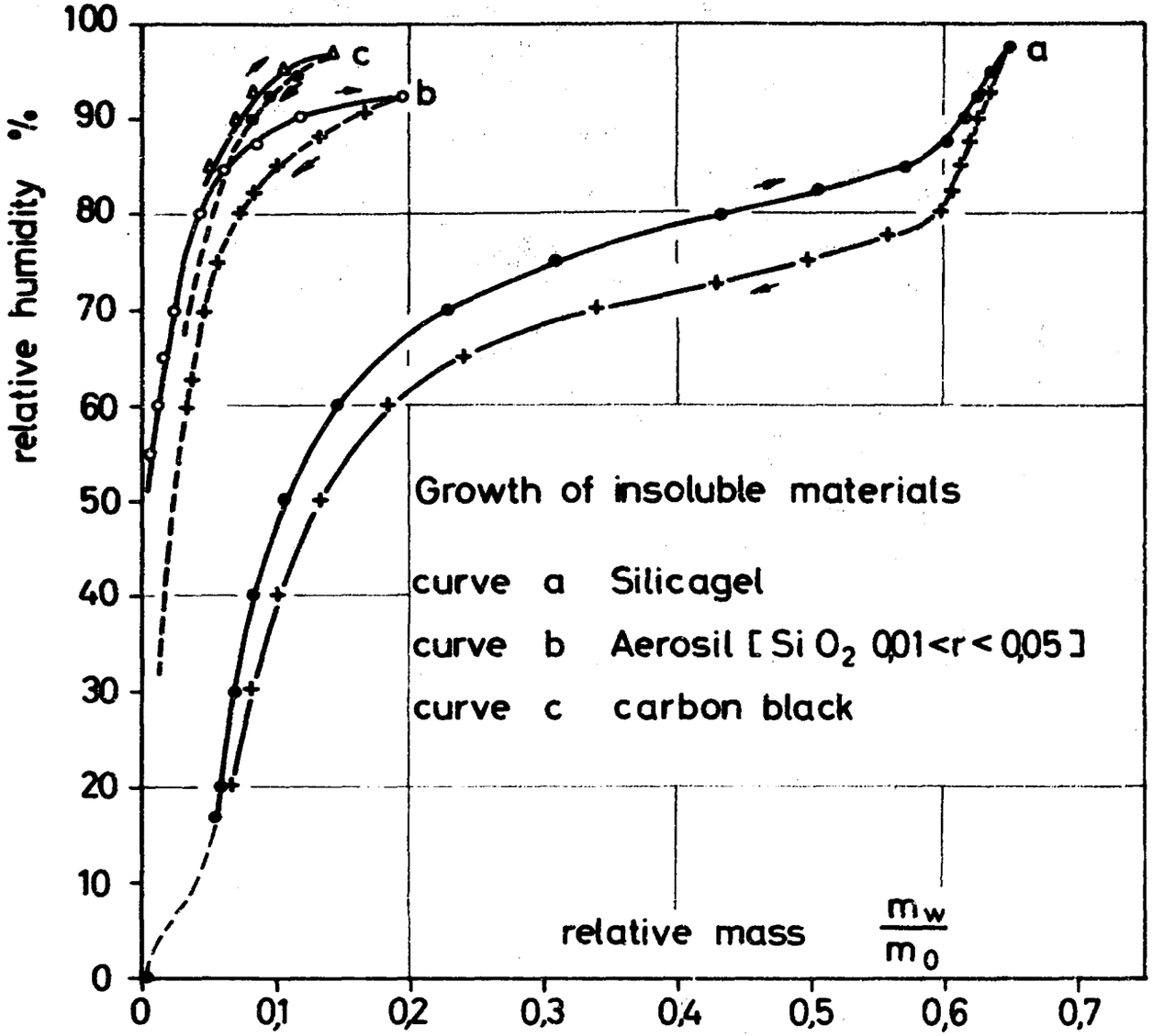
relative humidity %
100
90
80
70
60
50
40
30
20
10
0
0
0,1
0,2
0,3
0,4
0,5
0,6
0,7
a
b
c
Growth of insoluble materials
curve a Silicagel
curve b Aerosil [Si O2 0,01<r<0,05]
curve c carbon black
relative mass mw/m0

Fig. 9

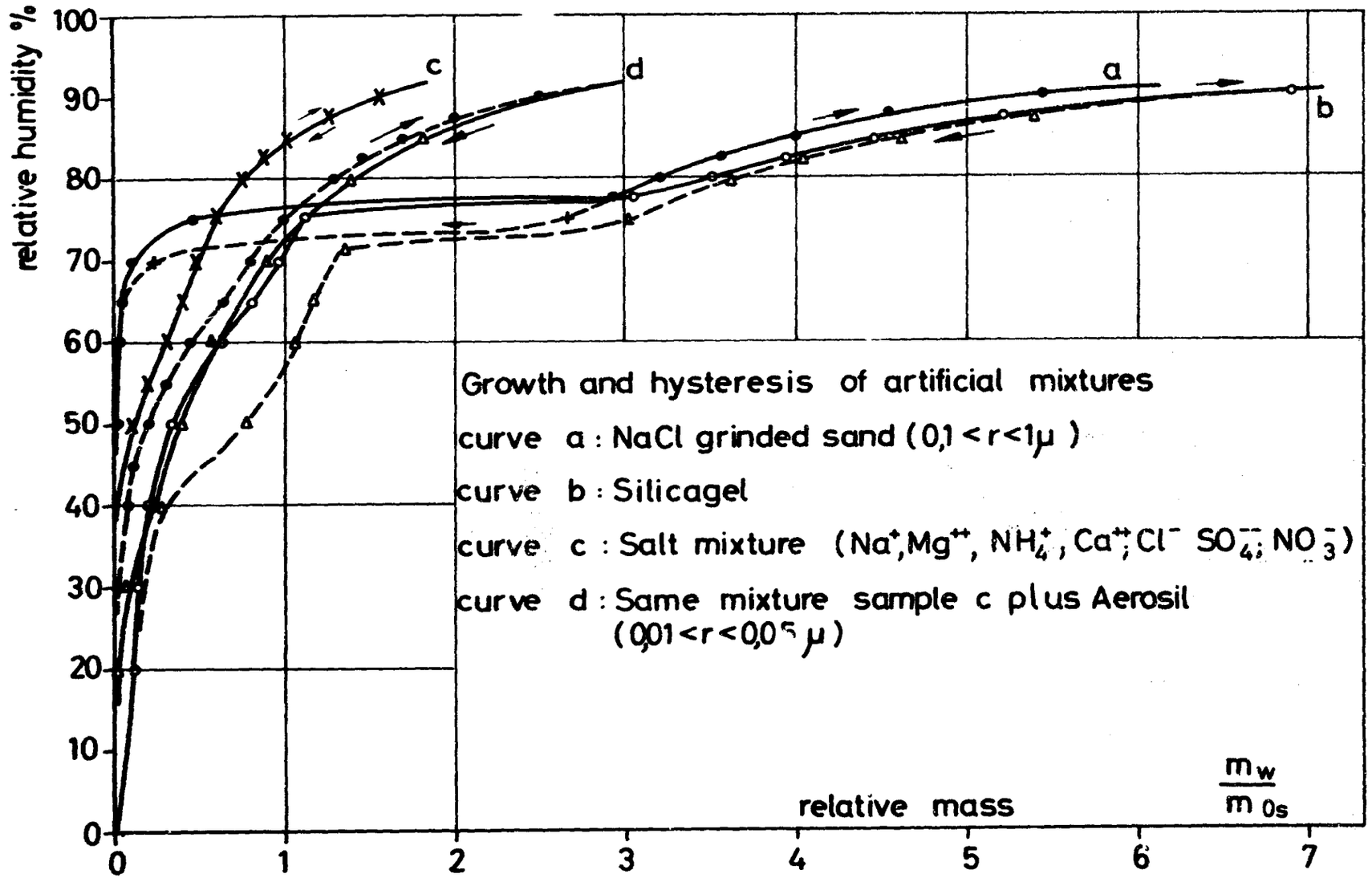
relative humidity %
100
90
80
70
60
50
40
30
20
10
0
0
1
2
3
4
5
6
7
relative mass
$\frac{m_w}{m_{0s}}$
a
b
c
d
Growth and hysteresis of artificial mixtures
curve a : NaCl grinded sand (0,1 < r < 1μ)
curve b : Silicagel
curve c : Salt mixture (Na^+, Mg^{++}, NH_4^+, Ca^{++}; Cl^- SO_4^{--}; NO_3^-)
curve d : Same mixture sample c plus Aerosil
(0,01 < r < 0,05 μ)

Fig.: 10

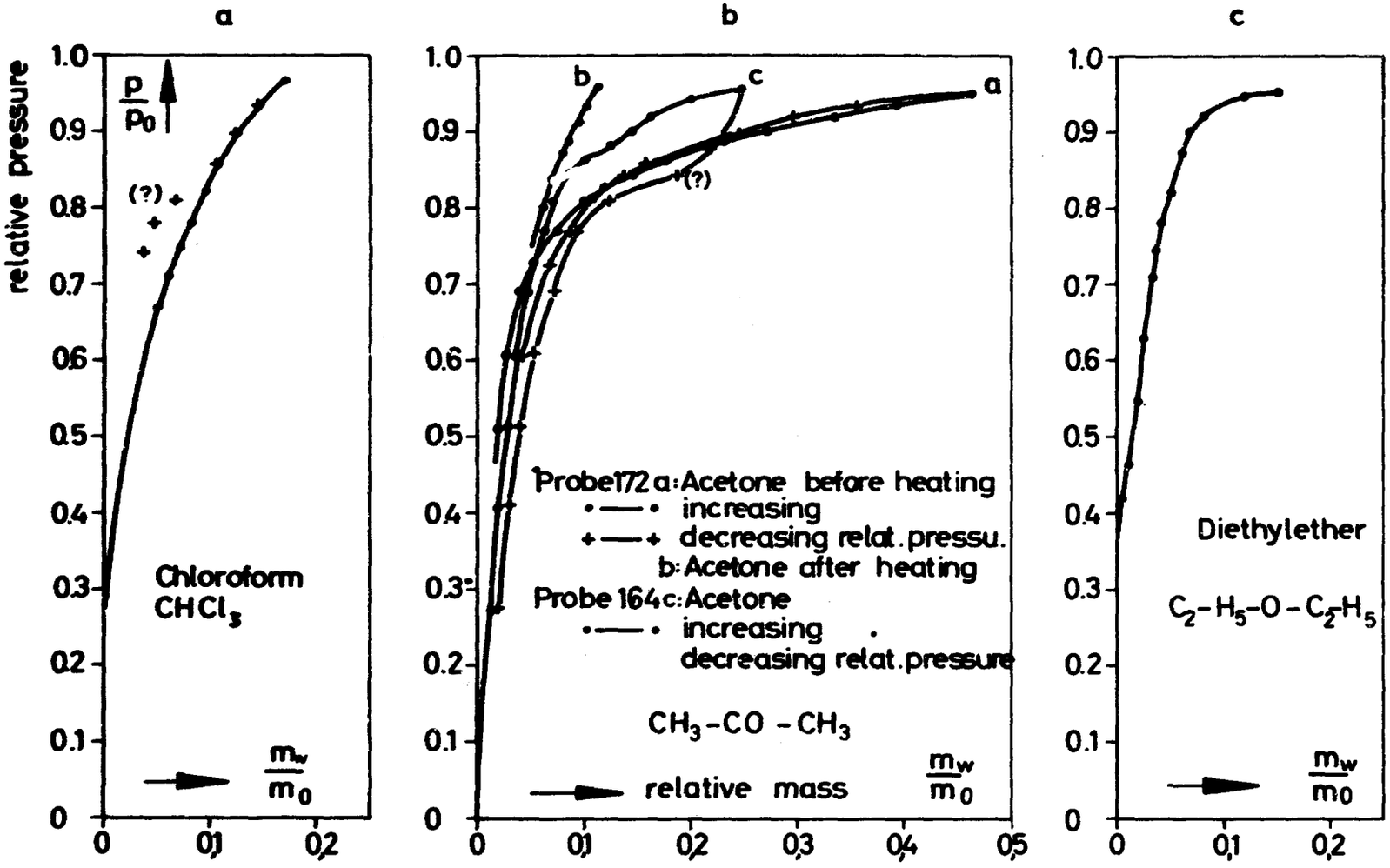
a
b
c
relative pressure
p/p0
(?)
Chloroform
CHCl3
mw/m0
Probe172 a: Acetone before heating
increasing
decreasing relat. pressu.
b: Acetone after heating
Probe 164 c: Acetone
increasing
decreasing relat. pressure
CH3-CO-CH3
relative mass
Diethylether
C2-H5-O-C2-H5

Fig.: 11

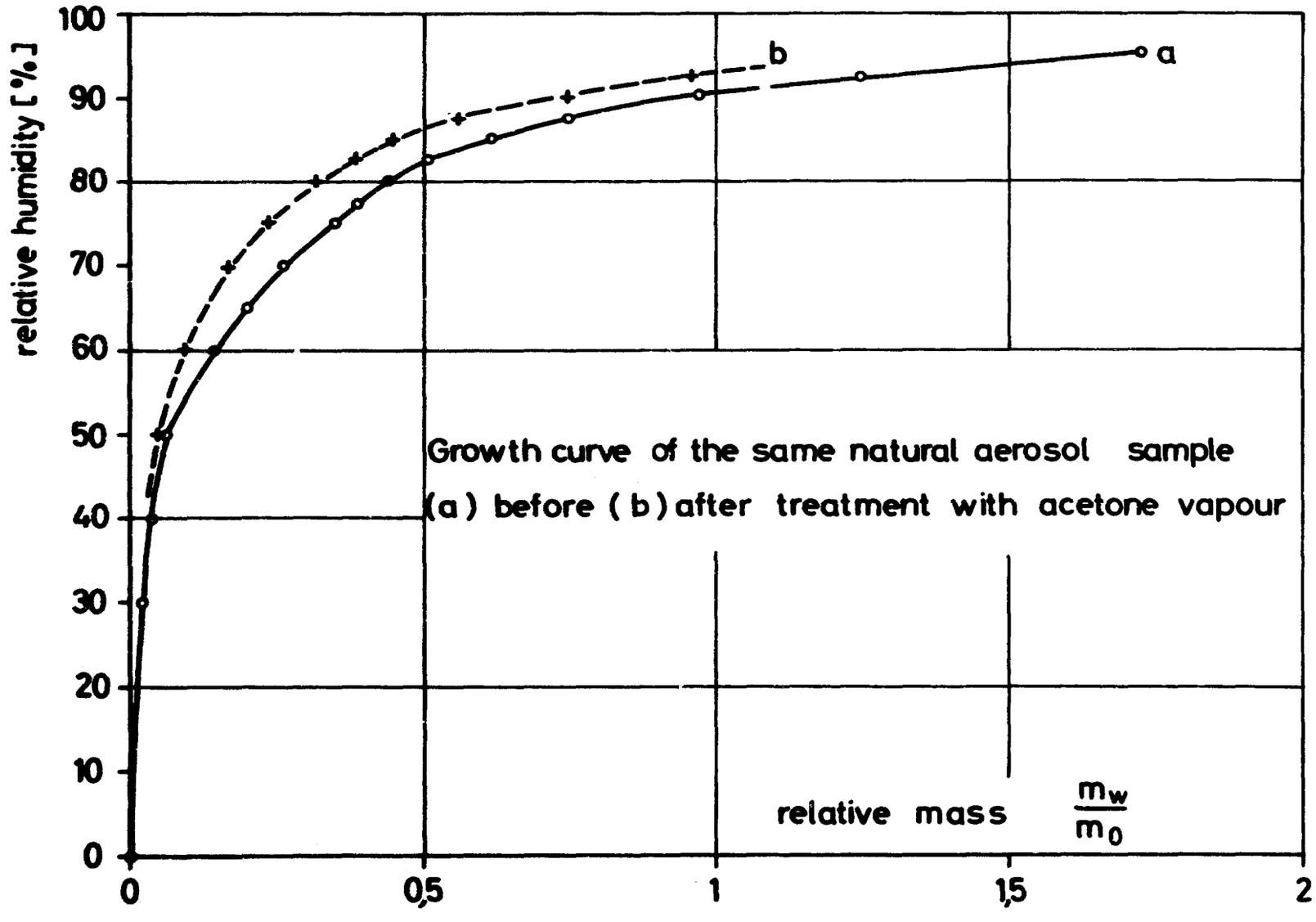
relative humidity [%]
100
90
80
70
60
50
40
30
20
10
0
0
0,5
1
1,5
2
b
a
Growth curve of the same natural aerosol sample
(a) before (b) after treatment with acetone vapour
relative mass $\frac{m_w}{m_0}$

Fig. : 12

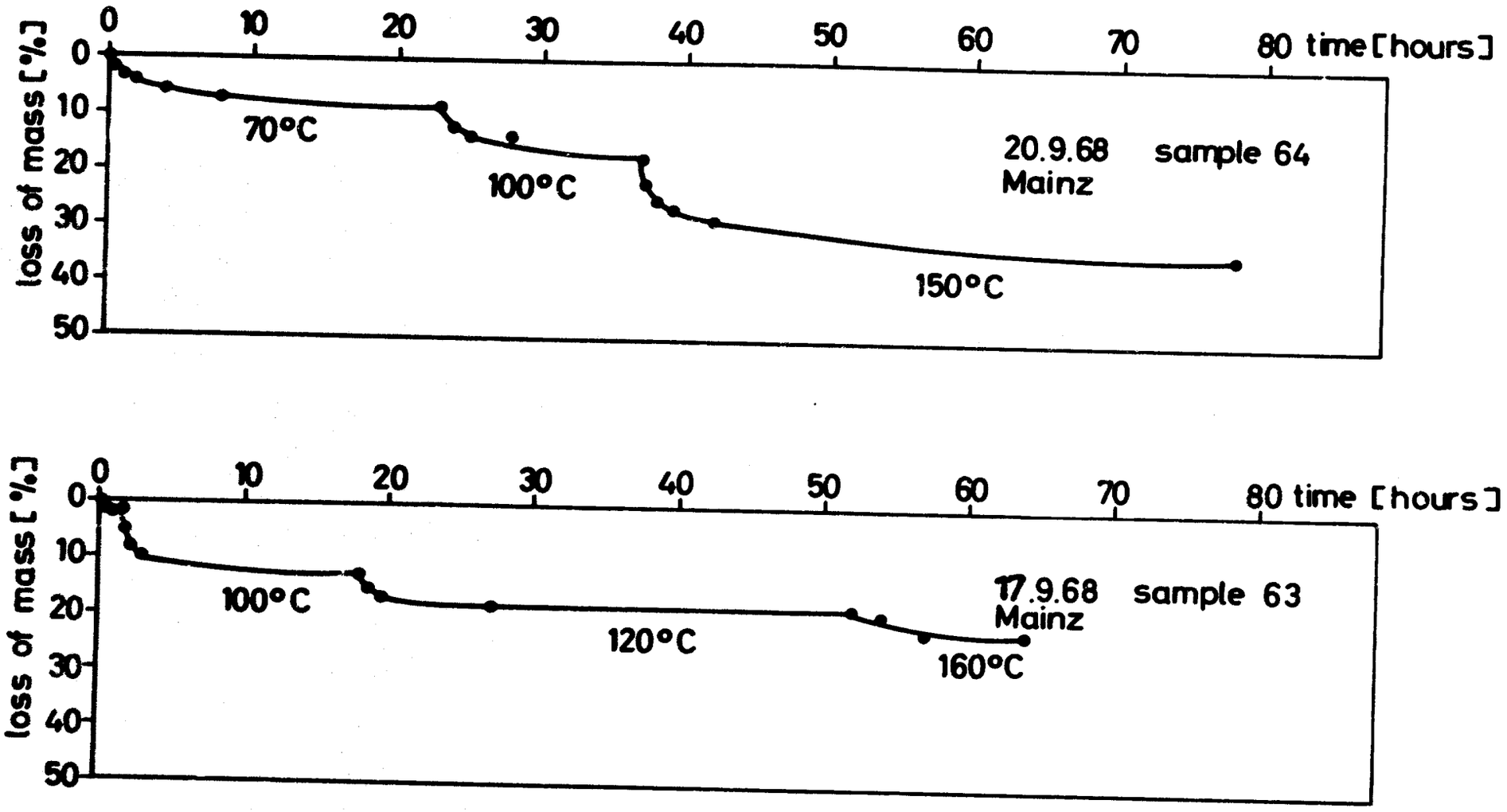

loss of mass of natural aerosol samples during heating

Fig. : 13

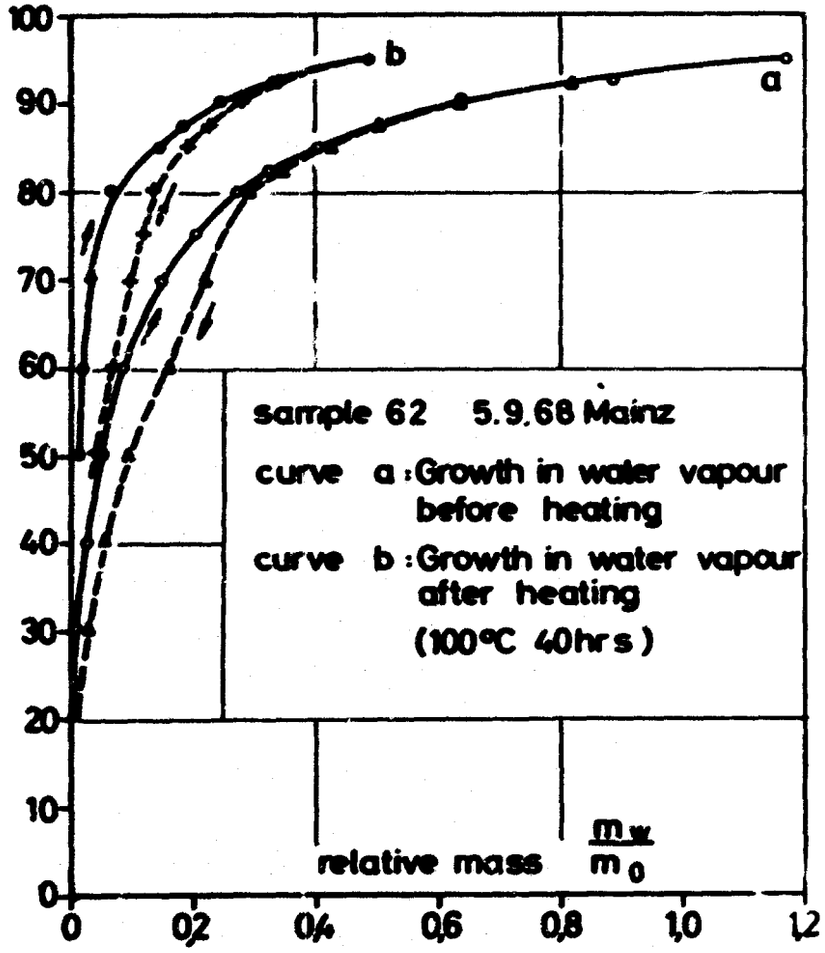
100
90
80
70
60
50
40
30
20
10
0
b
a
sample 62 5.9.68 Mainz
curve a : Growth in water vapour before heating
curve b : Growth in water vapour after heating
(100°C 40hrs)
relative mass $\frac{m_w}{m_0}$
0
0,2
0,4
0,6
0,8
1,0
1,2

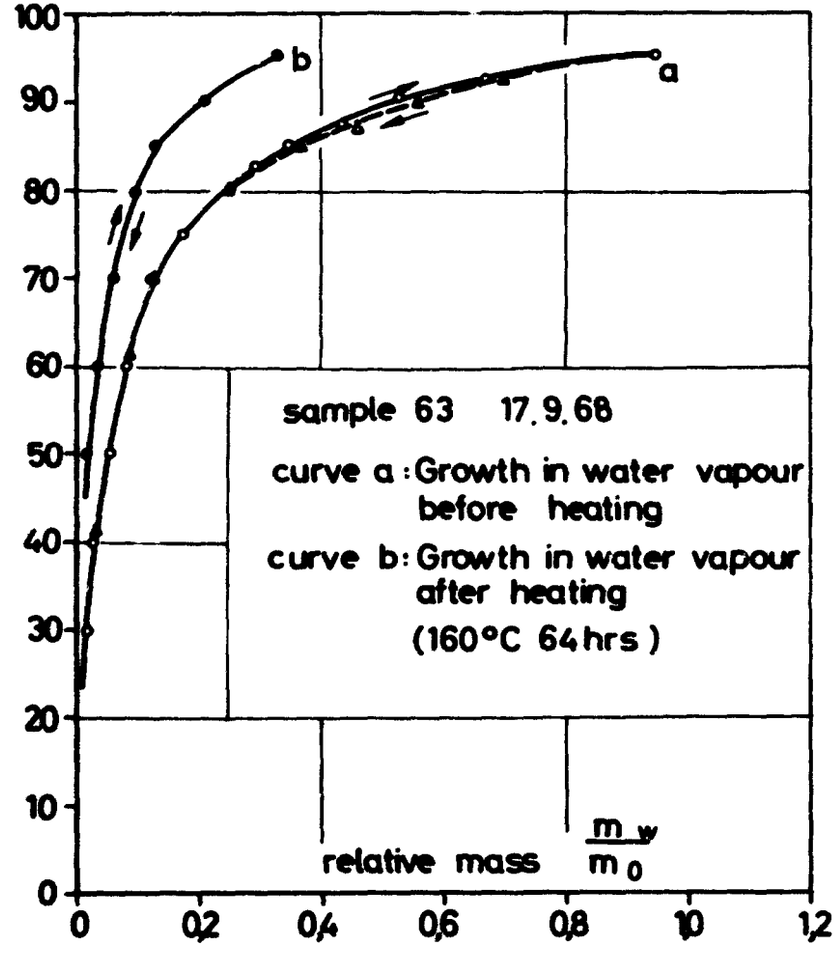
100
90
80
70
60
50
40
30
20
10
0
b
a
sample 63 17.9.68
curve a : Growth in water vapour before heating
curve b : Growth in water vapour after heating
(160°C 64hrs)
relative mass $\frac{m_w}{m_0}$
0
0,2
0,4
0,6
0,8
1,0
1,2

Fig.: 14

Unclassified

Security Classification

DOCUMENT CONTROL DATA - R&D

(Security classification of title, body of abstract and indexing annotation must be entered when the overall report is classified)

1. ORIGINATING ACTIVITY (Corporate author) Max-Planck-Institut für Chemie (Otto-Hahn-Institut) Mainz/Germany	2a. REPORT SECURITY CLASSIFICATION Unclassified 2b. GROUP

3. REPORT TITLE

STUDIES OF SIZE DISTRIBUTIONS AND GROWTH WITH HUMIDITY OF NATURAL AEROSOL PARTICLES

4. DESCRIPTIVE NOTES (Type of report and inclusive dates)

Scientific. Final. 1 Nov 1966 - 31 Dec 1968

5. AUTHOR(S) (Last name, first name, initial)

Abel, Nikolaus; Winkler, Peter and Junge, Christian

6. REPORT DATE	7a. TOTAL NO. OF PAGES	7b. NO. OF REFS
Jan 1969	104	31

8a. CONTRACT OR GRANT NO.	9a. ORIGINATOR'S REPORT NUMBER(S)
Contract AF 61(052) - 965 b. PROJECT NO. 7621 - 03 62405394 c. 681000 d.	9b. OTHER REPORT NO(S) (Any other numbers that may be assigned this report)

10. AVAILABILITY/LIMITATION NOTICES

This document has been approved for public release and sale; its distribution is unlimited

11. SUPPLEMENTARY NOTES	12. SPONSORING MILITARY ACTIVITY
TECH, OTHER	Air Force Cambridge Research Laboratories (CROA) Lg Hanscom Field Bedford/Mass. 01730

13. ABSTRACT

Part I. A sensitive large-ion counter was developed for determination of mobility distributions at low particle concentrations in clean atmospheres. If electrical charge equilibrium is assumed aerosol size distributions can be derived for the range of 10^{-6} cm to 10^{-5} cm particle radius, and for total particle concentrations larger than about 500 per cm^3. Results obtained at mountain stations and on sea are shown.

Part II. A gravimetric method is described for determination of the growth of aerosol samples in vapors of water and of organic solvents. Experiments with natural and artificial aerosols have been performed to study the form and the hysteresis effect of the growth curve of natural continental aerosols. Growth curves in organic vapors show that reactions of the vapors with the sample can occur. A "solution" method was developed for determination of the organic components in natural aerosols.

DD FORM 1 JAN 64 1473

Unclassified

Security Classification

Unclassified

Security Classification

14. KEY WORDS	LINK A		LINK B		LINK C	
	ROLE	WT	ROLE	WT	ROLE	WT
Atmospheric Aerosols						
Aerosol Size Distribution						
Large-Ion Mobility Distribution						
Aerosol Electrical Charge Distribution						
Ion Counter						
Microbalance						
Growth Curves						
Hysteresis						
Organic Matter in Natural Aerosols						

INSTRUCTIONS

1. **ORIGINATING ACTIVITY:** Enter the name and address of the contractor, subcontractor, grantee, Department of Defense activity or other organization *(corporate author)* issuing the report.

2a. **REPORT SECURITY CLASSIFICATION:** Enter the overall security classification of the report. Indicate whether "Restricted Data" is included. Marking is to be in accordance with appropriate security regulations.

2b. **GROUP:** Automatic downgrading is specified in DoD Directive 5200.10 and Armed Forces Industrial Manual. Enter the group number. Also, when applicable, show that optional markings have been used for Group 3 and Group 4 as authorized.

3. **REPORT TITLE:** Enter the complete report title in all capital letters. Titles in all cases should be unclassified. If a meaningful title cannot be selected without classification, show title classification in all capitals in parenthesis immediately following the title.

4. **DESCRIPTIVE NOTES:** If appropriate, enter the type of report, e.g., interim, progress, summary, annual, or final. Give the inclusive dates when a specific reporting period is covered.

5. **AUTHOR(S):** Enter the name(s) of author(s) as shown on or in the report. Enter last name, first name, middle initial. If military, show rank and branch of service. The name of the principal author is an absolute minimum requirement.

6. **REPORT DATE:** Enter the date of the report as day, month, year, or month, year. If more than one date appears on the report, use date of publication.

7a. **TOTAL NUMBER OF PAGES:** The total page count should follow normal pagination procedures, i.e., enter the number of pages containing information.

7b. **NUMBER OF REFERENCES:** Enter the total number of references cited in the report.

8a. **CONTRACT OR GRANT NUMBER:** If appropriate, enter the applicable number of the contract or grant under which the report was written.

8b, 8c, & 8d. **PROJECT NUMBER:** Enter the appropriate military department identification, such as project number, subproject number, system numbers, task number, etc.

9a. **ORIGINATOR'S REPORT NUMBER(S):** Enter the official report number by which the document will be identified and controlled by the originating activity. This number must be unique to this report.

9b. **OTHER REPORT NUMBER(S):** If the report has been assigned any other report numbers *(either by the originator or by the sponsor)*, also enter this number(s).

10. **AVAILABILITY/LIMITATION NOTICES:** Enter any limitations on further dissemination of the report, other than those imposed by security classification, using standard statements such as:

(1) "Qualified requesters may obtain copies of this report from DDC."

(2) "Foreign announcement and dissemination of this report by DDC is not authorized."

(3) "U. S. Government agencies may obtain copies of this report directly from DDC. Other qualified DDC users shall request through _____."

(4) "U. S. military agencies may obtain copies of this report directly from DDC. Other qualified users shall request through _____."

(5) "All distribution of this report is controlled. Qualified DDC users shall request through _____."

If the report has been furnished to the Office of Technical Services, Department of Commerce, for sale to the public, indicate this fact and enter the price, if known.

11. **SUPPLEMENTARY NOTES:** Use for additional explanatory notes.

12. **SPONSORING MILITARY ACTIVITY:** Enter the name of the departmental project office or laboratory sponsoring *(paying for)* the research and development. Include address.

13. **ABSTRACT:** Enter an abstract giving a brief and factual summary of the document indicative of the report, even though it may also appear elsewhere in the body of the technical report. If additional space is required, a continuation sheet shall be attached.

It is highly desirable that the abstract of classified reports be unclassified. Each paragraph of the abstract shall end with an indication of the military security classification of the information in the paragraph, represented as *(TS)*, *(S)*, *(C)*, or *(U)*.

There is no limitation on the length of the abstract. However, the suggested length is from 150 to 225 words.

14. **KEY WORDS:** Key words are technically meaningful terms or short phrases that characterize a report and may be used as index entries for cataloging the report. Key words must be selected so that no security classification is required. Identifiers, such as equipment model designation, trade name, military project code name, geographic location, may be used as key words but will be followed by an indication of technical context. The assignment of links, rules, and weights is optional.

GPO 863-551

Unclassified

Security Classification